Increasing Recoverable Oil in the Northern Afghanistan Kashkari Oil Field by Low-Salinity Water Flooding

Dissertation submitted to Akita University
in Partial Fulfillment of the Requirements
for the Degree of Doctor of Engineering

By
Zabihullah MAHDI

Dissertation Supervisor
Prof. Hikari FUJII

March 2024

Acknowledgment

I extend my sincere gratitude to my esteemed advisor, Prof. Hikari Fujii and Dr. Kazunori Abe, whose unwavering support, patience, motivation, and profound knowledge have been instrumental throughout my Ph.D. study and related research. Their guidance has been a beacon, shaping my research endeavors and enriching the writing of this thesis. I am immensely grateful for the privilege of having such a dedicated advisor and mentor.

Furthermore, I express my heartfelt appreciation to the honorable members of thesis committee: Prof. Shigemi Naganawa and Prof. Shun Chiyonobu. A special thanks to Hiroyuki Kosukegawa for his insightful instructions and our laboratory technical assistant, Dr. Saeid Mohammadzadeh Bina for his supportive presence along this research journey.

Their insightful comments, encouragement, and challenging questions spurred me to broaden my research perspectives.

Special appreciation is due to Dr. Naweed Seddiqi, and my fellow lab mates for their stimulating discussions, the collaborative efforts during sleepless nights leading up to deadlines, and the camaraderie that enriched the past four years. Gratitude extends to my friends at Akita University for their companionship, with a special acknowledgment to Prof. Hikari Fujii for offering a first glimpse into the world of research.

Last but certainly not least, heartfelt thanks go to my family, especially my father Dr. Mohaiuddin Mahdi and my beloved wife Fereshta Mahdi, their unwavering spiritual support throughout the thesis writing process and in all aspects of my life.

Abstract

Afghanistan is located in a tectonically complex and dynamic area, surrounded by rocks that originated on the mother continent of Gondwanaland. The northern Afghanistan basin, which runs along the country's northern border, has the potential for petroleum generation and accumulation. The Amu Darya basin has the largest petroleum potential in the region. Sedimentation occurred in the Amu Darya basin from the Jurassic to the Eocene epochs. Kashkari oil field is located in northern Afghanistan's Amu Darya basin. The field structure consists of a narrow northeast-southwest (NE-SW) anticline with two structural highs, the northwest limb being mild and the southeast limb being steep.

The first oil production well in the Kashkari oil field was drilled in 1976, and a total of ten wells were drilled in the area between 1976 and 1979. The amount of original oil in place (OOIP) in the Kashkari oil field, based on the results of surveys and calculations conducted by research institutions, is estimated to be around 140 MMbbls. The objective of this study is to increase recoverable oil reserves in the Kashkari oil field through the implementation of low-salinity water flooding (LSWF) enhanced oil recovery (EOR) technique.

The LSWF involved conducting a core flooding laboratory test consisting of four sequential steps with varying salinities. The test commenced with the use of formation water (FW) as the initial salinity, which was subsequently reduced to a salinity level of 0.1%. Afterwards, the numerical simulation model of core scale oil recovery by LSWF was designed by Computer Modelling Group's General Equation Modeler (CMG-GEM) software to evaluate the applicability of the technology to the field scale. Next, the Kahskari oil field simulation model was designed, and the LSWF method was applied to it. To obtain reasonable results, laboratory settings (temperature, pressure, rock, and oil characteristics) are designed as far as possible based on the condition of the Kashkari oil field, and several injection and production patterns are investigated. The relative permeability of oil and water in this study was obtained using Corey's equation.

In the Kashkari oilfield simulation model, three models: 1. Base model (with no water injection), 2. FW injection model, and 3. The LSW injection model were

considered for the evaluation of the LSWF effect on oil recovery. Based on the results of the LSWF laboratory experiment and computer simulation analysis, the oil recovery increased rapidly after the FW was injected into the core. Subsequently, by injecting 1% salinity water, a gradual increase of 4% oil can be observed. About 6.4% of the field, is produced by the application of the LSWF technique. The results of LSWF (salinity 0.1%) on the Kashkari oil field suggest that this technology can be a successful method for developing Kashkari oil production.

Table of Content

List of Figures

List of Tables

Chapter One

1 Introduction and Literature Review

1.1 Introduction

The oil consumption accounts for over 33% of the world's energy resources. The petroleum industry is planning on increasing the amount of oil that it can extract from formations by implementing enhanced oil recovery (EOR) techniques. This method can help recover up to 60% of the initial oil. On the other hand, only around 10% of the oil can be recovered during the primary recovery process [1, 2]. The first step in the oil recovery process is to use one of the reservoir natural drive mechanisms [3]. Various types of drive mechanisms can be used, such as water drive, gas cap drive, gravity drainage, and solution gas drive. However, once the reservoir pressure is dropped, it is not possible to produce a sufficient amount of oil [4]. Water-flooding is the next step in the secondary oil recovery process [5]. The process for recovering oil is to remove the residual oil from the reservoir. In the tertiary oil recovery process, various methods are used to recover the remaining oil [3].

Various technological advancements have allowed scientists to develop new techniques that can enhance the oil recovery process in reservoirs [2, 6-8]. The low-salinity water flooding (LSWF) can be on of those methods that can enhance the oil recovery process.

Recently, laboratory tests and field applications have shown that LSWF is one of the valuable enhanced oil recovery (EOR) methods in terms of its advantages in chemical cost, environmental impact, and field-scale implementation compared to conventional chemical EOR methods [9, 10]. The first signs of prospective oil recovery improvement during LSWF correspond to a study by Reiter [11] when he found an increase in the oil production rate within the water injection at different salinity. Later on, Bernard [12] examined the relative effectiveness of fresh water and salty water during water flooding and demonstrated that oil recovery increased when water salinity was reduced from 15,000 to 100 ppm. Tang and Morrow [13] also investigated the benefit of brine salinity reduction on oil recovery performance.

In terms of low-salinity water injection, extensive numbers of published data have demonstrated that the interplay of many factors, such as crude oil properties, brine salinity, brine composition, rock mineral composition, and reservoir temperature, can affect oil recovery [14]. Jadhunandan and Morrow [15] and Yildiz and Morrow [16] confirmed that brine composition impacts oil recovery in water flooding and it can be changed to optimize water flooding recovery. Austad et al. [17, 18], Fathi et al. [19], Zhang et al. [20], and Qiao et al. [21], also suggested that improved oil recovery is not only achieved by low salinity, but also by the specific composition of the injection water matter [22]. Based on numerous laboratory studies conducted on carbonate and sandstone reservoirs, Mg^{2+}, Ca^{2+}, and SO_4^{2-} ions present in seawater have proven to be the potential determining ions responsible for incremental oil recovery during LSWF [23-27].

Tang and Morrow [28] proposed a theoretical interpretation of the mechanism behind the effect of composition and salinity in LSWF. However, experimental core flooding tests conducted by Jerauld et al. [29] showed that the oil recovery enhancement does not generally depend on the salinity below a certain threshold. They reported this threshold salinity to be in the range of 1000–7000 ppm. Zhang et al. [30] demonstrated that a low-salinity concentration of 1500 ppm is required during the tertiary oil recovery process. Furthermore, Webb et al. [31] realized that by decreasing salinity from 5600 to 1500 ppm, the recovery has slightly increased; Morrow et al. [32] have also figured this behavior, but with a different threshold. More investigations have also taken place regarding this matter [13, 33-38].

Several field applications of LSWF indicated its feasibility at the reservoir field scale. Webb et al. [39] reported a decrease in oil saturation of about 25%–50% during LSWF. In 2005, McGuire et al. [40] expressed a substantial increase from 6 to 12% of the recovery of original oil in place after LSWF, using a single well chemical tracer test. Lager et al. [41] have also observed this phenomenon in the North Slope of Alaska. Skrettingland et al. [42] confirmed the efficiency of LSWF during his core flooding experiments in the North Sea. Moreover, there is a lot of research, that has compared the effectiveness of seawater injection due to its lower salinity over the injection of produced water [43, 44].

However, several authors have reported that injecting low-salinity brines can increase oil recovery by a factor of up to 40% compared with conventional high-salinity water injection in different sandstone reservoirs because low-salinity brines have a

better effect on changing reservoir wettability. Research by Morrow [45] shows that based on experimental studies, the lower salinity brine injection improves the recovery factor by about 29% more than the higher salinity brine injection. LSWF has a bright future because 50% of the world's conventional oil reservoirs are located in sandstone reservoirs and most of them contain clay minerals, which are favorable conditions for LSWF. The ionic composition of injected brine could impact oil recovery in sandstones. Many experimental data and industrial results demonstrate that higher oil recovery is observed in the low salinity process compared to water flooding [46]. Additionally, compared to other chemical EOR technologies, LSWF can achieve considerable low-cost recovery with relatively simple operations. The cost of LSWF is inexpensive because there are no expensive chemicals required. Also, according to industry reports, by using LSWF, the amount of oil recovery can increase by 6%–12% of OOIP, and residual oil saturation can decrease by 25%–50% [40]. An improvement in oil recovery is seen within lab experiments and single-well chemical tracer tests by as much as 38%, and an additional recovery of 29% in reservoir cores is obtained by reducing the salinity of the injected water.

Even though the oil mines of northern Afghanistan have been extracted for many years and the country's economy is dependent on more oil production, this country has never succeeded in increasing the efficiency and oil extraction of its mines by applying the EOR methods. The use of water-based techniques for greater efficiency and increased oil extraction in this industry has a long record in industrial countries, but the use of these cheap and profitable methods in Afghanistan has not had much history. Applying LSWF methods after recognition and stimulation of ions inside the reserves and finally producing more oil using this work has not even been considered in Afghanistan's oil industry. Afghanistan has petroleum resources [47-50], but their exploitation has been limited. Improving the economic conditions in Afghanistan will require the availability of energy resources, particularly by exploiting the country's petroleum reserves [51].

In this research, the use of LSWF is proposed to increase oil production from the Kashkari oil field in northern Afghanistan. The Kashkari oil field was developed by the China National Petroleum Corporation International (CNPCI) and the Watan Oil and Gas Group, Ltd. (WOGL) during the years from 2012 to 2016 [48, 49, 51-59]. The recovery of this oil field is offered by LSWF through a sandstone core sample and numerical simulation studies. First, the core flood test is conducted to calculate oil

recovery with injection in four steps. The first step is the injection of formation water (FW) with 3% salinity, which is designed based on the chemical composition of the reservoir's FW, and then the other steps are the injection of low salinity water with a salinity of 1%, 0.5%, and 0.1% respectively. The test model was simulated by the Computer Modelling Group's General Equation Modeler (CMG-GEM), for simulation studies of the recovery of oil by LSWF. Then, the core flood test and numerical simulation model results are compared by adjusting the simulated model for its application in the Kashkari oil field. In the last part of this research, the simulation model of the Kashkari oil field is established to apply and study the effect of the LSWF on the actual recovery of oil in the Kashkari oil field.

1.2 Sources and References

The sources and references used in this article contain hundreds of pages of official reports, various experiments on rock and oil samples, and Kashkari oil field development plans. Other detailed reports on each Kashkari well were made available to the author, using which the properties of the rock, oil, extraction, and other characteristics of the wells were analyzed.

One of the most important official documents used in conducting this research have been the daily reports of CNPCI and WOGL companies for the extraction and operation of wells in the Kashkari oil field. Meanwhile, the CNPCI and WOGL have repeatedly requested the SGS Afghanistan Ltd. company to analyze the oil and sample rock properties, and the results have been made available to the author.

In 2015, WOGL applied to Emerson Electric Co. for a geological model of the Kashkari oil field. Emerson Electric Co. started to work in the Kashkari oil field in the same year using the software SKUA-GOCAD and GEOLOG to build a three-dimensional geological model, but due to the company's interior problems this model was not completed successfully.

Another detailed report called "Formation Evaluation & Geo-modeling Study, Kashkari Field" was prepared in 2017 by Emerson company and its subsidiary PARADIGM GEOPHYSICAL, which was provided to the author by WOGL.

In addition to all these and dozens of reports and other research documents collected by researchers from various sources, WOGL shared the incomplete geological model of the Kashkari oil field prepared by Emerson. Some parts of this incomplete geological model have used all available sources and information about Kashkari.

Because SKUA-GOCAD software is not designed for LSWF simulation studies, the information and features in this model were transferred to CMG-GEM, which took up enough time and resources. In particular, parts of the information contained in the SKUA-GOCAD program could not be transferred to the CMG independently. Therefore, some of the information in the model built by SKUA-GOCAD was first transferred to the PETREL, and by adjusting the model in this software, the remaining features were transferred to CMG-GEM.

1.3 Research Background

The first operation for oil and gas exploration in Afghanistan was carried out in 1956. Between 1959 and 1966, fifty more exploratory wells were drilled in this basin, which led to the discovery of 3 large gas fields: Yatimtaq gas field (1960), Khwaja Gogerdak gas field (1961), and Khwaja Burhan gas field (1964). Although such discoveries were not 100% accurate, from 1966 to 1981, at least two small oil fields, a large gas field in Jarqodoq, and two other gas fields were discovered in the northwestern part of the country.

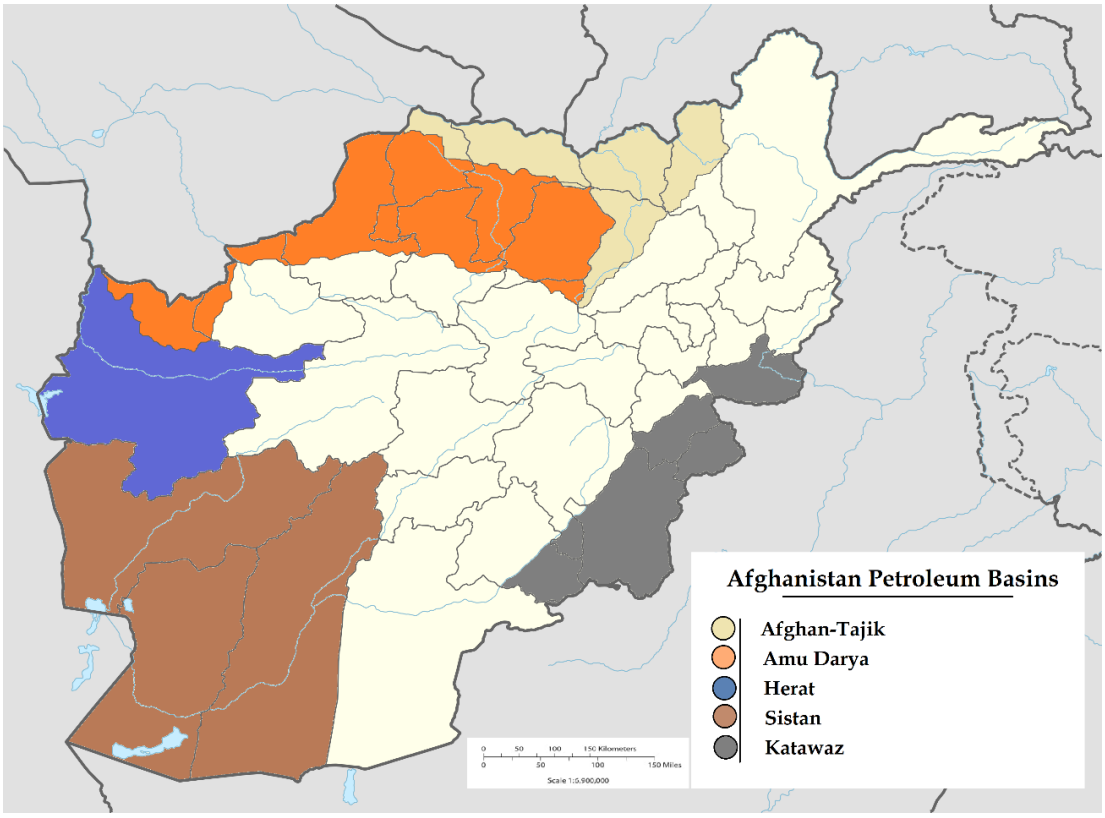

Figure. 1.1: Afghanistan's petroleum basins.

According to recent research, the northern basin is a part of the huge oil and gas basin of the Amu Darya, which ranks 15th among the 152 discovered oil and gas basins in the world in terms of reserves. This basin has an area of 400,000 square kilometers and extends into four countries: Afghanistan, Iran, Turkmenistan, and Uzbekistan; the research conducted by NASA revealed that there are more than 100 oil and gas spots in Afghanistan.

According to the amount of global consumption and the reserves of the major oil-producing countries, Afghanistan will not be considered among the major exporters; but can provide domestic needs for many years [49]. Figure 1.1 shows the basins of oil and gas in northern and other parts of Afghanistan.

1.4 Problem Statement

Nowadays, the technique of low salinity waterflooding (LSWF) has rapidly increased among academic and oil production companies. The successful improvement of oil recovery by ion exchange acceleration has convinced oil research institutions and companies to spend more budget and time for further development of this method. Up to now, most research has focused on the core scale by conducting core flooding and imbibition experiments. These tests serve as the main proof that low-salinity waterflooding can lead to additional oil recovery.

Typically, it is accepted that if the flooding experiments show positive changes in relative permeability curves, field application is justified provided the economic considerations are also favorable. In addition, together with field pilots, these tests resulted in several suggested trends and underlying mechanisms related to low-salinity water injections that potentially explain the additional recovery.

1.5 Objective

The overarching objective of this thesis is to advance the fundamental understanding and applicability of LSWF methods to enhance oil exploration and production. The research will primarily focus on the Kashkari oil field in northern Afghanistan, and aims to investigate the optimal salinity range of the injected water, alterations of the well and reservoir fluid's ionic relationships, and other factors that could affect the LSWF performance.

The thesis will commence with a comprehensive review of LSWF theory, its development, and applications in the oil industry. The review will delve into the

mechanisms that underlie the LSWF technique and its effectiveness in enhancing the oil recovery rate. Based on these findings, the research will examine the characteristics of the Kashkari oil field and investigate the factors that influence its oil production and decline.

The research will then shift towards experimental and simulation studies to determine the optimal range of salinity in the injected water that could improve the oil recovery rate in the Kashkari oil field. The experiments will involve the preparation and characterization of different brine solutions with various salt concentrations and testing them on core samples from the oil reservoir. The results of these experiments will be used to select the optimal salinity range for the field-scale LSWF method.

In addition, the thesis will explore the effects of modifying the well and reservoir fluid's ionic relationships on the LSWF's performance. This study will involve the alteration of effective ions inside the well and fluid to observe their effects on the oil recovery rate. The research will also analyze the production data from the Kashkari oil field and utilize reservoir simulation models to predict the performance of the LSWF under different scenarios, such as varying salinity ranges, flow rates, well patterns, and other factors.

Overall, the research outcomes of this Ph.D. thesis are expected to contribute to advancing the LSWF method as an efficient and sustainable approach to enhance oil exploration and production through Kashkari oil field. Furthermore, the findings of this thesis could provide practical insights and recommendations for the adoption of LSWF in other oil reservoirs, thus contributing to paving the way for environmentally and economically sustainable energy solutions in the oil industry.

1.6 Thesis Contents

This thesis comprises six comprehensive chapters and one annex that presents a detailed analysis of LSWF methods for enhanced oil recovery in the Kashkari oil field.

Chapter one provides a comprehensive overview of the research and sets out the framework of the thesis. The chapter starts with the background information of the research, highlighting the challenges faced in the oil industry concerning declining oil production and shrinking reserves. The chapter explains how LSWF methods have emerged as a promising solution to enhance oil recovery in mature oil fields and presents the research objectives.

The significance of the research is explained with a focus on the Kashkari oil field in northern Afghanistan. The chapter also describes the research methodology, summarizing the experimental and simulation approaches used to evaluate the LSWF technique and optimize oil recovery in the field. The research questions and aims of each chapter are outlined, and the significance of the study of the petroleum engineering field is emphasized.

Chapter two presents a detailed geological description of the Kashkari oil field, including its tectonic setting, geological complexities, stratigraphy, structure, and total petroleum system. The chapter discusses the Kashkari oil field's significance as an important strategic oil reserve, examining its geologic origins and characteristics, such as reservoir rock properties, permeability, and fluid composition.

The chapter reviews various geological formations in the Kashkari oil field. The chapter also describes the structural configuration of the field, such as anticlinal and synclinal features, faults, and folds. The geological and geophysical factors that have influenced reservoir modeling and simulation are discussed, including the effects of heterogeneity and anisotropy on fluid flow and oil recovery.

The chapter also discusses the practical applications of the theory to the Kashkari oil field, emphasizing the need for a thorough understanding of various parameters, such as injected water, reservoir rock properties, and fluid composition.

Chapter three describes the laboratory experiments conducted to assess the effectiveness of the LSWF technique in the Kashkari oil field. The chapter begins with the methodology used to prepare the LSW solutions, core flooding tests, and data analysis. The chapter provides a detailed description of the experimental set-up and procedure, including the selection of core samples, fluid injection, data acquisition, and analysis. The chapter presents the experimental data obtained from the tests conducted at different salinity ranges and compares the results to evaluate the technique's effectiveness.

Chapter four focuses on the simulation studies conducted to investigate the LSWF method's effectiveness in the Kashkari oil field. The chapter describes the design of the laboratory and field-scale LSWF simulation model and the creation of the Kashkari reservoir geological model. The chapter presents a comprehensive analysis of the LSWF simulation model's performance and evaluates the model's predictions in terms of the Kashkari oil field's production and recovery rates.

Chapter five presents practical insights and recommendations for sensitivity analyses of the LSWF technique's effectiveness for EOR in the Kashkari oil field. The chapter discusses the significance of each parameter that affects the technique's performance, such as the injection rates, well patterns, and different salinity ranges. The chapter proposes various scenarios, and simulation studies, analyses sensitivity the LSWF technique's efficiency while reducing costs and environmental impacts. The chapter concludes with a discussion of the potential applications of the optimized LSWF technique to other mature oil fields worldwide.

Chapter six summarizes the key findings and contributions of the research presented in the thesis. The chapter revisits the research objectives, research questions, and aims of each chapter, emphasizing how the study has contributed to the petroleum engineering field's understanding of the LSWF method. The chapter also discusses the implications of the study for the oil industry's future, emphasizing the significance of enhanced oil recovery techniques to meet the ever-increasing energy demands worldwide.

Annex provides a detailed overview of the Buckley-Leverett (BL) frontal displacement theory. The annex describes the theoretical basis of the method, including the principles of fluid displacement, relative permeability curves, and capillary pressure. The annex explains the BL theory's assumptions and limitations and provides a framework for the LSWF simulation studies conducted in this thesis.

1.7 Methodology

The literature review conducted for this research plays a crucial role in providing an overview of existing studies on the topic. It highlights the shortcomings of previous research and identifies gaps that need to be addressed. This information helps formulate research questions that guide the study. Additionally, it forms the foundation for developing hypotheses that can be tested through empirical data.

The LSWF laboratory analysis involved a core flood test in which the San Saba sandstone core sample was subjected to different salinity percentages. This experiment was conducted using a range of equipment and techniques, including core flooding apparatus, and pressure transducers. The results obtained from this experiment were critical in developing a numerical simulation model that was used to assess LSWF's efficiency in different scenarios.

The numerical simulation model was developed using CMG-GEM software. The simulation modeled the core flooding laboratory test, and its results were compared with those obtained through LSWF laboratory analysis. The model allowed for adjustments to simulate the real conditions present in the Kashkari oil field, which provided more reliable and accurate results.

Overall, the integration of different approaches and techniques in this research study has made it possible to obtain comprehensive findings. The methodology used in this research can be applied in future studies to enhance the understanding of oil recovery mechanisms and optimize production efficiency. The below diagram at Figure 1.2 explains the methodology of LSWF oil recovery on the Kashkari oil field.

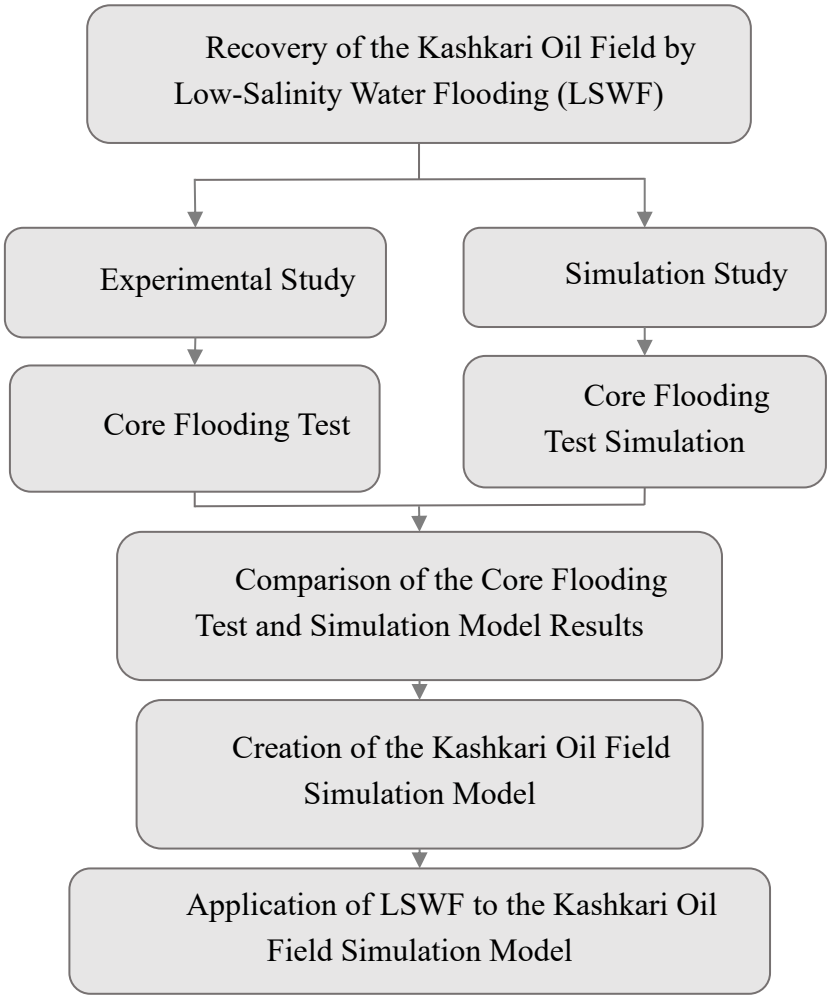

Figure. 1.2: Diagram of Kashkari oil field recovery by LSWF.

Chapter Two

2 Geological Setting of Kashkari Oil Field

2.1 Regional Geology of Afghanistan

Afghanistan lies in a tectonically complicated and active area, surrounded by the blocks originated from the mother Gondwanaland. Afghanistan is in Alpine-Himalayan orogenic belt, situated in central Asia formed during Late Paleogene by the collision between Indian Plate, Eurasian Plate and Arabian Plate. The tectonic evolution of this region relates to the closing of the Tethys Ocean during the Paleozoic and Mesozoic times. During this evolutionary stage, different blocks were originated from Gondwanaland and accreted to the southern margin of Eurasian plate which gave rise to a complex assemblage tectonic zones in Afghanistan [60]. There are following three tectonic zones in Afghanistan.

i. Afghan Tajik Platform;

ii. Katawaz Basin;

iii. Afghanistan Centre Block.

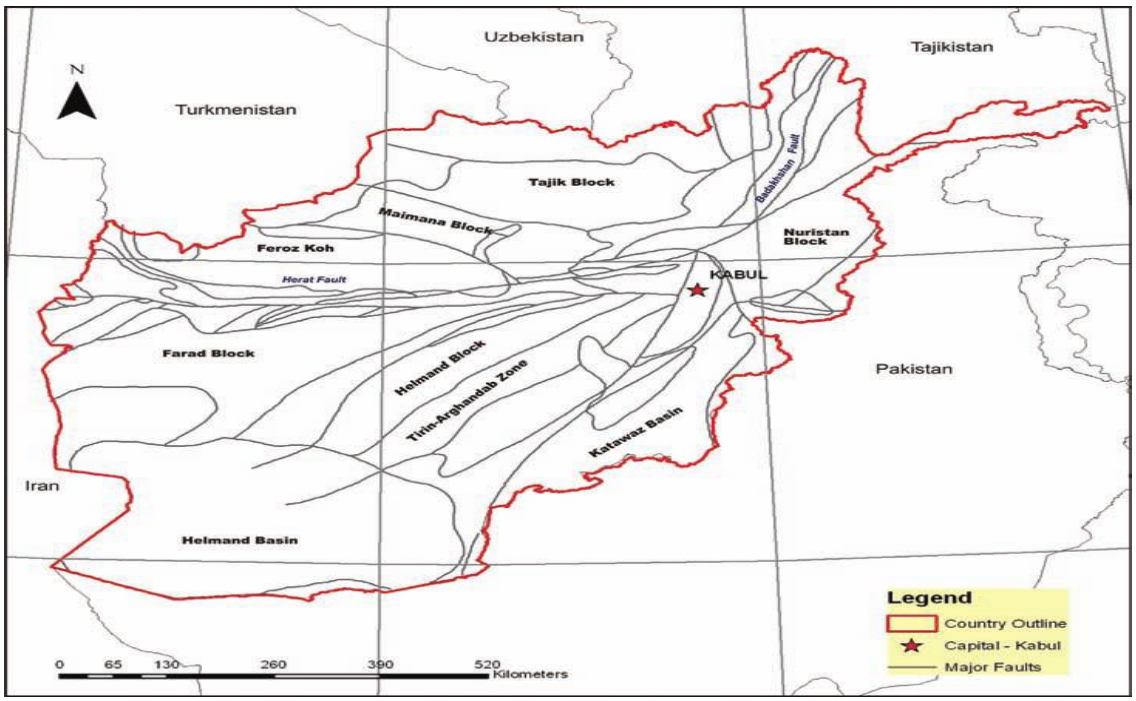

Figure 2.1: Tectonic Map of Afghanistan representing all zones [61].

As the geology of Afghanistan is complex, it has limited areas which show favorable conditions for the generation, accumulation, and production of oil and gas. Sedimentary accumulations in Afghanistan are categorized into three different areas.

i. North Afghanistan Basin along the northern boundary;

ii. Southwestern Afghanistan Basin;

iii. Katawaz Basin.

2.1.1 North Afghanistan Basin

North Afghanistan Basin locates along the northern boundary of the country and the southeastern part of the Turanian Platform, sedimentary basin which has sufficient potential for petroleum accumulation. The Amu Darya basin is the only region of Afghanistan having petroleum prospect. The targeted oil field Kashkari is located in this region.

2.1.2 Southwestern Afghanistan Basin

Southwestern Afghanistan Basin has a thick sedimentary cover, but here the petroleum prospect is not considerable as the rock sequence is intensively folded and faulted.

2.1.3 Katawaz Basin

This basin has sedimentary rocks ranging in age from Permian to Oligocene up to 3,000 m thick, but the sedimentary strata are highly folded and faulted. Rocks in this region are highly metamorphosed in the northern parts and intensity of metamorphism decreases towards south and there are no considerable accumulations of petroleum products [62].

2.2 Geological Settings of the Amu Darya Basin

The Amu Darya basin is located in northwest of Afghanistan, in Faryab and Sar-e-pul provinces. The extension of this basin is far beyond the Afghanistan [47]. This basin is extended into Turkmenistan, Uzbekistan, Afghanistan, and a small portion in Iran, covering an area of 400,000 km^2.

In the southwest, the Kopetdag foldbelt marks the boundary of the Amu Darya basin. This foldbelt is comprised of Jurassic and Cretaceous clastic and carbonate strata which overlie the Triassic and Paleozoic sequence unconformable. The north slope of Bande Turkestan foldbelt marks the southern boundary of the basin. It is a mountainous range comprised of clastic, carbonate and volcanic rocks of Permian and Triassic age which

overlie the metamorphic rocks of Paleozoic age and overlain by the rocks of Jurassic and Paleogene with an unconformable contact. In the east of the Amu Darya basin, the Afghan Tajik basin is present, these two basins behaved as a single basin until Miocene time so the stratigraphy of both of them ranging from Jurassic to Oligocene age is similar. From Miocene time to recent, the Afghan Tajik basin experienced a deformation due to Pamir Block and this compression resulted to the formation of a series of anticlinoria and synclinoria in the Afghan Tajik basin and this series is underlain by a thrust and detachment surface provided by the salts of Jurassic age. The Kyzylkum high is present on the north side of the Amu Darya basin and this high comprised of metamorphic and igneous rock sequence of Paleozoic age. To the northwest side, the Karakum regional high is present, and the basin boundary crosses this high. The crest and southern and eastern slopes of the high have hydrocarbon potential and these areas are included in the Amu Darya basin [63].

2.3 Stratigraphy of the Amu Darya Basin

The Amu Darya basin is significantly a depression of Jurassic-Tertiary age underlain by Paleozoic basement rocks and Permian-Triassic rift system. The composition of the basement is poorly known to geoscientists, but the extrapolation from the margins of basin suggested that the basement comprised of several terrane of Hercynian age. After the Hercynian orogeny, the development of the Amu Darya basin started. The rocks of the basement are deformed and metamorphosed. Undeformed basement strata may be present beneath the Jurassic-Tertiary strata in deeper parts of the basin [64].

In the Amu Darya basin sedimentation took place during Jurassic to Eocene time. The sedimentation covered the older rocks in the basement. Lower to middle Jurassic rocks are at the base and generally comprised of continental clastic rocks as confirmed by the drilling. Some marine beds are also present while the basal portion is covered with clastic strata which also contains some coal beds [47]. The stratigraphic column along with the geological formation and their lithologies is shown in Figure 2.2.

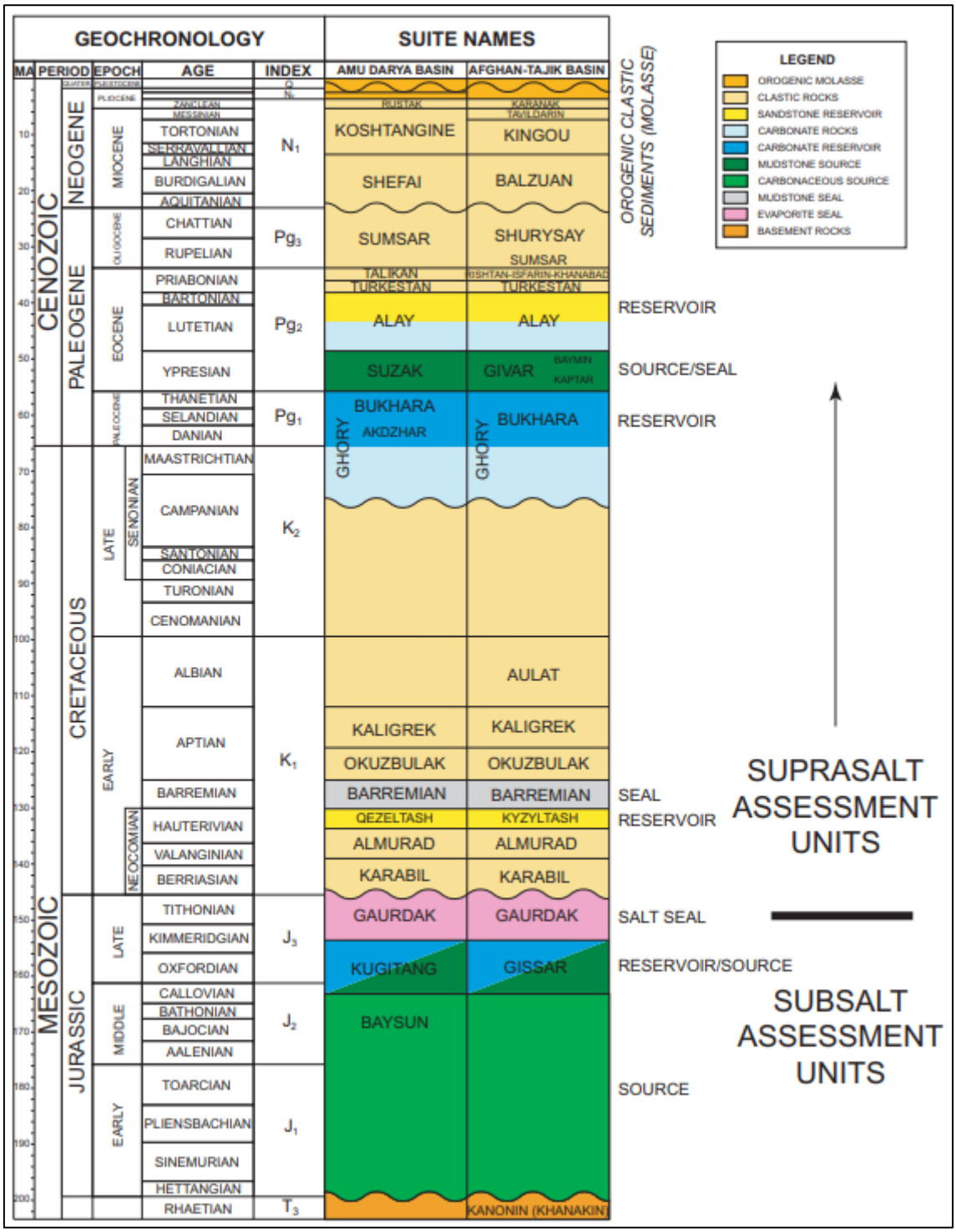

Figure 2.2: Stratigraphy of Amu Darya basin.

During Bathonian-Callovian, marine transgression occurred and began. During this time, Baysun suite was deposited as basal shale. This suite comprised of mudstone of

dark gray color, marl and some clayey limestone which reaches in thickness up to 200 m. This suite also has sandstone, and the thickness of sandstone decreases towards the edge of the Amu Darya basin [63].

From Callovian-Oxfordian time, carbonate sedimentation took place over the basal shale. During this time interval, the Amu Darya basin was partitioned into shallow water shelves on its margin and a deep-water sea on the southeastern side (Figure 2.3). During this period, Kugitang suite was deposited which is mainly comprised of carbonate deposits extending from west to east. This suite has a complex of barrier reefs, pinnacle reefs and atolls which form along the marginal areas and on shallow water shelves. The lithology distribution of this suite indicates that the environment of deposition was not the same all around the basin, it was lagoonal-tidal flats in the south, shelf, and barrier reef in north and deep basinal environment.

Gaurdak suite was deposited Kimmeridgian-Tithonian time, and it is an evaporate deposit. This suite comprised of two units i.e., lower anhydrite unit and upper salt and anhydrite unit. The age of Gaurdak suite is determined by the fauna of marine gastropods and pelecypods. This formation also extends into the Afghan Tajik basin. This unit is conformably overlain by the Karabil suite.

Karabil suite was deposited during Upper Tithonian-Valanginian time and consists of both lagoonal and continental sediments of red color.

During Valanginian-Hauterivian times, Almurad Formation was deposited which comprised of continental and lagoonal sediments. This suite also has marine sediments as there was a minor marine transgression occurred which led to the deposition of limestone in the western premises of the Amu Darya basin and in the eastern part of the basin dolostone and anhydrite was deposited.

Qezeltash suite deposited during the Hauterivian-Barremian time consisting of continental deposits of siltstone, mudstone, and conglomerates.

During Lower Aptian times, the Qezeltash suite graded into Okuzbulak suite, which comprised of marl and limestone with ammonites.

During Upper Aptian times, Kaligrek suite was deposited comprising of beds of sandy unit with marl and limestone interbeds.

Ghory suite was deposited during Paleocene and represents a continuous rock series of Campanian-Paleogene age.

The rocks of Paleocene age are present at the top of the sedimentary fill of the basin. During Middle-Upper Paleocene time, Bukhara Formation was deposited which consist of shallow water carbonates which contain clastic and anhydrite beds.

The Eocene stratigraphy of the Amu Darya basin is represented by Suzak suite, Alay suite, Turkestan suite and Talikan suite. This whole sequence is comprised of shale, siltstone, and sandstone. Calcareous beds are also present throughout the sequence but are more abundant in the western areas of the basin (Figure 2.2).

Oligocene-Miocene time is represented by Sumsar suite, Shefai suite, Koshtangine suite. The strata during this time were deposited in a variety of sedimentary environments, but the most of the strata has lacustrine and alluvial indications. Overall, it has clastic nature. The Quaternary deposits are comprised of orogenic molasse and clastic sediments and are present at the top of sedimentary cover of the Amu Darya basin. These sediments are thickest ranging in thickness from 1000-1700 m [63] [47].

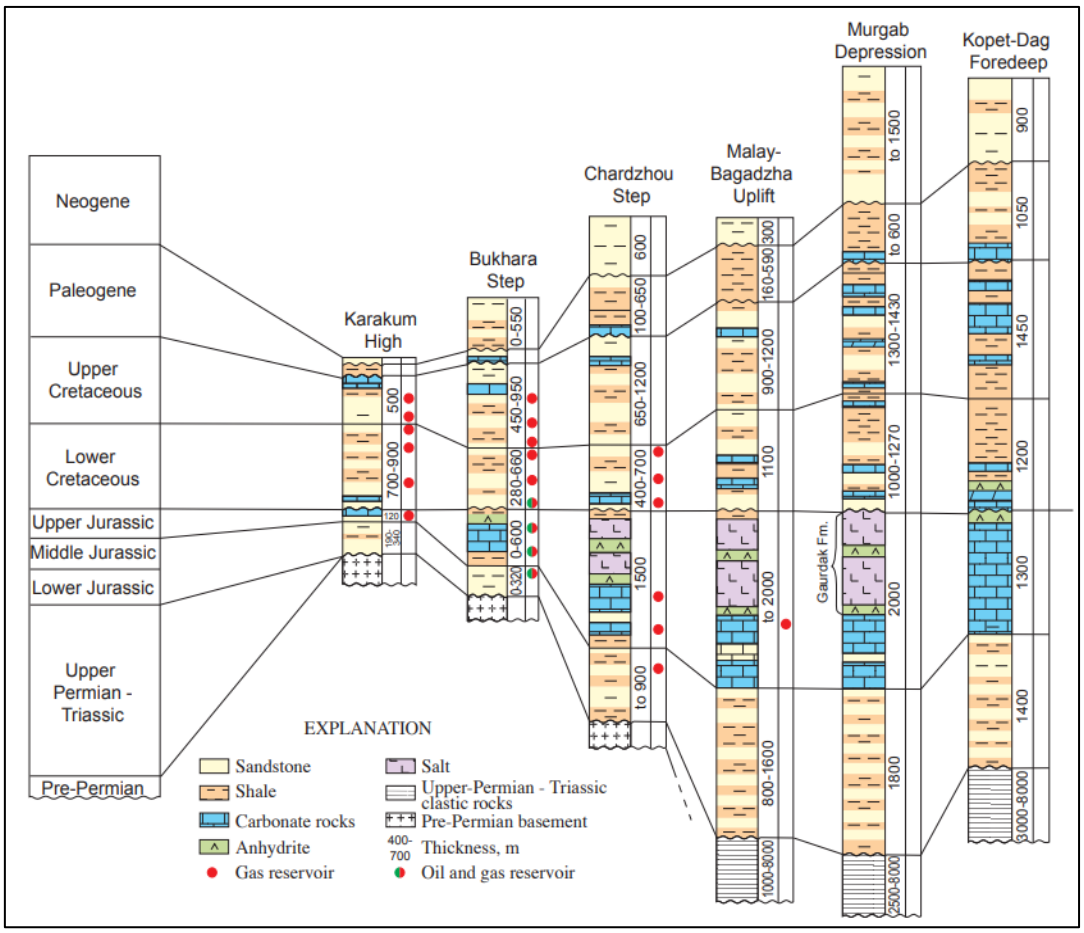

Figure 2.3: Lithostratigraphic column of the Amu Darya basin representing the variation in lithology and thickness of geological units along the extent of the basin.

2.4 Petroleum System of the Amu Darya Basin

In Afghanistan, there are five sedimentary basins which are being explored for petroleum potential and production. These basins are:

i. Amu Darya Basin;

ii. Afghan Tajik Basin;

iii. Herat Basin;

iv. Helmund Basin;

v. Katawaz Basin.

The Amu Darya basin is in the northwest of Afghanistan and has most of the petroleum reserves of the country. The total petroleum system (TPS) of the basin is represented by Jurassic-Cretaceous petroleum system. The major reserves of the TPS are consisted of gas i.e., 6.5 trillion cubic meters while the liquid reserves of the system are smaller in quantity i.e., 2 billion barrels and out of these reserves almost 60% comprised of condensate and 40% is oil [65].

TPS of Amu Darya basin includes the sedimentary cover of age ranging from Triassic to Cenozoic but most of the components of petroleum system i.e., source rock and reserves lie on rocks of Jurassic-Cretaceous age.

2.4.1 Source Rock

There are two source rocks in TPS of the Amu Darya basin.

i. Coaly shale of lower to middle Jurassic, dominantly gas prone type III kerogen;

ii. Marine black shale of Upper Jurassic has kerogen type II.

The composition of biomarkers reveals that several condensate accumulations were produced in the thermal gas-window zone′s depths and that terrestrial organic materials can be found in the source rocks [66]. The Chardzhou step is thought to contain condensates associated with the disintegration of primary oil pools in gas. There are not many oil pools and most of them are actually retrograde condensates [67]. Natural gas from the Amu Darya basin is a dry methane gas with 0.005-6% of hydrogen sulfide and shows higher maturity. Natural gas reserves of the southern areas of the Amu Darya basin showed up to 1% of sulfur.

2.4.2 Maturation of Source Rock

The source rocks of the Amu Darya basin are deeply buried in the gas generation window and shows a high level of maturation. At the end of the Early Cretaceous, the source rocks were buried to a depth of 2 km, the maximum depth at which petroleum

could be produced, with a geothermal gradient of 45 °C per km. The Murgab depression in northwest Afghanistan served as the source location of hydrocarbon accumulations. It is speculated that the two stages of expulsion took place: the first stage involved the expulsion of oil with little gas, and the second stage involved gas generated from high temperatures [63].

The crude oil pools are present only in those areas where there is no natural gas accumulation, and natural gas pools in Cretaceous rocks are present only in those locations where the Jurassic strata also has a natural gas accumulation. The crude oil generation window started at depths of 2,200 to 2,500 m with paleotemperatures of 90 to 105 °C and extends to 2,200 to 4,000 m and deeper at 140 °C based on the geothermal gradients of the Amu Darya basin.

2.4.3 Reservoir Rock

Most of the hydrocarbon reserves of the Amu-Darya basin have been identified in two reservoir sequences: *Hauterivian Shatlyk Bed sandstones* and *Upper Jurassic carbonates*.

Most of the natural gas, gas condensate, and oil reserves in Uzbekistan are found in Upper Jurassic carbonates, and the majority of them located on the Chardzhou and Bukhara steps. More than 90% of Turkmenistan's gas reserves are found in the Shatlyk Bed, mainly within the Murgab depression and the surrounding areas.

Upper Jurassic carbonate reservoir characteristics are intimately correlated with their depositional facies [68]. Reef carbonates range in permeability from 25–400 millidarcies (mD) and in porosity from 14–19 percent. Reservoir rocks may reach as thick as 200 m and constitute an average of 86% of the reef sequence's overall thickness [69].

2.4.4 Traps

All the known fields are in structural traps related to the Neogene compressional event, particularly broad anticlines. Fields that are yet to be identified are anticipated in structural traps, reefs, or a combination of the two. All known petroleum traps of the basin are comprised of the anticlines. Pinch out traps are also present in places where Jurassic strata pinch out.

2.4.5 Seals

The Kimmeridgian to Tithonian Gaurdak Formation, which contains salt and anhydrite associated carbonate layers, is the main regional seal of the basin [62]. The Gaurdak Formation in northern Afghanistan's Amu Darya basin has a thickness that varies from 130–180 m.

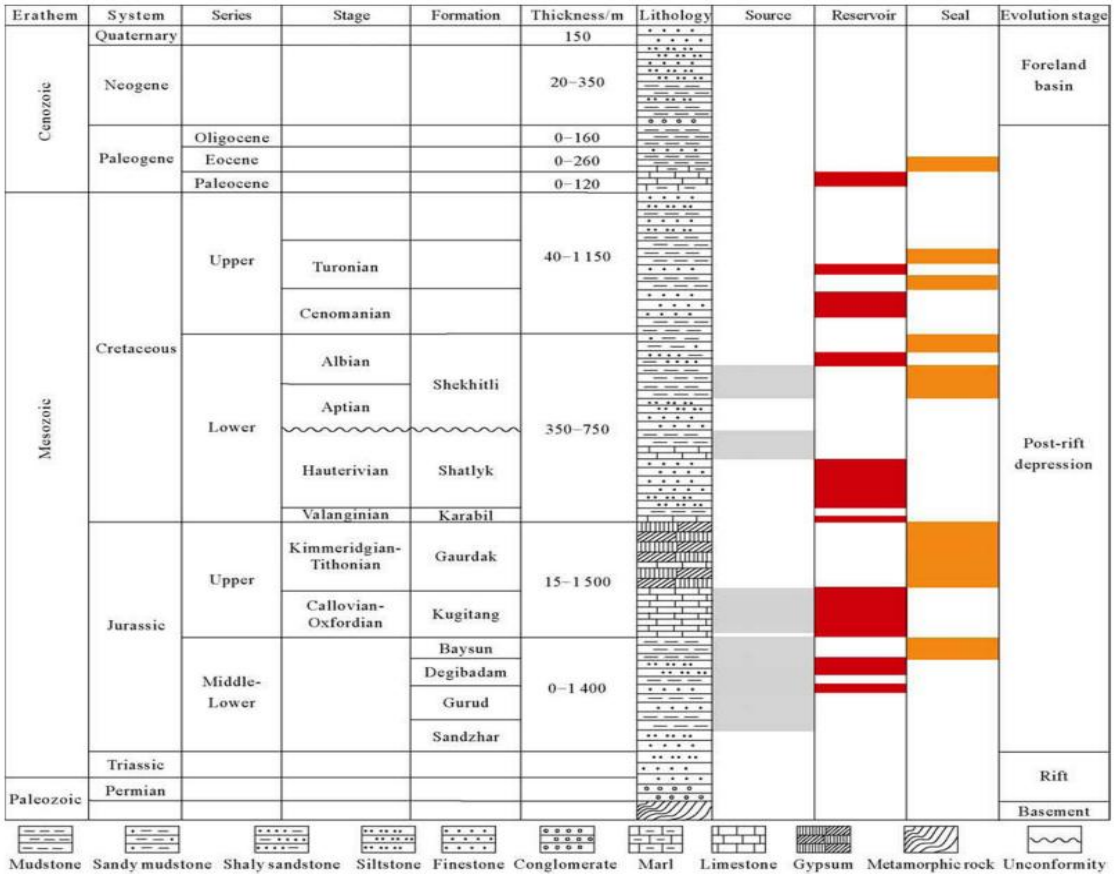

Figure 2.4: Stratigraphic column of Amu Darya basin along with the components of TPS [70].

2.5 Oil and Gas Fields in Amu Darya Basin

In the Amu Darya basin (Afghanistan), 15 petroleum fields are discovered and out of these, 7 are oil fields and 8 gas fields. According to the information primarily collected from the Afghanistan government, 370 wells have been drilled in northern Afghanistan. Over 100 of these wells are categorized as exploration, and over 200 are categorized as development [62, 63].

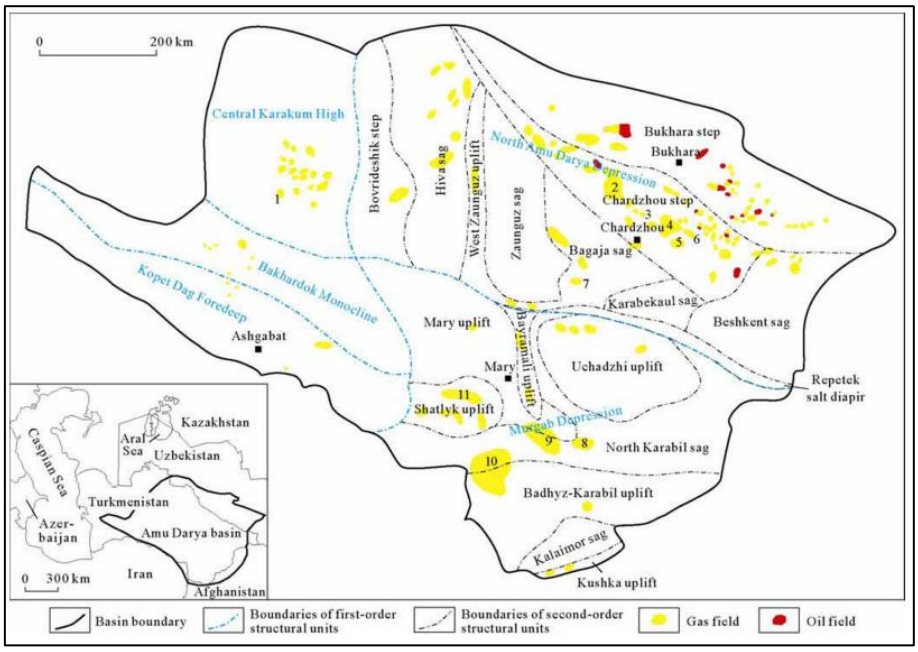

Figure 2.5: The oil and gas fields of Amu Darya basin map [70].

2.6 Kashkari Oil Field

The Kashkari oil field is located in the northern Afghanistan, Jowzjan and Sar-e-Pol provinces, in the Amu Darya basin. The oil field is located in the Kashkari block, which is connected to the 1,723 km^2 Zamarudsay block and the 1,103 km^2 Bazar-Kami block [71].

The southeastern border of the Amu Darya basin includes the sedimentary basin, a petroliferous region. It is located 12 km from the city of Sar-e-Pol in the southeast, 10 km from the Angut oil field, 5 km from the Ak-Darya oil field in the southwest, and 27 km from the Bazarkami oil field in the southeast. It is located in the eastern portion of the Amu Darya basin's oil zone, adjacent to several mountains. The most significant Afghanistan gas zone is to the north of the block. Low levels of exploration and development have been made at the Kashkari oil field, and no seismic prospecting has been conducted there. The wells were drilled during the 1960s and the 1980s, and their location was mostly determined by gravity and magnetic data and surface geological studies [72].

The first producing well for the Kashkari oil field in northern Afghanistan was drilled in 1976, and by 1979, a total of ten wells had been drilled. According to surveys and assessments made by research organizations, the Kashkari oil field has approximately 140 million barrels of original oil in place (OOIP) [73].

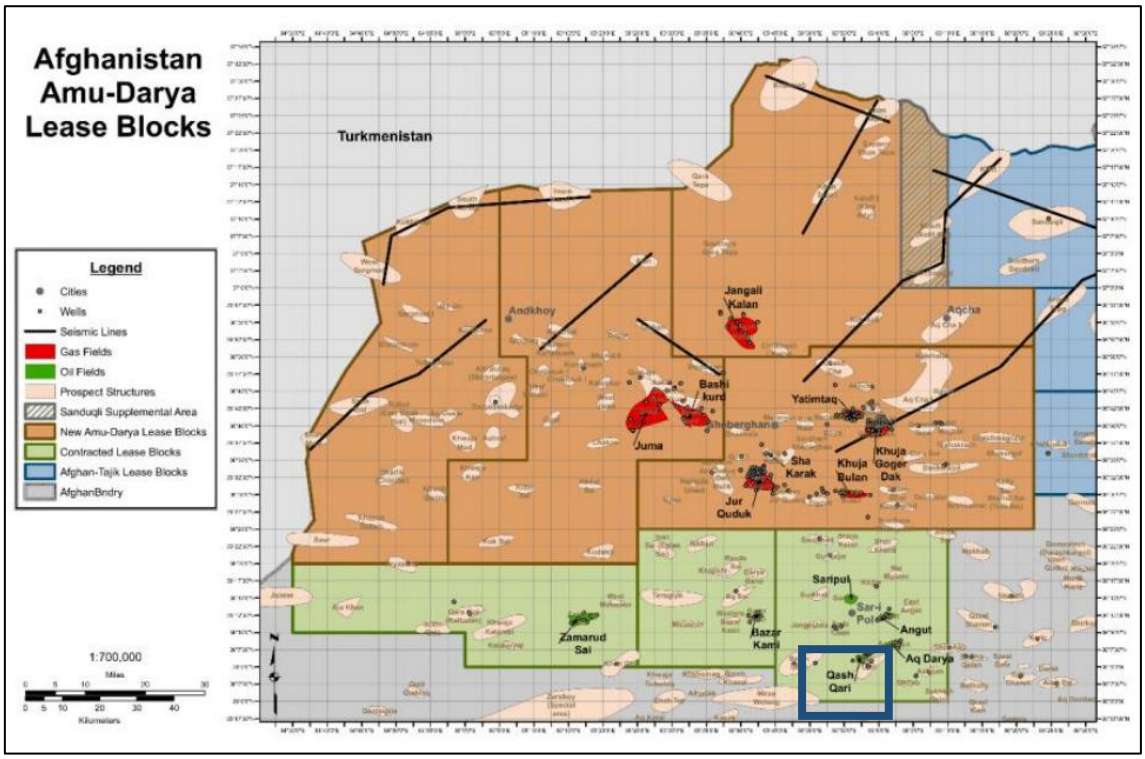

Figure 2.6: Location of Kashkari oil field marked in blue square on map.

2.6.1 Lithostratigraphy and Structure of Kashkari Oil Field

The blocks are situated in a mountainous region with varying landforms. With a few Quaternary strata in a few locations, the outcropped stratum is primarily Guri. The results from the drilled wells indicate that the drilled stratum mainly consists of Cretaceous systematic layers. The Guri formation, Turonian, Cenomanian, Albian, Aptian, Barremian, Hauterivian, and Valanginian formations are drilled from top to bottom.

A narrow NE-SW anticline with two structural highs is the Kashkari field. The northwest limb is mild, whereas the southeast limb is steep. The current underground contour (UGC) maps have been generated using drilling data instead of seismic exploration, hence the accuracy of structural features in regions with less numbers of wells is not high.

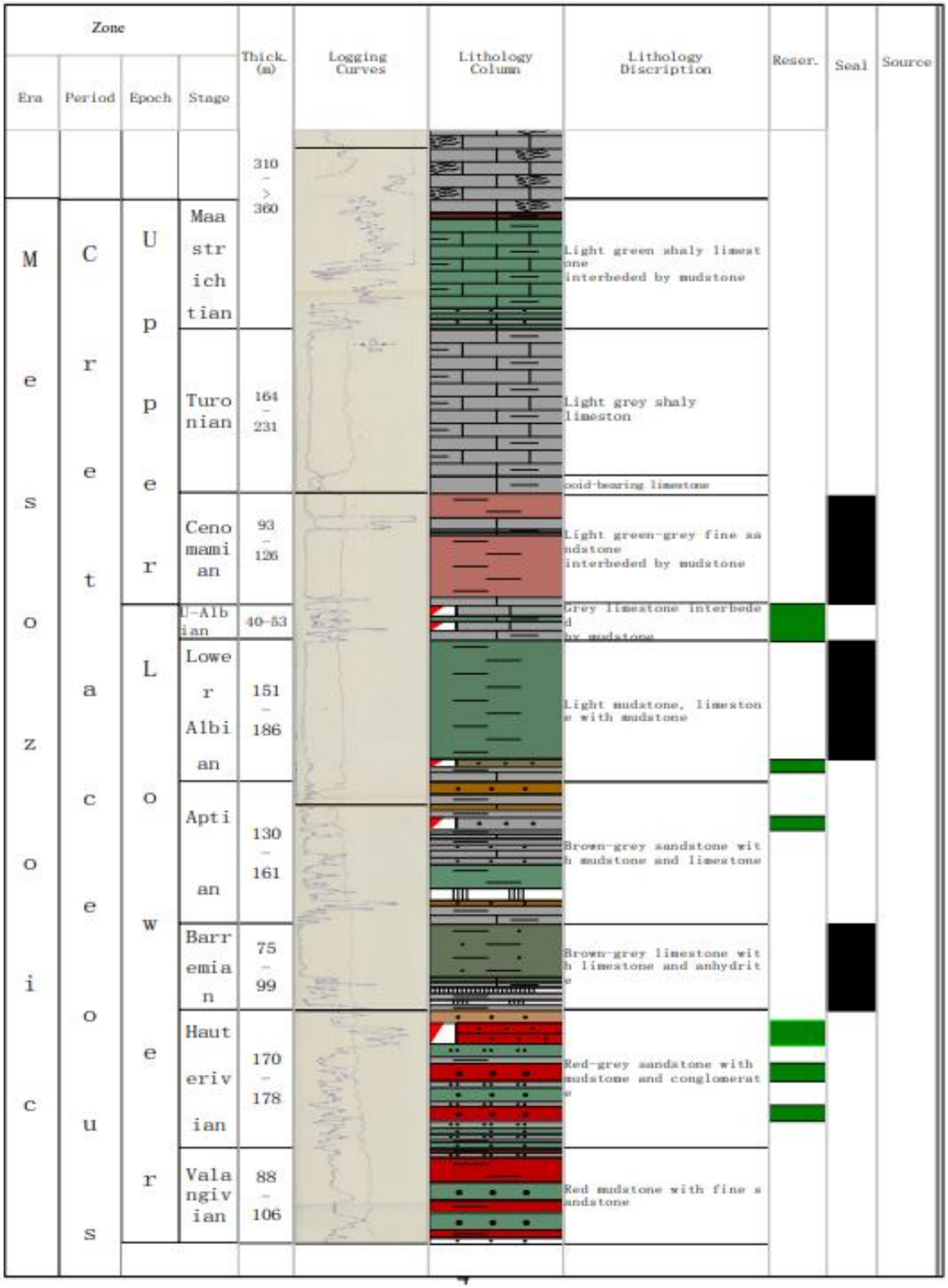

Figure 2.7: Lithostratigraphic chart of Kashkari oil field.

2.6.2 Properties of Fluid in Kashkari Oil Field

The crude oil from the Kashkari oil field has medium quality, it is a black color crude oil with minor quantities of sulfur and wax. The field includes dissolved gas, which consists mainly of CO_2 with a heavy hydrocarbon content of 26%, nitrogen having a content of 2.14%, and H_2S having a content of 0.00028%. The reservoir is an anticline-controlled edge water layered oil reservoir with four vertical reservoirs each of which have their own independent oil and water systems [74].

2.7 Enhanced Oil Recovery

Primary recovery depends on the pressure that built up naturally inside the oil reservoir to push oil to the surface. 85% to 95% of the oil is frequently left behind after primary recovery. When natural pressure is insufficient to force oil to the surface, secondary oil recovery introduces external energy into the oil reservoir. It accomplishes this by flooding the reservoir with water or by pushing compressed gases there. The properties of the oil reservoir itself have a limit on the success of secondary oil recovery, and it can quickly lose effectiveness. 50% to 80% of the oil is not recovered during secondary oil recovery.

The remaining oil that was not possible to recover using conventional methods is recovered through Enhanced Oil Recovery (EOR) method. Oil's value rises along with global demand, in the long run, renewable energy sources must take the place of fossil fuels. But for the time being, EOR is the only practical way to recover up to 80% of the world's oil reserves [75].

2.7.1 Model of Kashkari Oil Field

A simulation model for EOR studies has been designed to get the production from Kashkari oil field. The model is designed by following all the given geological description of the oil field to get the better and reality-based simulation results which can be applied to recover the leftover oil reserves from the already drilled wells.

This simulation model is designed for the LSWF recovery. The salinity-dependent oil/water relative permeability functions resulting from wettability change are used in the model to simulate LSWF.

A promising new method to EOR in both sandstone and carbonate reservoirs is LSWF. Over the past ten years, the oil sector has become interested in LSWF because of its potential. In addition to the few successful field applications of LSWF, numerous

investigations in this area have been carried out recently. Injecting low-salinity brine oil reservoirs, which is depleted in divalent cations compared to in-situ brine, is the recovery process for this method. By applying this approach, significant results can be obtained as compared to brine waterflooding [76].

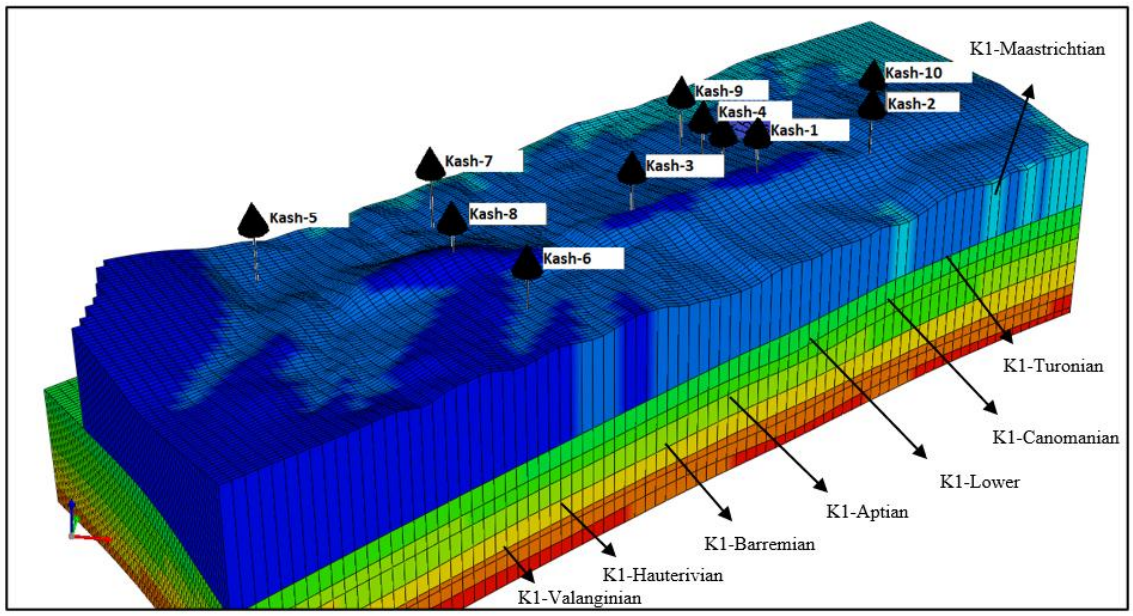

Figure 2.8: EOR model of Kashkari Oil Field, Afghanistan.

The Kashkari oil field was subjected to the intended LSWF from the core flooding experimental section and its simulation in CMG-GEM. To produce oil, five wells (Kash-1, Kash-3, Kash-4, Kash-9, and Kash-10) were in use. The remaining six wells (Kash-2, Kash-5, Kash-6, Kash-7, Kash-8, and Kash-21) either were not activated yet or fails to fulfil the conditions necessary for an oil reservoir. The Kashkari oil field is an anticline-structured, double-high layered-edge-water oil reservoir. Albian Group XIa, Aptian Groups XIIa and XIIb, and Hauterivian Group XIV are the pay zones. Mostly continental unsolid sandstone comprises most of the lithology. The narrow interbeds that make up the oil layers are distinctive. Sandstone reservoirs XIV and XIIa have good physical characteristics and range in permeability from medium to high.

For an EOR model of Kashkari oil field, a model of eight layers is designed because these layers have all the targeted wells (Figure 2.8 and Table 2.1). The well and their corresponding reserves are tabulated below for better understanding of the model and reserves.

Table 2.1: Wells incorporated in model and their corresponding reserves.

Wells	Reserves	Stratum	Layers
Kash-1	XIIa, XIIb, XIV	K1_Br, K1_H	6, 7
Kash-3, Kash-9, & Kash-10	XI, XIIa, XIIb, XIV	K1_Al_1, K1_A, K1_Br, K1_H	4, 5, 6, 7
Kash-4	XI, XIIa	K1_Al_1, K1_A, K1_Br	4, 5, 6

2.8 Summary

Kashkari oil field is located in the Amu Darya Basin of northern Afghanistan. The Amu Darya Basin is the only sedimentary basin of Afghanistan which has sufficient petroleum potential and has been explored to produce oil and gas. The petroleum system of the basin consists of on the rocks of age ranging from the Jurassic-Cretaceous. The Kashkari oil field was discovered with the drilling of the first well in 1976. Total 10 wells have been drilled in Kashkari oil field. As we know that, with growing population, the demand for oil is increasing day by day and the conventional oil reserves are depleting. We also know that during the primary production almost 80% of the oil left behind in the well so there is a need to recover those left oil. EOR is an emerging method to recover the oil from the well to meet the needs of a growing population. There are several methods which can be adopted for enhanced oil recovery, but this project explains the LSWF technique for oil recovery. This technique is beneficial for sandstone reservoirs which have a significant quantity of clays. The lab testing shown, this method derives the improvement of the residual oil recovery from Kashkari field. Wells Kash-1, Kash-3, Kash-4, Kash-9 and Kash-10 are used for EOR experiment and the results are positive showing the increase in the flow towards the surface. The model will help in enhanced oil recovery targeted wells.

Chapter Three

3 Experimental Studies of Low-Salinity Water Flooding

The concept of enhancing oil recovery (EOR) through the use of low or reduced salinity water was first reported by Bernard in 1967 [12]. This marked a shift in thinking about extraction techniques and marked the beginning of an ongoing area of study within the field. Some years later, in 2004, Webb broke new ground by being the first to document results from a single-well test, providing conclusive field evidence that residual oil levels could indeed be effectively reduced through the application of low-salinity water, as outlined in Webb et al. 2004 [39].

This sparked renewed interest in LSWF which matured notably around the mid-nineties. This was largely driven by numerous influential publications originating from Dr. Morrow's research group at the University of Wyoming. These works were predominantly rooted in laboratory core flood experiments.

Despite this surge in attention, it is interesting to note that the level of interest in LSWF remained relatively steady but modest up until around the year 2005. However, the five-year period from 2005 to 2010 witnessed a remarkable intensification in the focus on low-salinity research. A steep increase, indeed practically exponential in nature, was observed in the publication of papers related to low-salinity. As Morrow and Buckley reported in 2011, a grand total of 25 such papers were published in 2010 alone.

However, despite this growing academic and industrial interest in LSWF, a definitive and consistent explanation for the mechanistic operation behind the process had not been agreed upon, as per the findings of Morrow and Buckley in 2011[45]. A similar situation could be observed even half a decade later in 2016. This difficulty in reaching a consensus could, in part, be attributed to variations in test procedures, particularly concerning different types of rocks and crude oils.

The issue of great complexity concerning the minerals, crude oils, and aqueous-phase compositions that are involved and the interactions among this multitude of variables may also contribute significantly to the lack of universally accepted mechanisms for the low-salinity effect. This indicates a vast range of varying conditions and circumstances under which the LSWF may prove either successful or unsuccessful.

Such wide-ranging results hint at the possibility that more than one mechanism may be operative in the process of LSWF.

Out of a total of 64 articles published from 1967 to 2015, 53 focused on the impact of water chemistry and 34 emphasized wettability in the process of LSWF. Other cases such as the importance of clay, initial water saturation (Sw_i), and temperature were emphasized 29 times, 14 times, and 8 times respectively. Other parameters such as porosity, permeability, oil type, and viscosity have also been examined a few times.

The technique of LSWF has been the subject of extensive research, with numerous authors documenting its positive effects on oil recovery. Despite the considerable amount of research conducted, there's still no unanimous agreement regarding the primary mechanisms that control this advanced recovery method. There's a growing consensus in the industry that certain conditions must exist for the benefits of low-salinity injection to be observed, yet no single mechanism has been universally recognized as applicable across all situations.

The majority of the literature that has been analyzed points to an increase in oil recovery due to LSWF, as exhibited in laboratory core flooding experiments. Moreover, the beneficial effects of LSWF have also been realized in practical field applications, underscoring its potential value as a viable oil recovery method.

An illustrative study on this topic was conducted by Dang et al. in 2013 [77]. In their extensive review, they researched into the mechanism behind LSWF over the last two decades, attempting to shed light on the scientific foundations of this method. Further to the theoretical analysis, they also conducted a comparative evaluation of laboratory and field studies, an important step in aligning theoretical understanding with practical outcomes.

The investigation into the mechanisms of LSWF is an ongoing process and the evolution of understanding continues in this critical area of enhanced oil recovery. Despite the lack of a universally accepted mechanism, the tangible benefits of the technique - as documented in both laboratory and field studies - advocate its ongoing use and exploration within the oil industry.

This research aims to provide a comprehensive understanding of the impact of LSWF on the Kashkari oil field by core flooding test with the different salinity percentages. Traditional waterflooding techniques, which are the oldest and most frequently used methods to EOR beyond what can be achieved through simple reservoir depletion, are widely recognized within the field. However, LSWF represents a more

recent advancement in EOR techniques. In this innovative approach, the salinity of the injection water is deliberately reduced to further enhance the extraction of oil. While this method might be newer when compared to its conventional counterparts, it has been steadily gaining traction in contemporary oil recovery discourse.

3.1 Field Information

As explained in details about the geological properties of Kashkari oil field in the second chapter of this research, we know that the main lithology of this field is light grey sandstone and siltstone. The sandstone is mainly quartz and silicate; the content of the cement material is 15%–20%, mainly calcspar, and dolomite, including a small quantity of anhydrite and kaolinite. According to the core analysis data of the 8 wells and considering the logging interpretation results, all Kashkari reservoirs are located in four formations. The XIa and XIIb groups belonged to a medium porosity and medium-low permeability reservoir; XIIa and XIV's groups belonged to a medium porosity and medium-high permeability medium-level reservoir, with the porosity and permeability calculated to be 19.15% and 43.75 mD respectively.

According to the temperature statistics of 7 wells and 19 test points in the Kashkari oil field, the temperature gradient of the oil reservoir is confirmed as 2.82 °C/100m. The original stratum pressure of XIa is 12314 kPa, and XIIa, XIV, and XIIb wells are 12824 kPa, 12755 kPa, and 16188 kPa, respectively. The average pressure and temperature of the Kashkari oil field are 13520 kPa and 61.1°C respectively.

Table 3.1: Kashkari oil field FW salinity and ion contents.

Formations	Reservoir	Wells	Type	(g/L)
Albian	Xia	Kash-5, Kash-7	Na_2SO_4	33–39
Aptian	XIIa, XIIb	Kash-1, Kash-2, Kash-6, Kash-7	Na_2SO_4	26–35
Hauterivian	XIV	Kash-2, Kash-3, Kashk-5	$NaHCO_3$	11–16

Ion Contents (mg/L)					
Cl^-	SO_4^{2-}	HCO^{3-}	Ca^{2+}	Mg^{2+}	$K + \& Na^+$
12456.3	4172.8	2091.6	402.5	75.5	10321.3

Samples of FW data from 6 wells show that FW in the XIV strata of the Kashkari oil field is of the $NaHCO_3$ type mineralization of 11–16 g/L, while FW in stratum XI and XII is the Na_2SO_4 type mineralization increased from the bottom to the top gradually. The

FW salinity was derived from the tests conducted by USSR research group in 1980 and described at the Production Report of the Kashkari Oil Field, the details are summarized in Table 3.1. Due to discrepancies, in the stated salinities used in previous studies, the final salinity values used in this analysis were back-calculated as equivalent NaCl, from the concentration of total solids detailed in the work of the Russians. This represents the most reliable summary of the FW properties, as it is derived directly from samples acquired when testing the various reservoirs [78].

Table 3.2: Pressure and viscosity of Kashkari oil field's crude oil under normal temperature.

Zone	Pressure (kPa)	Viscosity (cp)
XIa	6398.0	2.1
XIIa	4212.9	2.19
XIIb	4398.0	3.4
XIV	2978.1	7.6

The crude oil, containing sulfur and wax and with a density of 0.81-0.87g/cm^3 and viscosity of 2.64-5.38cp, is a black oil reservoir under normal temperature and pressure (Table 3.2) [49, 51].

3.2 Core Flooding Laboratory Test

In the scope of this particular study, we selected a cylindrical core sample from the San Saba region for our LSWF experiments. The chosen sample was especially suitable due to a combination of factors such as its geological composition, its accessibility, as well as its compatibility with the requirements of our intended line of investigation.

The various physical properties of the selected core sample were meticulously measured in the lab, the details of which are elaborated in Table 3.3. These properties include factors such as porosity, permeability, bulk volume, and others, all of which play a crucial role in oil recovery processes like LSWF.

The laboratory-based core flood test involved several stages of preparation before the actual LSWF procedure was executed. The core preparation procedure primarily involved making sure that the core sample was adequately saturated. We initiated the process by saturating the core sample with FW. This was a crucial preparatory step, as it ensured that the core sample replicated the initial real-life conditions found in oil reservoirs.

Subsequent to the saturation with FW, we proceeded to saturate the core sample with crude oil. This step was integral and served to replicate the oil-impregnated conditions of a typical oil reservoir environment within the sample. The crude oil used for this purpose was carefully chosen, duly considering its consistency with sourced oil in real oil fields.

One essential factor in our core flood test was the aging process. The plan was for the aging period to span three weeks in a 60°C. This duration was selected based on a combination of practicality and the need to mimic reservoir conditions as closely as possible in the controlled setting of a lab.

With the core prepared meticulously as described, we proceeded to execute the core flood test. The intricacies and finer details of the entire process, both in terms of the core preparation procedure and the actual test process, are explained step-by-step in the following sections. This careful procedural approach ensured the reliability of our research and findings, contributing to a more comprehensive understanding of LSWF and its applications.

The core sample was initially filled with FW with a salinity of 3% at a rate of 0.2 ml/min until the core was fully saturated. Subsequently, oil injection was carried out at the same flow rate until the entire San Saba core was saturated. The core was then aged for three weeks at the reservoir temperature (60°C) to restore its wettability. After aging, the core was subjected to FW flooding at a rate of 0.2 ml/min until it reached residual oil saturation (Sor). Different brine solutions with varying salinity levels (step-1, step-2, and step-3) were then injected to observe the impact of low-salinity water on oil recovery. This process of LSWF is further detailed in Figure 3.1.

Figure 3.2 provides a visual representation of the core flood test apparatus used in this experiment, specifically, the SRP-350 model. This version comes equipped with accumulators of oil, FW, and LSW, which are crucial components for the test.

The materials utilized in the experiment, namely the San Saba core sample and the crude oil, are depicted in Figure 3.3. These were specifically selected to be representative of typical elements in an oil recovery operation. The crude oil used here had a viscosity of 7.7 cP at 20°C and dropped to 3.5 cP at 60°C. These properties closely align with the characteristics of the crude oil obtained from the Kashkari oil field, reinforcing the relevance of the test results.

Table 3.3: Core sample physical properties.

Core ID	Sandstone
Core type	San Saba sandstone
Core Diameter (mm)	25.14
Core Length (mm)	50.63
Core Weight (g)	52.13
Gas permeability (mD)	63.68
Pore volume (cc)	5.44
Bulk volume (cc)	25.13
Porosity (%)	21.6
Water permeability (mD)	25

Table 3.4: FW and LSW ion contents.

Ion Contents (PPM)	Cl^-	SO_4^{2-}	HCO^{3-}	Ca^{2+}	Mg^{2+}	Na^+	Total
FW (3%)	12488	4172	2091	402	75	10278	29506
LSW (1%)	4162	1390	697	134	25	3426	9834
LSW (0.5%)	2081	695	348	67	12	1713	4916
LSW (0.1%)	416	139	69	13	2	343	982

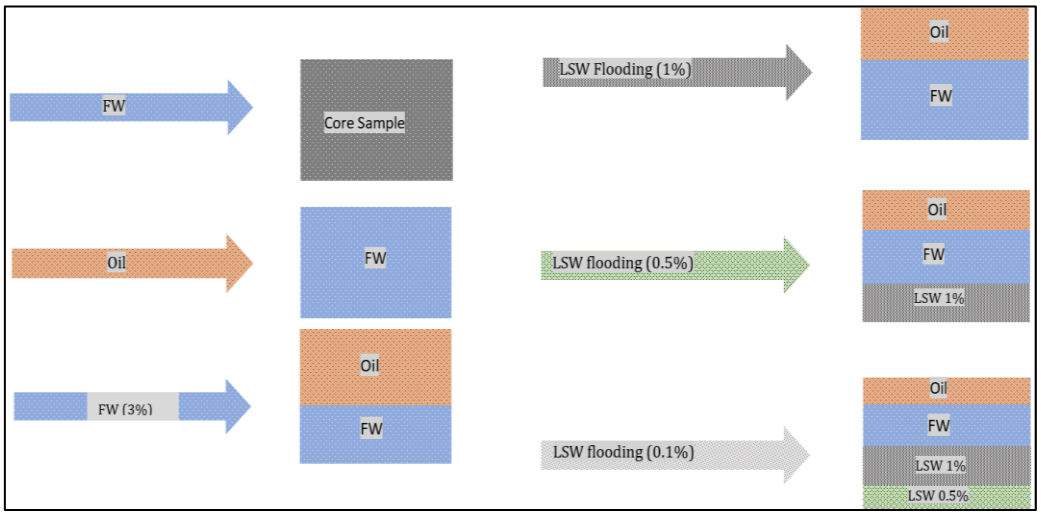

Figure 3.1: Core preparation and four steps LSWF process.

The core test incorporated four sequential stages of salinity water injection. These steps are explicitly detailed in Table 3.4. Each stage represented varying salinity levels, providing a comprehensive analysis of how changes in salinity impacted oil recovery, particularly under conditions similar to those within the Kashkari oil field. This structured and detailed testing methodology facilitated not only an understanding of

the LSWF process but also provided data to optimize oil recovery in real-world scenarios.

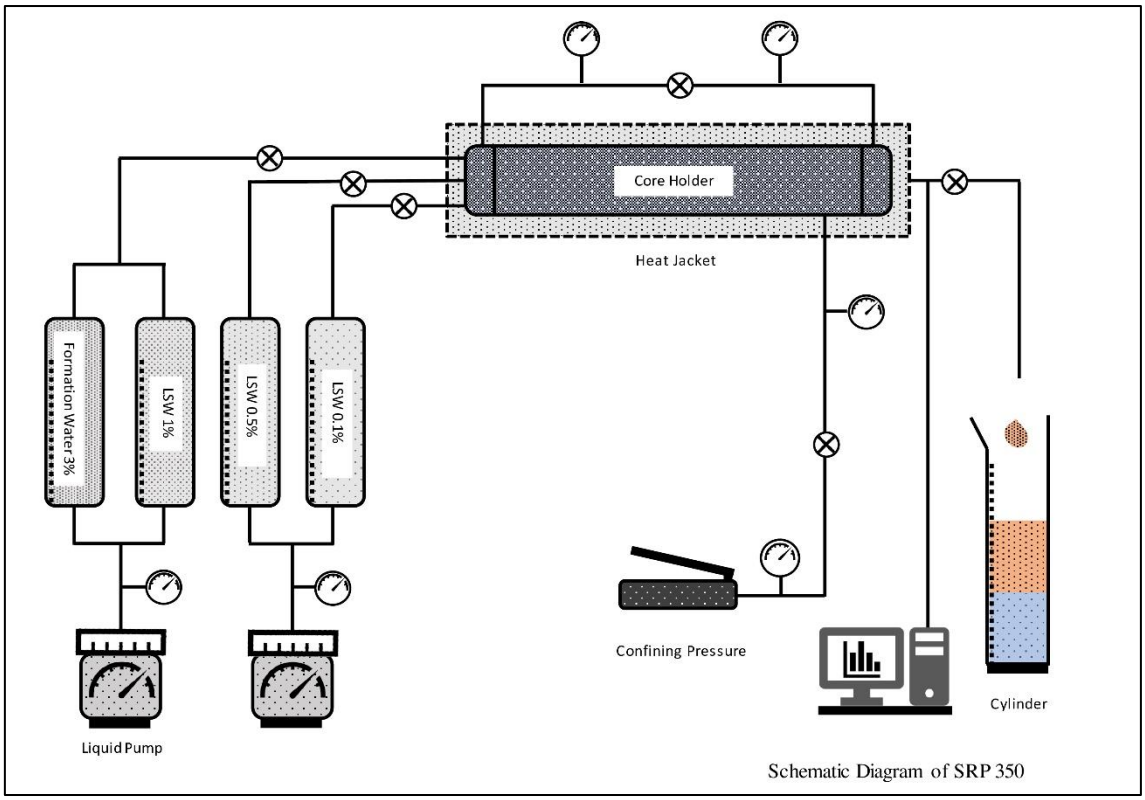

Figure 3.2: Apparatus used for the core flooding test (SRP-350).

Figure 3.3: Crude oil and core samples.

3.3 Experiment Result

The LSWF core test was performed under specific conditions that mirrored the actual conditions in the Kashkari oil field. The core test was implemented at a temperature of 60°C, which corresponds to the temperature within the Kashkari oil field. Additionally, the test was conducted under a confining pressure of 20684 kPa and a steady flow rate of 0.2 ml/min.

The process of oil recovery utilizing LSWF is graphically represented in Figure 3.4. This figure is based on the results obtained from the four-step core flooding laboratory test, which evaluates the impact of different salinity levels on oil recovery outcomes.

In the initial phase of the test, FW with a salinity level of 3% was introduced into the core. This resulted in a swift and substantial increase in oil recovery, as can be observed from Figure 3.4. By this stage, the oil recovery rate had already reached an impressive 44%.

The subsequent second step involved LSWF at a reduced salinity level of 1%. This step resulted in a further enhancement of oil recovery. More precisely, the graph displayed an additional 4% increase in oil recovery during this phase, demonstrating the direct impact of reduced salinity water flooding on oil extraction.

In the third step of the process, the salinity was further reduced to 0.5%. This stage saw a relatively smaller but still significant increase of 1% in oil recovery. This continued the trend of incremental oil recovery corresponding to reduced salinity levels.

In the final step, LSW with a salinity content of just 0.1% was introduced into the core. This stage witnessed yet another increase in oil recovery — this time by 1.7%.

As a result, upon completion of the four-stage LSWF laboratory test, the overall oil recovery registered at an impressive 51%. This comprehensive experiment provides invaluable insights into the efficacy of varying salinity levels on oil recovery rates in a controlled laboratory setting. It also further supports the increasing interest and research into the application of LSWF as a method for enhanced oil extraction.

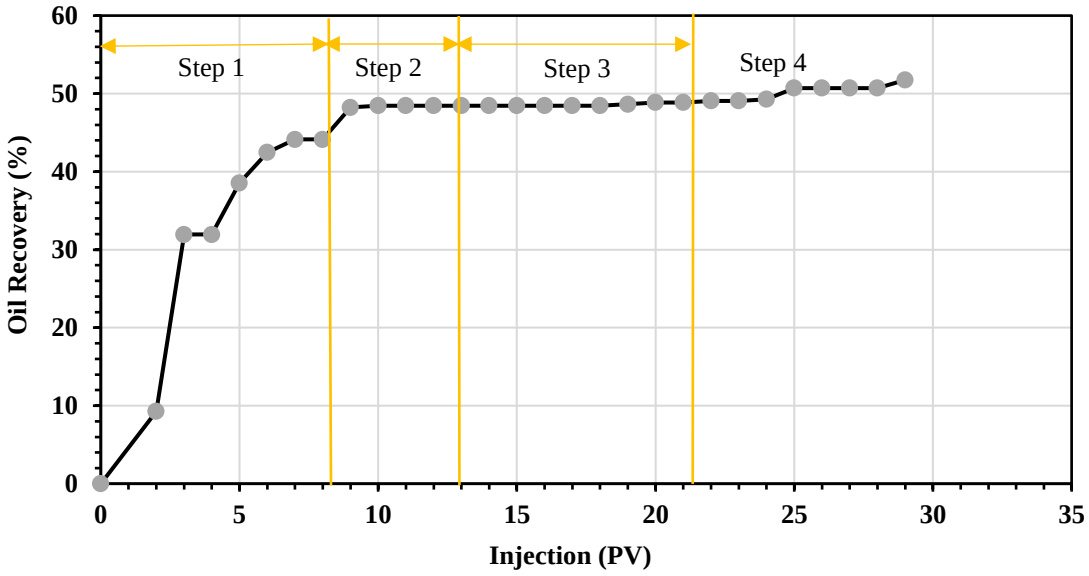

Figure 3.4: LSWF laboratory test results with four steps, step-1 with the salinity of 3wt%, 1wt%, 0.5wt%, and 0.1wt% is the salinity of steps 2, 3, and 4 respectively.

3.4 Discussion

LSWF technology continues to gather significant interest from the industry, primarily due to its simplicity and cost-effective nature. The operational and financial benefits of LSWF extend beyond mere affordability; its easy application and high accessibility also contribute to making it a desirable option. Additionally, LSWF requires notably lower capital investment compared to some other extraction techniques, making it a particularly appealing choice from an economic standpoint.

Decades worth of research have concluded that injecting brine with a salinity of 1000-2000 ppm can significantly improve interactions between crude oil, brine, and rock (COBR). Furthermore, these interactions have been observed to lower remaining oil saturation, thereby enhancing oil recovery.

However, despite the markedly increasing interest towards LSWF, a universally recognized mechanistic explanation underlying its functionality still remains elusive. This can be attributed to the complexity and multitude of parameters involved in COBR interactions, which create a level of uncertainty around the mechanisms that induce LSW.

Complicating the matter further is the fact that the efficacy of LSWF varies greatly depending on the specific conditions. Such a broad spectrum of outcomes implies the simultaneous operation of more than one mechanism within the process of LSWF.

Clay minerals, which make up a large portion of sedimentary rocks, carry a negative surface charge. This trait induces positively charged ions, such as Ca^{2+}, Mg^{2+}, Na^{+}, or K^{+}, to adhere to it. Particularly, divalent cations such as Ca^{2+} and Mg^{2+} are found in abundance in FW. These cations play an instrumental role in promoting the adsorption of oil onto rock surfaces, thereby rendering the rock oil-wet and causing a significant amount of the oil to remain trapped within the reservoir.

Interestingly, upon injection of LSW, the clay minerals, due to their unique ion exchange capabilities, will replace the divalent cations with monovalent ones (as demonstrated in Figure 3.5 (a)). The divalent cations, along with the desorbed oil, are subsequently removed from the rock surfaces (Figure 3.5 (b)). Since monovalent ions only have one active site, their adsorption onto the clay surfaces doesn't lead to any further oil absorption, hence creating a water-wet conditions and aiding in oil recovery (Figure 3.5 (c)). This intricate process, monitored and documented at a microscopic level, provides valuable insights into LSWF's oil recovery capabilities.

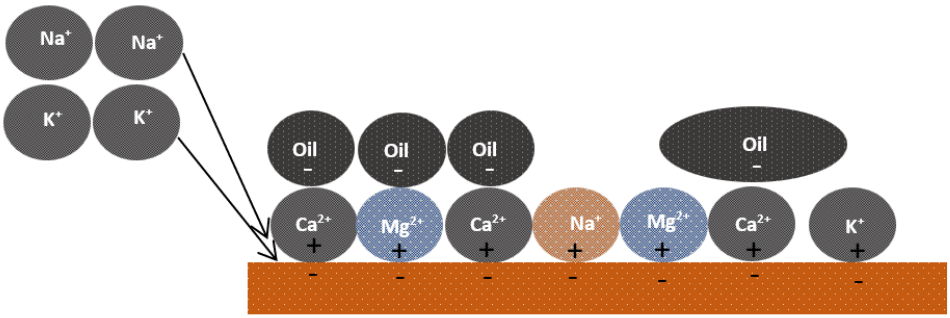

(a)

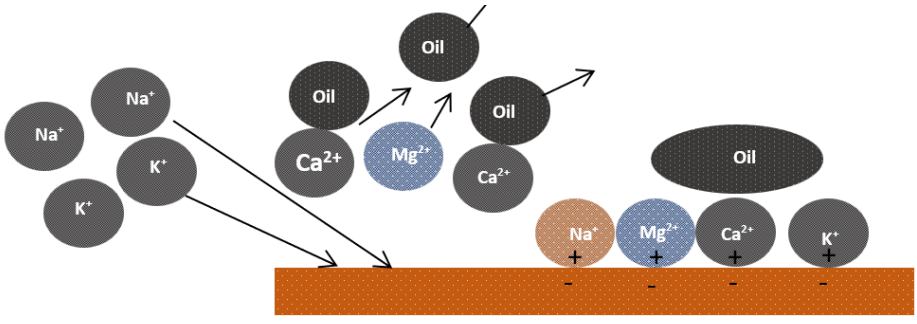

(b)

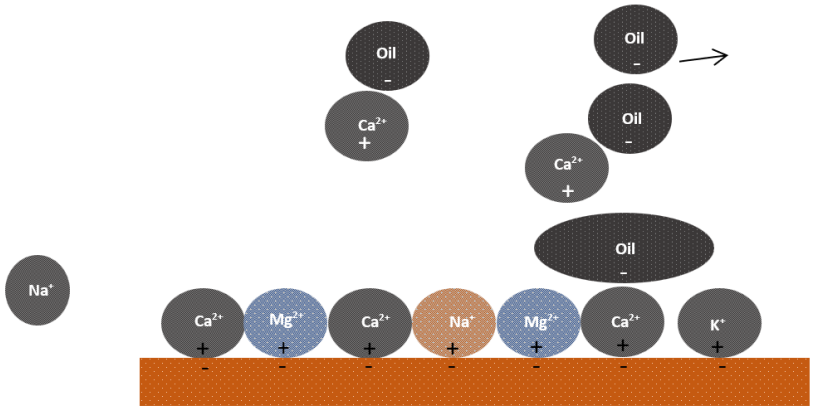

(c)

Figure 3.5: Ion exchange mechanism process, (a) LSW injection; (b) monovalent cations take the role of divalent cations; (c) Monovalent cations do not adsorb any additional oil.

This experimental study into LSWF examines a COBR system wherein the FW is primarily comprised of divalent cations prior to the introduction of LSW. The presence of these divalent ions leads to the formation of a thin water film between the rock surface and the crude oil.

This water film carries a positive charge and, as a result, it more strongly attracts the negatively charged acidic components found in crude oil compared to its positively charged basic components. This interaction forms an essential element of the LSWF process and plays a significant role in the recovery of oil.

Assuming the operation of the multiple-component ion exchange (MIE) mechanism in this context, the process of replacing divalent cations like Ca^{2+} and Mg^{2+} from rock surfaces follows a specific sequence — starting from potassium (K), progressing to sodium (Na), calcium (Ca), and finally to magnesium (Mg). Essentially, this mechanism suggests that a LSW solution composed of KCl at the optimal concentration will be more effective at displacing Mg^{2+} or Ca^{2+} cations than Na^{+}, Ca^{2+} and Mg^{2+} would be.

This phenomenon could likely be explained on the basis of the reactivity series (RS), a vital guiding principle that ranks elements based on their reactivity. According to the RS, K is the most reactive of the elements under consideration, thus it has a stronger tendency to interact with and bind to clay surfaces. Sodium (Na) is the next most reactive ion, followed by calcium (Ca^{2+}), and finally magnesium (Mg^{2+}). This gradient of reactivity plays a critical role in determining the efficiency of ion exchange and,

consequently, the effectiveness of LSWF for oil recovery. This study, thus, provides essential insights to further optimize LSWF practices and achieve greater oil recovery rates.

3.5 Summary

The findings of the experimental trials carried out in this study corroborate these existing research conclusions and validate the efficacy of the LSWF method. One of the key conclusions drawn from these laboratory core flooding tests is that implementing LSWF with precise salinity levels —specifically, 1%, 0.5%, and 0.1% — has the potential to significantly increase oil recovery. In fact, this method yielded an impressive maximum oil recovery increase of up to 7% following the initial FW injection.

Each experimental phase of these trials, characterized by varying salinity percentages, was treated as an independent step. Each of these steps had a distinct effect on oil recovery, contributing to the overarching results. Some stages of the experiment yielded less impactful outcomes compared to others. However, the overall increase in recovery could be attributed to the efficacy of all the steps combined.

One particular result worth noting is the relatively significant gain in oil recovery observed following the FW injection stage. The LSWF injection phase at a salinity level of 1% demonstrated a considerably high oil recovery increase of 4% in comparison to the subsequent two steps that utilized lower salinity levels.

In conclusion, the results of these laboratory core flooding tests add credence to the claim that LSWF represents a highly efficient strategy for EOR. It is particularly effective in reservoir environments such as the Kashkari oil field, which boasts significant clay content. However, as each stage of injection, characterized by different salinity levels, yielded varying results, it also highlighted the need for careful consideration of these levels in the practical application of LSWF as part of an optimized strategy for EOR.

Chapter Four

4 Numerical Simulation of LSWF to Kashkari Oil Field

4.1 Introduction

Reservoir modeling is a valuable tool for the verification and validation of experimental results and predictions of conditions beyond the scope of the experimental work [79]. Jerauld presented one of the first models on LSWF, which considered salt as an additional component lumped in the aqueous phase. Relative permeability, capillary pressure, aqueous phase density, and viscosity were all modeled as functions of salinity. S_{orw} was assumed to be linearly dependent on salinity. Although the same scaling factor proposed by Jerauld et al. [29] is currently used in most LSWF models, the need to use scaling parameters for handling relative permeability and capillary pressure of oil and water separation has been highlighted by Al-Shalabi et al. [80].

Dang et al. [46, 81] developed a comprehensive ion exchange model that captures the geochemical reactions that occur during LSWF. The model was coupled with the compositional simulator GEM from CMG and was validated with the ion exchange model PHREEQC (Mathematical software) and two core flood experiments, for a North Sea reservoir and a heterogeneous Texas sandstone reservoir core. The geochemistry model was used to evaluate LSWF optimization through well placed, and the authors investigated the potential of a hybrid enhanced oil recovery process that involved combining LSWF and CO_2 injection in a miscible water-alternating-gas (WAG) process.

A geochemical model that uses the equivalent fraction of divalent cations (Ca^{2+} and Mg^{2+}) was proposed by Awolayo and Sarma [82]. The model was used to history match several carbonate core-flood experiments. Based on the simulation results, they concluded that the interplay between surface charge alteration and mineral dissolution was the key to improved oil recovery at the core scale.

The CMG-GEM 2021.10 reservoir simulators were used in this research for modeling the LSWF of the San Saba sandstone core. The GEM simulator packages in CMG are widely employed as compositional tools in the petroleum industry, with the capacity to develop reservoir models. A cartesian grid system with specified divisions along X-axis

and the development model was simulated to match the LSWF laboratory test [83, 84]. Porosity, permeability, and crude oil properties were introduced as input data for reservoir characterization.

4.1.1 Special Core Analysis

The special Core analysis mainly consists of relative permeability, capillary pressure (Pc), rock wettability, and formation rock compressibility (C_f) measurements. The relative permeability and Pc depend on both the reservoir rock and reservoir pore fluids. The formation of rock compressibility depends on the rock type and porosity. To study fluid flow in reservoir pores, relative permeability analysis in the drainage and imbibition states is required. To apply the endpoint of the relative permeability curve, the residual water, and oil saturation were obtained from the core analysis results.

Usually, the Pc curve is obtained from both petrophysical logs and core analysis results and then compared with the other. In the absence of reservoir measured relative permeability and Pc curves, measured data of neighboring reservoirs that have similar rock properties are taken, otherwise, correlation data and empirical relations are used. The three main criteria for selecting representative relative permeability and Pc measurements are rock type, $\sqrt{\frac{K}{\emptyset}}$ and wettability. In the Kashkari oil field, there is not any scale test at all, so according to the client′s viewpoint, empirical correlations have been used for determining relative permeability and capillary pressure curves from reliable references.

Corey combined predictions of a tube-bundle model with his empirical expression for capillary pressure to obtain expressions for gas and oil relative permeability. Brooks and Corey extended Corey's results for capillary pressure to obtain the following expressions for oil and gas relative permeability.

The following "power-law" relationships are often used to describe oil, water, and gas relative permeabilities, respectively:

$$K_{ro} = K_{ro,max}\left(\frac{S_o - S_{or}}{1 - S_{or} - S_{wc} - S_{gc}}\right)^{n_o} \tag{4.1}$$

$$K_{rw} = K_{rw,max}\left(\frac{S_w - S_{wr}}{1 - S_{or} - S_{wc} - S_{gc}}\right)^{n_w} \tag{4.2}$$

$$K_{rg} = K_{rg,max}\left(\frac{S_g - S_{gr}}{1 - S_{or} - S_{wc} - S_{gc}}\right)^{n_g} \tag{4.3}$$

The exponents n_o, n_w, and n_g range from 1 to 6. The maximum relative permeability, $k_{ro\ max}$, $k_{rw\ max}$, and $k_{rg\ max}$ are between 0 and 1. These expressions are often referred to as modified Brooks-Corey relations, reflecting their similarity to the Brooks-Corey expression for oil and water relative permeability. Figures 4.1 and 4.2 demonstrate the relative permeability and capillary pressure data calculated from Eqs. 4.1-4.3 used in the simulation model, respectively.

4.1.2 Governing Equations

During LSWF, the initial thermodynamic equilibrium of a system is disrupted through geochemical reactions that occur at the rock or brine interface [85-87]. The geochemical reactions can be divided into homogeneous and heterogeneous reactions. Homogeneous reactions occur among the aqueous phase components and are known as intra-aqueous reactions whereas heterogeneous reactions occur between the aqueous components and mineral species, such as mineral dissolution/precipitation and ion exchange reactions [84]. The two types of reactions are typically represented as chemical equilibrium and rate-dependent reactions, respectively because intra-aqueous reactions are faster than mineral dissolution or precipitation reactions.

Fluid flow in the reservoir or any porous medium is governed by Darcy's law. The diffusion and dispersion of components in the aqueous phase also contribute to the movement of the aqueous phase components [84]. The three different species involved in the geochemical reactions during LSWF include hydrocarbon components (n_h) that may be soluble in the aqueous phase, aqueous phase components (n_a), and mineral components (n_m).

4.1.3 Intra-Aqueous Reactions

According to Bethke, [88] equilibrium constants are used in modeling chemical equilibrium reactions. For a chemical reaction to be in thermodynamic equilibrium, the rate of the forward and backward reactions must be equal; implying that the activity product of the reaction must be equal to its equilibrium constant. This concept creates the governing equations for chemical equilibrium reactions.

$$Q_\alpha - K_{eq,a} = 0,\ \ a = 1, \dots, R_{aq} \tag{4.4}$$

$$Q_\alpha = \prod_{i=1}^{n_{aq}} a_i^{via} \tag{4.5}$$

Where $K_{eq,\alpha}$ is the equilibrium constant for the aqueous reaction α, R_{aq} is the number of aqueous phase reactions, Q_α is the activity product, and a_i and $v_{i\alpha}$ are the activity of component k and the stoichiometry coefficients, respectively. The aqueous phase components consist of both components that only exist in the aqueous phase (n_a components) and gaseous components soluble in the aqueous phase, n_c. The total number of components in the aqueous phase, n_{aq}, is the sum of the two. Aqueous species can also be divided into independent (primary) and dependent (secondary) aqueous species.

Tables of values of the equilibrium constants for many reactions as a function of temperature can be found in the works by Delaney and Lundeen [89] and Kharaka et al. [90]. The relationship between the activities of a species i, a_i and its molality, m_i, is given in Eq. 4.6 The molality of a species is its moles per kilogram (mol/kg) of water and is expressed in units molal (M).

$$a_i = \gamma_i m_i, \qquad i = 1, \dots, n_{aq} \tag{4.6}$$

γ_i in the above equation is the activity coefficient. The activity of an ideal solution is equal to its molality because $\gamma_i = 1$. However, most solutions are non-ideal and a value other than one is required for γ_i. Many models exist for calculating the activity coefficients of electrolytic solutions, such as the Debye-Hückel equation, the Davies equation, and the B-Dot model [88]. An activity coefficient model describes the relationship between a species' activity coefficient and the ionic strength (I) of the solution. The Davies and B-Dot models are variants of the Debye-Hückel equation developed by Debye and Hückel in 1923 [88]. In STARS™, computations of the ionic activity coefficients are done using the B-Dot model. The model is widely applied in many geochemical models because it can accurately predict the activity coefficients of species over various temperatures (0–300°C) and molality (up to 3M ionic strength of a solution NaCl as the dominant solute), compared to the other models. The expressions for the B-Dot equation and ionic strength are given in Eqs. 4.7 and 4.8.

$$log\gamma_i = -\frac{A_\gamma z_i^2 \sqrt{I}}{1+\dot{a}_i B_\gamma \sqrt{I}} + \dot{B} \tag{4.7}$$

$$I = \frac{1}{2}\sum_{i=1}^{n_{aq}} m_i z_i^2 \tag{4.8}$$

A_γ, B_γ and $\dot{B}$ are temperature-dependent coefficients, $\dot{a}_i$ is the ion size parameter (constant), z_i is the valence number of species i, and m_i is its molality [88].

4.1.4 Mineral Dissolution and Precipitation Reactions

The Reactions involving minerals and aqueous species are slower than aqueous reactions and are modeled using kinetic rate laws [88]. The expression of the rate law for mineral dissolution and precipitation is given in Eq. 4.9.

$$r_\beta = \hat{A}_\beta k_\beta \left(1 - \frac{Q_\beta}{K_{eq.\beta}}\right), \qquad \beta = 1, \dots R_{mn} \tag{4.9}$$

Where r_β is the reaction rate reactive surface area is the reactive surface area for mineral β, and k_β, $K_{eq.\beta}$, and Q_β is the rate constant, equilibrium constant, and activity product for mineral reaction β, respectively. Q_β is similar to the activity product for aqueous chemical equilibrium reactions given in Eq. 4.5.

$$Q_\beta = \prod_{i=1}^{n_{aq}} a_i^{via} \tag{4.10}$$

The activities of the minerals are equal to unity and are therefore not included in the above equation. The ratio $(Q_\beta / K_{eq.\beta})$ in Eq. 4.9 is called the saturation index. Mineral dissolution occurs if $\log (Q_\beta / K_{eq.\beta}) > 0$. If $\log (Q_\beta / K_{eq.\beta}) = 0$, the mineral is in equilibrium with the aqueous phase and no reaction occurs ($r_\beta = 0$). Eq. 4.9 applies to minerals only. The rate of formation/consumption of different aqueous species is obtained by multiplying r_β by the respective stoichiometry coefficient [91].

$$r_{k\beta} = v_{k\beta} \cdot r_\beta \tag{4.11}$$

The reaction rate constant for different reactions is normally reported at a reference temperature, T_o (usually 25°C). The temperature of petroleum reservoirs is typically higher than T_o. To calculate the rate constant at a different temperature T, Eq. 4.12 is used.

$$k_\beta = k_{0\beta} exp\left[-\frac{E_{a\beta}}{R}\left(\frac{1}{T} - \frac{1}{T_0}\right)\right] \tag{4.12}$$

Where $E_{a\beta}$ and $k_{o\beta}$ are the activation energy for the reaction β (J/mol) and the rate constant for reaction β at the reference temperature, T_o, R is the universal gas constant (8.314J/mol-K). Both T and T_o are in Kelvin (K). The activation energy (E_a) needed for the chemical reactions that result in wettability modification during LSWF is critical

because if the reaction rate is slow, no new equilibrium would occur during the LSWF interval and thus no low salinity effects would be observed [92]. The activation energy is related to how strongly the polar oil components are bonded to the mineral surface, the solvency of the polar components in the actual phases, and the reactivity of the ions in the injected water. The bonding energy between polar compounds in oil and carbonates is generally higher than that between the oil and clay in sandstones [92].

The equilibrium constants for aqueous and mineral reactions can alternatively be calculated using a fourth-order polynomial expression as a function of reservoir temperature, T.

$$log(K_{eq}) = a_0 + a_1T + a_2T^2 + a_3T^3 + a_4T^4 \qquad (4.13)$$

The default values of a_o, a_1, a_2, a_3, and a_4 for the different reactions are specified in STARS' internal library, and the reservoir temperature, T, is 60 °C.

As mineral dissolution/precipitation occurs, the surface area available for reactions also changes, and therefore, the reactive surface area is an important parameter when calculating the reaction rate. The change in the reactive surface area as minerals dissolve/precipitate is calculated using Eq. 4.14 [91].

$$\hat{A}_\beta = \hat{A}^0_\beta \cdot \frac{N_\beta}{N^0_\beta} \qquad (4.14)$$

Where $\hat{A}^0_\beta$ and N^0_β are the reactive surface area and the number of moles of a mineral β per unit grid block bulk volume af time o and N_β is the number of moles of a mineral β per unit grid block bulk volume at the current time.

Additionally, both the void volume (porosity) and permeability of the porous medium are altered because of mineral dissolution and precipitation. Eq. 4.15 and 4.16 are the expressions used in calculating the change in porosity.

$$\widehat{\emptyset}^* = \emptyset^* - \sum_{\beta=1}^{n_m}\left(\frac{N_\beta}{\rho_\beta} - \frac{N^0_\beta}{\rho_\beta}\right) \qquad (4.15)$$

$$\emptyset = \widehat{\emptyset}^*[1 + c_\emptyset(P - P^*)] \qquad (4.16)$$

Where $\emptyset$ is the new porosity, $\emptyset^*$ is the reference porosity with no mineral dissolution/precipitation, $\widehat{\emptyset}^*$ is the porosity with dissolution/precipitation, ρ_β is the mineral's molar density, $c_\emptyset$ is the rock compressibility, and p and p^* are the current and reference pressures, respectively.

To calculate the change in permeability, the Kozeny-Carman equation is used.

$$\frac{k}{k^0} = \left(\frac{\emptyset}{\emptyset^0}\right)^3 \cdot \left(\frac{1-\emptyset^0}{1-\emptyset}\right)^2 \tag{4.17}$$

Where k° is the initial permeability and $\emptyset^0$is the initial porosity.

4.1.5 Ion Exchange Reactions

When water with a different ionic composition to the FW is injected, multiple ion exchange and geochemical reactions occur between the ions in the aqueous phase and the rock surface. The exchange reactions are fast and homogeneous and are therefore modeled as chemical equilibrium reactions. The multiple ion exchange and geochemical reactions are key to the increase in oil recovery during LSWF. However, they differ from the reservoir rock type.

In this research, multicomponent ion exchange and the resulting wettability alteration during LSWF are modeled using the exchange of divalent cations; Ca^{2+} and Mg^{2+}. The ion exchange reactions are shown in Tables 4.1 and 5.2. The X in the reactions represents the ion exchanger on the carbonate rock surface. During LSWF, Ca^{2+} and Mg^{2+} are taken up by the exchanger, while Na^+ is released. The reverse process occurs during high-salinity water flooding. Ion exchange reactions are characterized by equilibrium constants, to chemical equilibrium reactions.

$$K_{Na/Ca} = \frac{[a(Ca^{2+})]^{1/2} a(Na-X)}{a(Na^+)[a(Ca-X_2)]^{1/2}} \tag{4.18}$$

$$K_{Na/Mg} = \frac{[a(Mg^{2+})]^{1/2} a(Na-X)}{a(Na^+)[a(Mg-X_2)]^{1/2}} \tag{4.19}$$

Where a is the activity. It is, however, difficult to evaluate the activity coefficients of Na-X, Ca-X_2, and Mg-X_2, and thus, selectivity coefficients are used in place of equilibrium constants according to the Thomas-Gaines convention [93]. Rewriting Eqs. 4.18 and 4.19 in terms of the selectivity coefficient results in the expressions in Eqs. 4.20 and 4.21.

$$K'_{Na/Ca} = \frac{\varsigma(Na-X)[m(Ca^{2+})]^{0.5}}{[\varsigma(Ca-X_2)]^{0.5}m(Na^+)} \cdot \frac{[\gamma(Ca^{2+})]^{0.5}}{\gamma(Na^+)} \quad (4.20)$$

$$K'_{Na/Mg} = \frac{\varsigma(Na-X)[m(Mg^{2+})]^{0.5}}{[\varsigma(Mg-X_2)]^{0.5}m(Na^+)} \cdot \frac{[\gamma(Mg^{2+})]^{0.5}}{\gamma(Na^+)} \quad (4.21)$$

Where ζ (i–X_a) (i = Na^+, Ca^{2+} or Mg^{2+} and a is the valency) is the ion exchange equivalent fraction on the exchanger, m is the molality and γ is the activity coefficient. An important property of the exchanger is its cation exchanger capacity (CEC), which describes the number of ions that can be adsorbed on its surface. The moles of all components in STARS™ are expressed as moles per grid block bulk volume, N. Thus, if V is the bulk volume of the rock, the total moles of the exchangeable species (Na-X, Mg-X_2, and Ca-X_2) would be $VN_{(i-Xa)}$. Eq. 4.21 must therefore be satisfied for a given value of CEC in the grid block. The equivalent fractions of the exchangeable species are calculated by the following:

$$\varsigma(Na-X) = \frac{N_{Na-X}}{\emptyset CEC} \quad (4.22)$$

$$\varsigma(Ca-X_2) = \frac{N_{Ca-X_2}}{\emptyset CEC} \quad (4.23)$$

$$\varsigma(Mg-X_2) = \frac{N_{Mg-X_2}}{\emptyset CEC} \quad (4.24)$$

where $\emptyset CEC = N_{Ca-X_2} + 2N_{Ca-X_2} + 2N_{Mg-X_2}$

Table 4.1 shows the various species used in the simulations presented in this thesis. All the intra-aqueous, mineral, and ion-exchange reactions used in the modeling of LSWF are provided in Table 4.2.

Table 4.1: A list of the aqueous, solid, and exchanged species used in core flood simulation.

Species	Elements
Independent aqueous species	H^+, Ca^{2+}, SO_4^{2-}, Mg^{2+}, Na^+, Cl^-, HCO_3^-, OH^-, HSO_4^-
Dependent aqueous species	$CaSO_4$, $MgSO_4$, $NaCl$, H_2O, CO_2
Solid species	Calcite ($CaCO_3$) and Dolomite ($CaMg(CO_3)_2$)
Exchange species	Na^+, Ca^{2+}, Mg^{2+}

Table 4.2: List of aqueous, mineral, and ion exchange reactions used in the simulations.

Aqueous Reactions	Equilibrium Constants
$CO_2 + H_2O \leftrightarrows H^+ + HCO_3^-$	$K_1^{eq} = 10^{-6.39}$
$H^+ + OH^- \leftrightarrows H_2O$	$K_2^{eq} = 10^{12.39}$
$Ca^{2+} + SO_4^{2-} \leftrightarrows CaSO_4$	$K_3^{eq} = 10^{-2.69}$
$Mg^{2+} + SO_4^{2-} \leftrightarrows MgSO_4$	$K_4^{eq} = 10^{-2.54}$
$H^+ + SO_4^{2-} \leftrightarrows HSO_4^-$	$K_5^{eq} = 10^{-3.06}$
$Na^+ + Cl^- \leftrightarrows NaCl$	$K_6^{eq} = 10^{1.06}$
$Ca^{2+} + HCO_3^- \leftrightarrows CaHCO^{3+}$	$K_7^{eq} = 10^{-1.51}$
Mineral Reactions	Solubility Product
$(CaCO_3) + H^+ \leftrightarrows Ca^{2+} + HCO_3^-$	$K_1^{SP} = 10^{6.41}$
$(CaMg(CO_3)_2) + 2H^+ \leftrightarrows Ca^{2+} + Mg^{2+} + 2HCO_3^-$	$K_2^{SP} = 10^{2.53}$
Ion Exchange Reaction	Selectivity Coefficient
$Na^+ + \frac{1}{2} Ca - X_2 \leftrightarrows \frac{1}{2} Ca^{2+} + Na - X$	$K_1' = 10^{0.67}$
$Na^+ + \frac{1}{2} Mg - X_2 \leftrightarrows \frac{1}{2} Mg^{2+} + Na - X$	$K_1' = 10^{0.58}$

4.2 Simulation Model of the LSWF Lab Test

The LSWF experimental test model was painstakingly reproduced using the Computer Modelling Group's General Equation Modeler (CMG-GEM). The software was able to accurately emulate a cylindrical sandstone core that was originally used for the experiment, with a volume of 24.95 cm^3.

To start with, a three-dimensional rectangular grid was established. This grid was made up of 40 individual blocks, each of one measuring 0.1267 cm in length. The grid itself was designed to be of a similar volume as the laboratory core sample, with a height and width both set at 2.5 cm.

It is important to note that the design of the model was informed by the core flood test model. In line with this, the top of the grid was assumed to have a measurement of 0.01 cm.

Further adjustments were made to the model to ensure it was as close as possible to the real-world core sample used in the LSWF test. The detailed measurements of the core sample's physical properties - porosity and permeability were key among these - and these were replicated in the model. The objective is to have a digital representation that can be manipulated in the virtual environment in order to better understand the properties and potential behaviors of the actual physical sample.

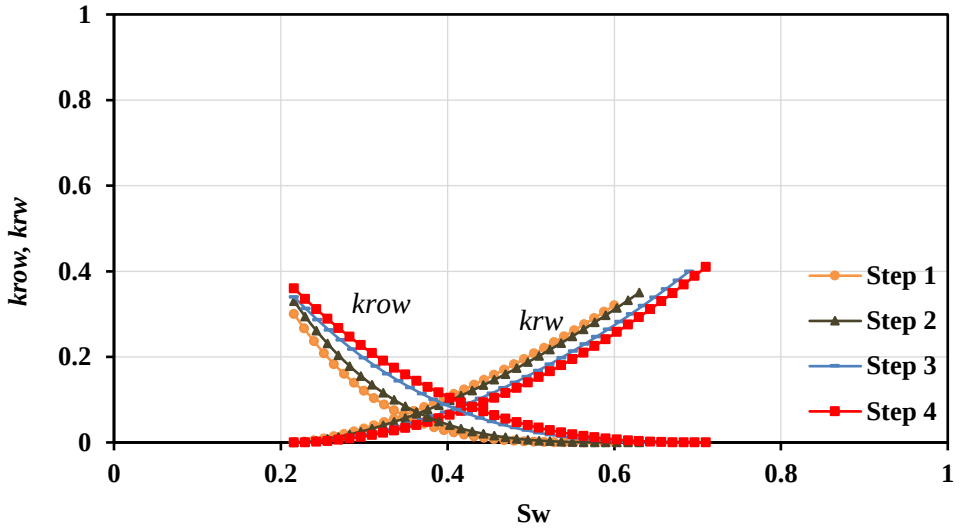

Figure 4.1: Relative permeability curves were used for LSWF simulation; salinities are considered as: step-1 with the salinity of 3wt% which is same as FW, and 1wt%, 0.5wt%, and 0.1wt% are considered as the salinity of steps 2, 3 and 4 respectively.

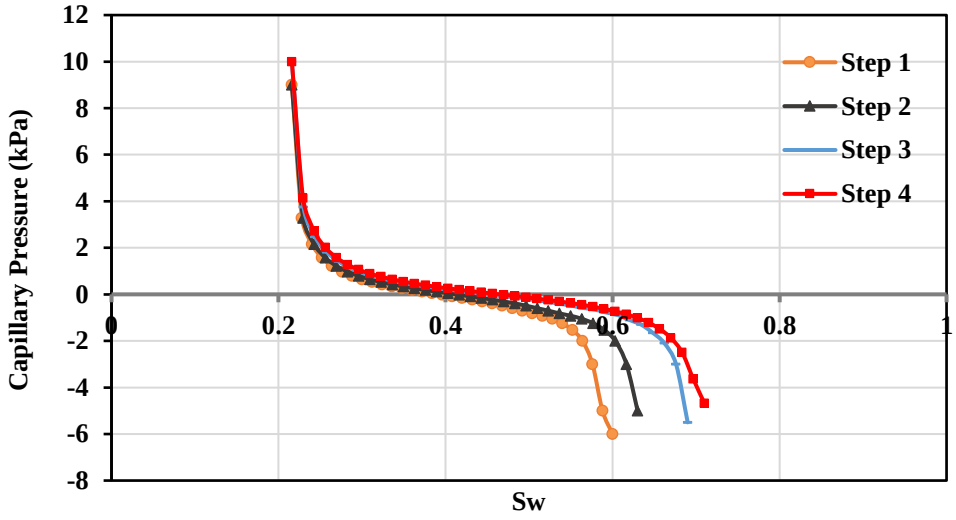

Figure 4.2: Capillary pressure curves used for LSWF simulation, salinities are considered as: step-1 with the salinity of 3wt% which is same as FW, and 1wt%, 0.5wt%, and 0.1wt% are considered as the salinity of steps 2, 3 and 4 respectively.

The composition of injected water used in simulation model is assumed as same as water used in core flooding test. As shown in Table 4.1 the mineral reactions, aqueous reactions, and aqueous components for relative permeability are set to the simulation model. The initial aqueous composition is set as FW, and it is injected as first step of oil

recovery. The initial mineral composition and pore volume are also assigned same as the San Saba core sample.

After building the reservoir grid model, the input or output frequency control was set and different variables relevant to our prescribed reservoir model were chosen. Initial oil saturation values were inputted as 70%. It was assumed that no solvent gas was present within the core, or during the recovery test. The injector well was created at the node (1 1 1), whereas the producer well was situated at (40 1 1).

The LSWF procedure involves a simulated model based on the laboratory core flood test to be flooded. The first step in this process entails saturating the simulated model with oil. This is followed by injecting formation water, often referred to as FW, as an important initial step in the oil extraction process.

FW is continuously injected until the oil production rate becomes stable, meaning it reaches a consistent output level. After achieving this steady state of oil production using FW, low salinity (1wt%) water is introduced in the second step of the simulation process. This approach is then repeated for the third (0.5wt%) and fourth (0.1wt%) steps, ensuring a detailed and comprehensive simulation.

To verify the accuracy and effectiveness of the LSWF simulation, the results of the oil recovery from the low-salinity water injection are compared with the outcomes from the laboratory tests conducted on the San Saba core sample. This comparison is crucial in order to validate the simulation model. If differences are apparent between the predicted extraction rates and the actual results, adjustments are made to minimize errors and improve the computational model's accuracy and reliability. The ultimate goal is to ensure the simulation results reflect the actual condition as closely as possible, thus improving the model's predictive capacity for future oil recovery strategies.

4.3 Kashkari Oil Field Simulation Model

4.3.1 Kashkari Oil Field

Figure 2.6 of chapter 2 shows the location of the Kashkari oil field in the Amu Darya basin in the Sar-e Pol and Jawzjan Provinces, northern Afghanistan. The oil field is in the Kashkari block, which is connected to the Bazar Kami block with an area of 1,103 $km^{2,}$ and the Zamarudsay block with an area of 1,723 km^2. The sedimentary basin is a petroliferous area at the southeastern margin of the Amu Darya basin. It is 12 km from Sar-e Pol city to the southeast, 10 km from the Angut oil field, 5 km from the Ak Darya oil field to the southwest, and 27 km from the Bazar Kami oil field to the southeast. It is

within the oil zone near the mountains to the east of the Amu Darya basin. To the north of the block is the major gas zone of Afghanistan [48, 51-59, 78, 94].

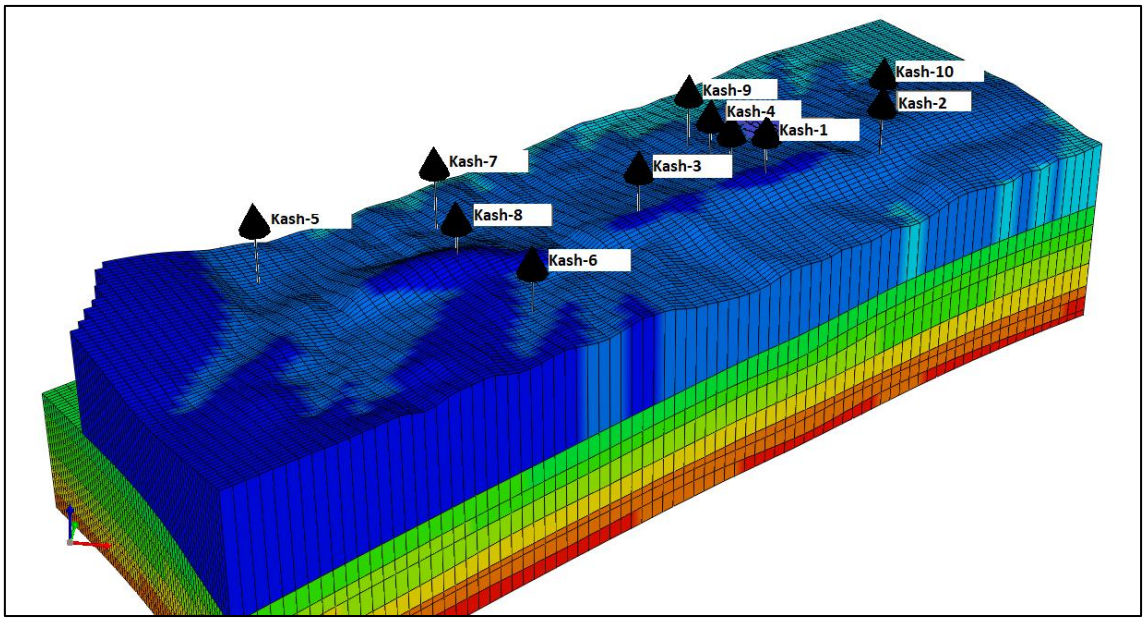

Figure 4.3: Kashkari oil field 3D model.

The Kashkari oil field has a low degree of exploration and development, and no seismic prospecting has been done. The wells drilled from 1976 up to 1980 were positioned mainly according to gravity and magnetic data and the surface geological survey and deployment [51, 52, 78, 94].

4.3.2 Geology and Reservoir Characteristics

The Kashkari oil field has considerable topographic irregularities and large differences in the exposed strata. Within the Kashkari oil field, the outcropped stratum is mainly Guri, with a few Quaternary strata in some parts. According to the data from the drilled wells, the drilled stratum consists mainly of Cretaceous systematic strata. From top to bottom, the strata are Guri formation, Turonian, Cenomanian, Albian, Aptian, Barremian, Hauterivian, and Valanginian. Within the area, the strata have relatively stable thicknesses horizontally that are easy to track. Longitudinally, the lithological association and division of each stratum are clear on the logging curve [51, 52, 94].

The Kashkari oil field is an asymmetrical and double-high layered-edge-water oil reservoir with an anticline structure. The pay zones are Albian Group XIa, Aptian Groups XIIa and XIIb, and Hauterivian Group XIV. The lithology is mainly continental unsolid sandstone. The oil layers are characterized by thin interbeds. Reservoirs XIV and XIIa have good physical properties and are sandstone medium porosity and medium-to-high permeability [51, 52, 94].

In the Hauterivian stratum (120–240 m), the lithology is mainly brown medium-to-small sandstone siltstone and clay interbeds and some thin anhydrite interbeds. The lower part is a conglomerate. Reservoir XIV is in a stratum whose lithology is sandstone and siltstone. The lithology of the Aptian stratum (80–210 m) is mainly gray sandstone and medium-to-coarse sandstone with limestone and anhydrite interbed. Reservoirs XIIa and XIIb are in a stratum whose lithology is mainly sandstone. The upper part of the Albian stratum (290–400 m) is dominated by gray-black limestone and light-green sandstone, and the lower part is dominated by mudstone with sandstone and limestone in some parts. Reservoir XIa is in a stratum whose lithology is mainly sandstone [51, 52, 94].

According to the core-analysis data for eight wells (Kash-1 to Kash-7 and Kash-9 were cored at reservoirs XIa, XIIa, and XIV), and considering the logging interpretation results from CNPCI, the XIa group indicates a medium-porosity and medium-to-low-permeability reservoir; the XIIa group indicates a medium-porosity and medium-to-high-permeability medium-level reservoir; the XIIb group indicates a medium-porosity and medium-to-low-permeability reservoir; and for the XIV groups, the porosity range is 21.5%–40.4% with an average of 32.6%, and the permeability range is 2.1–18,693 mD with an average of 352.6 mD. Thus, the reservoirs are characterized by mesoporosity and medium-to-high permeability [51, 94].

A comparison of the top structures of the Albian, Aptian, and Hauterivian stages indicates clearly that the structures of these three formations are similar in shape, and that the structural development and evolution of the oil field are partly inherited [51, 94].

The Kashkari oil field is a long and narrow NE–SW-trending asymmetric anticline with a relatively complete structure. Two structural highs are connected through a saddle 32°–35° in the northeast direction, 26.5° in the east direction, and 12° in the northwest direction. The oil column height of the Hauterivian stage is 150 m. No previous seismic exploration has been carried out, and the existing underground

contour maps were compiled based on drilling data, so the accuracy of the structural features in regions with fewer wells is low. The stratum groups XIa, XIIa, XIIb, and XIV were identified in the vertical drilling of the Kashkari field. Different oil layers have different oil or water contact, so four independent oil reservoirs formed vertically [72].

Table 4.3 lists the Kashkari oil field properties as obtained from CNPCI and WOGL [51, 94]. The four reservoirs have different oil or water contacts and the oil-bearing area is 2.41–8.57 km^2. According to the reserve estimation, the OOIP is 133.994 MMbbls. In the plane, the OOIP was estimated previously by the Soviet Union as 137.403 MMbbls [78].

Table 4.3: Effective thickness, porosity, and oil saturation of reservoirs in the Kashkari oil field [95].

Formation	Reservoir	Effective Thickness (m)			Porosity (%)			Oil Saturation (%)		
		Min.	Ave.	Max.	Min.	Ave.	Max.	Min.	Ave.	Max.
Albian	XIa	2	5	7	16.7	17	19	60	62	64
Aptian	XIIa	2.5	11.2	16.3	18.6	22	25.4	62	70	78
	XIIb	2.5	4.5	7.1	16.3	18.5	20.6	65	67	74
Hauterivian	XIV	5	14.1	25	19	20.1	22.5	60	71	74

4.3.3 The Establishment of the Initial Static Parameter

The simulation software used to build the Kashkari oil field simulation model is CMG-GEM. The CMG-GEM in the simulation model of the LSWF lab test section was able to get a better match with the laboratory data to simulate the results of the LSWF core test.

Since all the field data was not available to be entered in the static model and only the reports of the Kashkari oil field were available, the PETREL software was used to perform petrophysical modeling of the reservoir properties, including porosity and permeability. It has been tried that the characteristics entered into the program are compatible with the reported characteristics and do not exceed the range of real data. It should be noted that in the usual field development plan (FDP) studies of oil fields, the initial static parameters such as physical properties of the oil field (porosity and permeability), the system pressure and temperature, fluid distribution, volume coefficient viscosity, relative permeability, and rock and fluid compressibility along the field is done with the help of petrophysical logs, which are implemented by the

petrophysics team and static modeler. However, since all data of the petrophysical logs of the wells did not exist, and the static and petrophysical modeling team was not available, petrophysical and geophysical relationships were used to expand the reservoir parameters in the field and these parameters were expanded.

The relative permeability curve for water and oil for all models (with high and low salinity), which were expressed in the LSWF lab core test simulation sections, are used in this model (Figures 4.3 and 4.4).

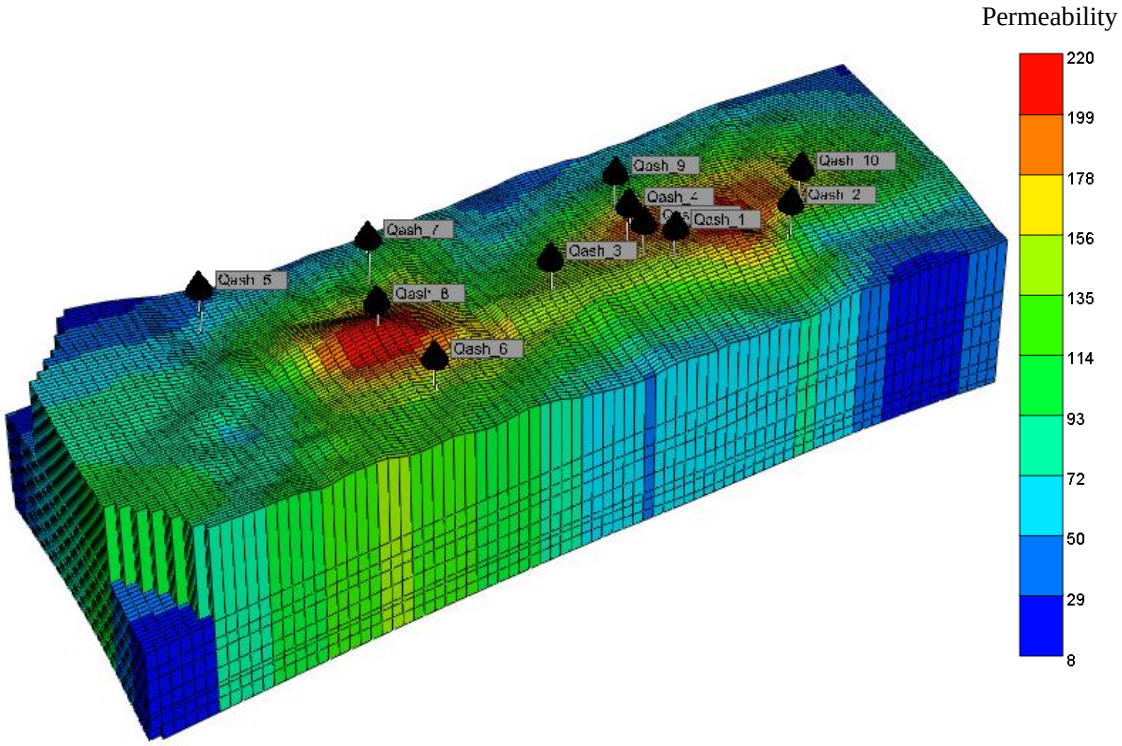

Figure 4.4: Kashkari oil field 3D model with the distribution of permeability.

The grid is divided according to the principle of dividing the layers toward the i and j directions, in which the step between each point is 26 m in the i direction and 75 m in the j direction. In the vertical direction, 8 layers are divided. The microstructure map of the small sand body thickness of the Kashkari block's rhythm section is used to control the tectonic fluctuation of the layers. In the simulation model, 76 cells in the x-direction, 82 cells in the y-direction, and 8 cells in the z-direction are considered, which consist of a total of 49856 cells. The pressure data mainly focus on flowing BHP. The production time ranges from 1976 to 2046 with the monthly time step are considered.

It is also necessary to explain that, the reservoir model chosen to evaluate the enhancement of oil recovery by LSWF at the field scale is based on a sector of the Kashkari sandstone oil field. This model was only used as an example in this study and is not a recommendation for a real development strategy in this field.

4.4 Application of LSWF in the Kashkari Oil Field

The LSWF proposed in the core flood experimental section and simulated in CMG-GEM is applied in the Kashkari oil field. Five wells (Kash-1, Kash-3, Kash-4, Kash-9, and Kash-10) are active and used for oil production purposes, and the remaining six wells (Kash-2, Kash-5, Kash-6, Kash-7, Kash-8, and Kash-21,) are not activated yet or do not meet the oil reservoir. In this simulation study, three models, the base model with no water injection, FW injection with a salinity of 3%, and LSW injection with a salinity of 0.1% were designed for 70 years to evaluate the EOR by LSWF in Kashkari oil field. The details of FW (3%) and LSW (0.1%) injected into the model are the same as the step one and step forth conducted in the lab test and its simulation model. The oil component is considered the same as the lab test simulation model. For the base model and FW injection model, the first step relative permeability illustrated in Figure 4.1 is used, while in the LSW injection model, the fourth step relative permeability is used. The wells Kash-2 and Kash-21 were considered injection wells. These injection wells had perforated all four reservoirs XI, XIIa, XIIb, and XIV. It should be noted that the flowing bottom hole pressure (BHP) is considered for well injection, and it is the same for all three models and the value of 2900 kPa is assigned.

4.5 Result

4.5.1 Experimental Simulation Result

The CMG-GEM simulated model of oil recovery and water cut by LSWF for comparing them with the laboratory test were shown in Figures 4.5 and 4.6. The oil recovery graph of the simulated model first increased rapidly same as the laboratory test result. The oil recovery in the simulation model is 52%, and both laboratory and simulated results are well matched. The water cut result of the laboratory LSWF test simulation model also compared with the lab test to confirm the simulation accuracy. Figure 4.6 illustrated the two graphs matching, after 5 PV injection of FW and during

the second step LSWF the result of simulation graph is well matched with the lab test.

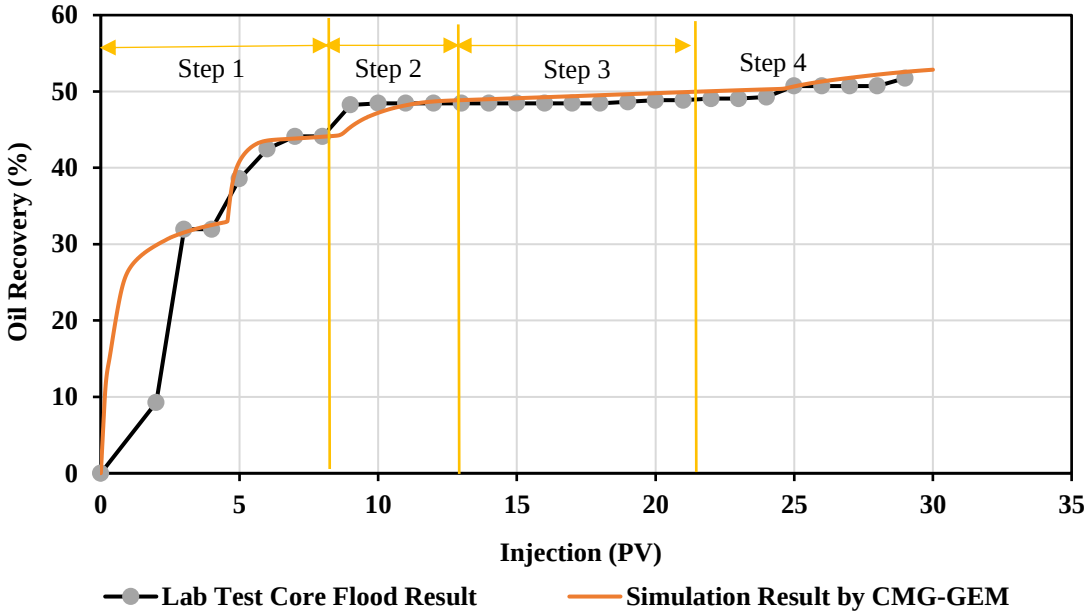

Figure 4.5: LSWF laboratory and simulation of oil recovery results.

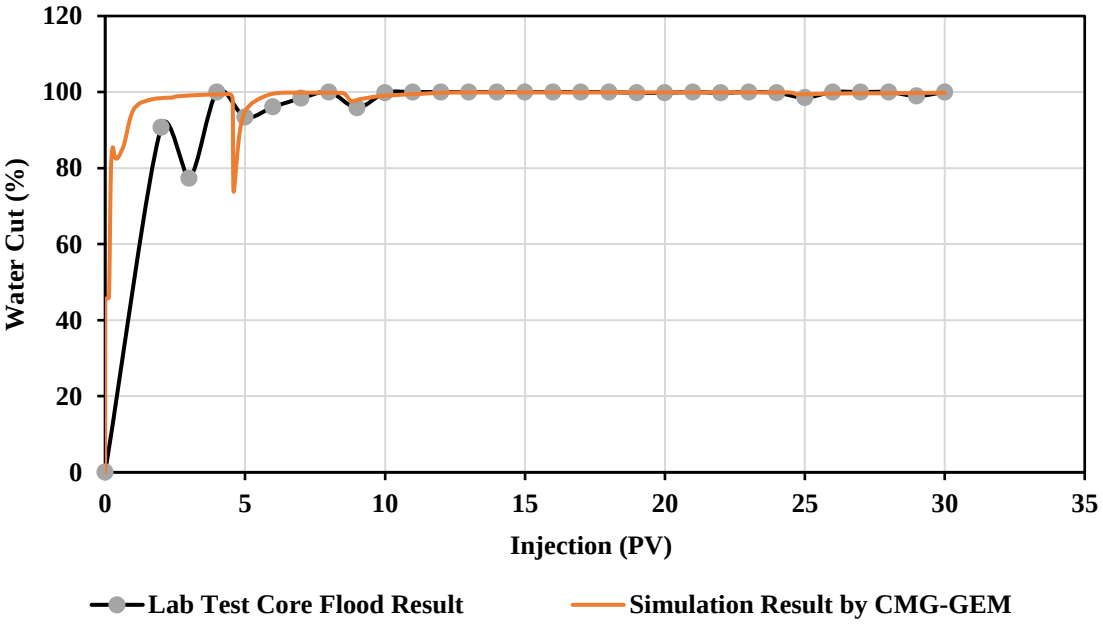

Figure 4.6: LSWF laboratory and simulation of water cut results.

4.5.2 The Application of LSWF to the Kashkari Oil Field Result

To evaluate the efficiency of LSWF in the Kashkari oil field, water reduction and oil increment during the effective period, average water reduction per day and average oil

increment per day, and cumulative oil production for 70 years by natural depletion (base model), FW injection and LSW injection with the salinity of 0.1% were evaluated.

The daily oil production, water cut, cumulative oil production, and oil recovery are illustrated in Figure 4.7. Figure 4.7 (a) shows the daily oil production which started from 200 m^3/day and gradually decreased to about 50 m^3/day. Figure 4.7 (b) shows the water cut of base, FW injection, and LSW injection models. Due to the non-implementation of water injection in the base model, its water cut is zero; but the water cut in the other two models increased considerably and reached 90 %. Figure 4.7 (c) illustrates the cumulative oil production of the base, FW injection, and LSW injection models. In Figure 4.7 (c) the cumulative oil production of the base, FW injection, and LSW injection models are 2.12, 7.3, and 10.4 MMbbls respectively. Figure 4.7 (d) illustrates the oil recovery of the base, FW injection, and LSW injection models. In this figure, the oil recovery of the three models are 1.3%, 4.5%, and 6.4% respectively.

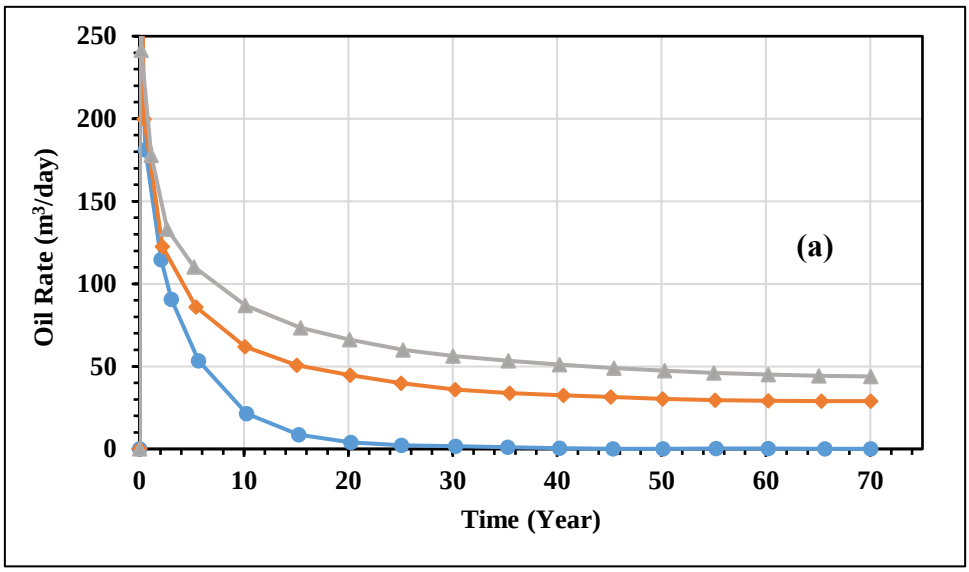

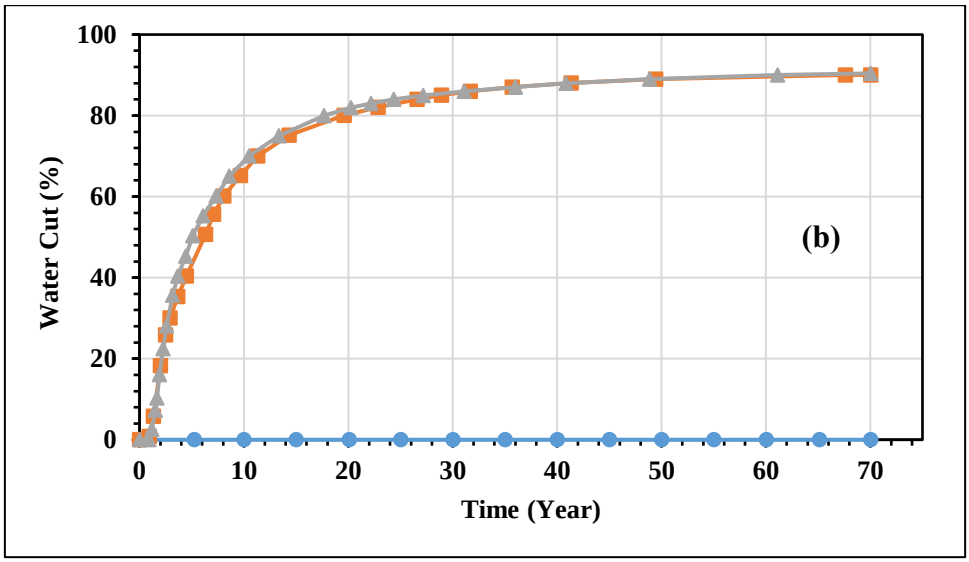
Water Cut (%)
100
80
60
40
20
0
0
10
20
30
40
50
60
70
Time (Year)
(b)

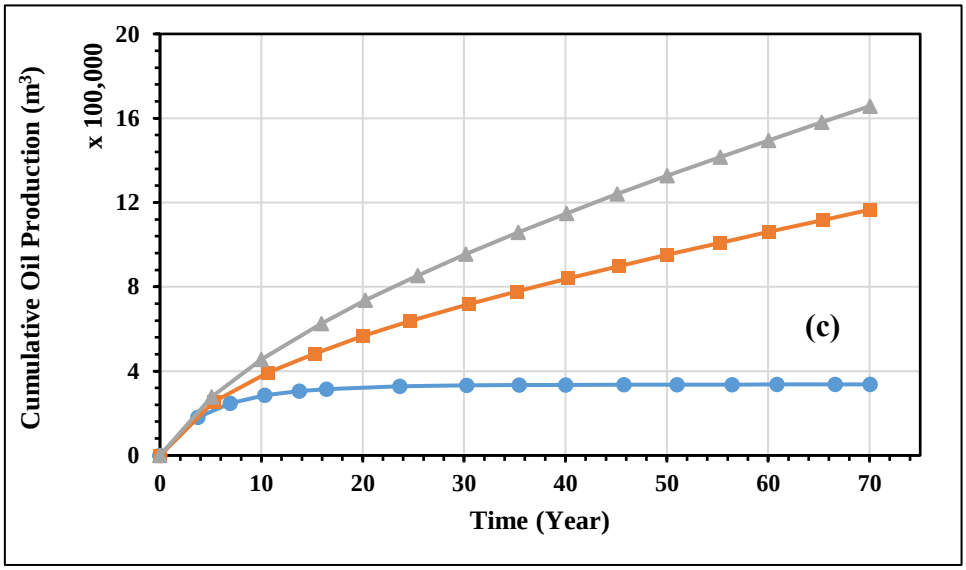
Cumulative Oil Production (m3)
x 100,000
20
16
12
8
4
0
0
10
20
30
40
50
60
70
Time (Year)
(c)

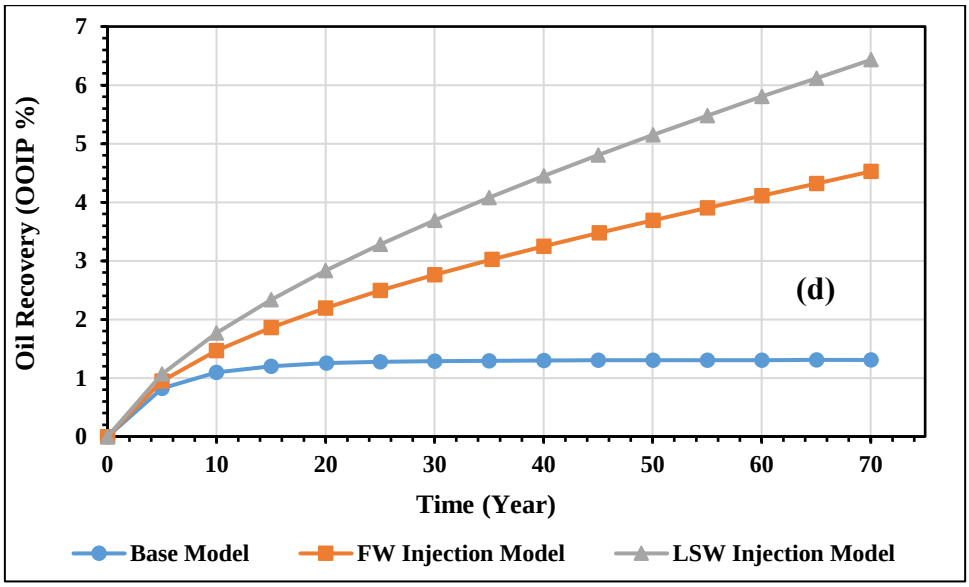

Figure 4.7: The influence of LSW injection on (a) oil rate daily production, (b) water cut, (c) cumulative water production, and (d) oil recovery in the Kashkari oil field.

Figure 4.8 illustrated the Kashkari oil field average pressure for the base, FW injection, and LSW injection models which are designed at 27,000 kPa for the initial condition. It seems from Figure 4.8 that the pressure on the base, FW injection, and LSW injection models from 27,000 kPa to 22,000 kPa, 25,500 kPa, and 25,700 kPa gradually decreased.

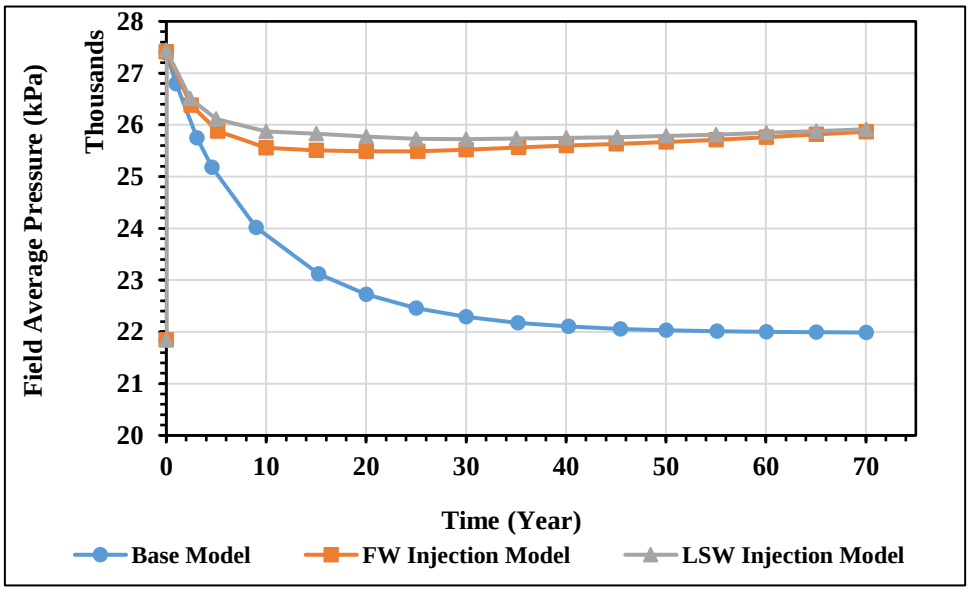

Figure 4.8: The average pressure evaluation of the base, FW injection, and LSW injection models of the Kashkari oil field.

Figure 4.9 shows the liquid, oil, and water production rates of three models (base, FW injection, and LSW injection models) from the Kashkari oil field. It seems from Figure 4.9 (a) illustrated the liquid, oil, and water rates of the base model. In this Figure due to not implementing water injection the water cut is zero and the oil production is decreasing considerably. Figures 4.9 (b) and (c) illustrated the liquid, oil, and water rates of FW injection and LSW injection models. The Figures show that the oil production is significantly decreasing while the water production is increasing in these two models.

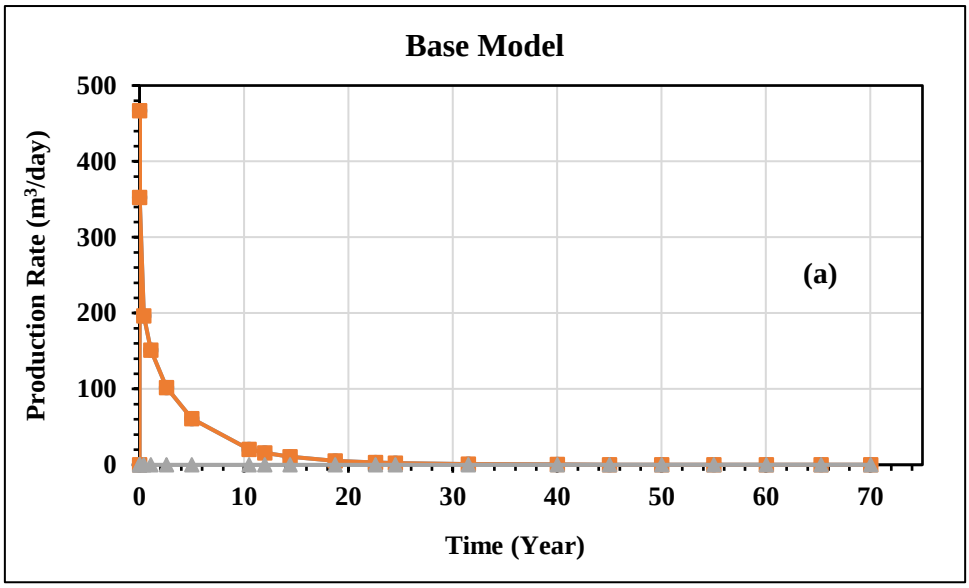

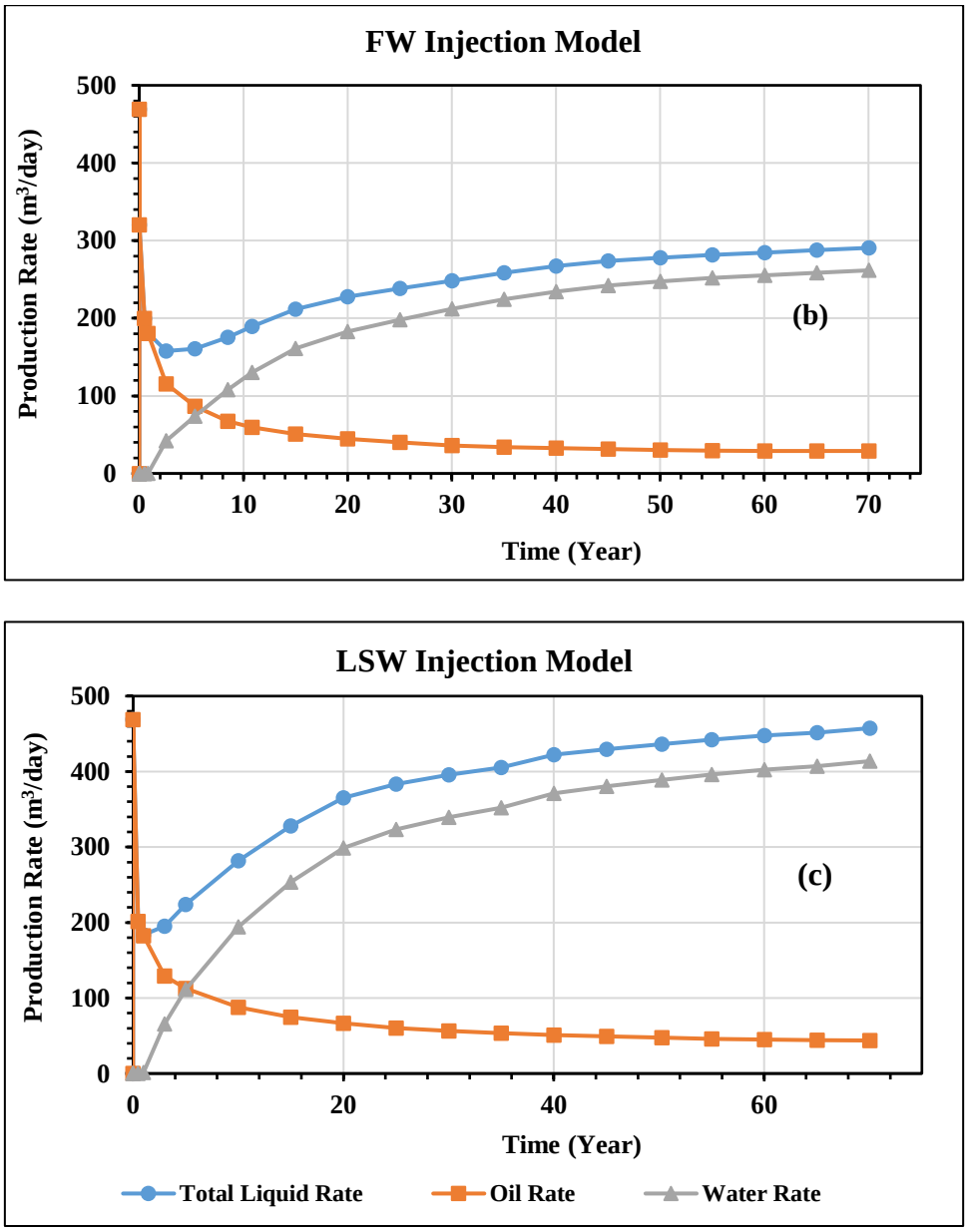

Figure 4.9: The liquid, oil, and water rates of the (a) base, (b) FW injection (c), and LSW injection models.

As seen from previous Figures the flow rate of produced oil expressively decreases over time, which is normal. With the production of oil and the reduction of the pressure, the oil production capacity of the Kashkari oil field is reduced and has a downward trend. This decrease in oil production rate is more in the FW injection model with a salinity of 3% than in the LSW injection model with a salinity of 0.1%, which indicates that the injection of water with low salinity is more effective in oil recovery of Kashkari oil field. In the base model where the injection water is not implemented and produced by

natural pressure, the oil recovery factor is 1.3%. By injecting FW with a salinity of 3%, this amount of recovery has increased by 3.2%, but when LSW with a salinity of 0.1% is injected into the oil field, oil recovery by 5.1% shows an increase compared to the base model.

Based on these Figures, the ionic changes in the injected water have led to the activation of the mechanisms for increasing the extraction of the aqueous base, including the change in wettability. In Figure 4.1, during the activation of the mentioned mechanism, the relative permeability curve of oil has increased and the curve of water has decreased, in other words, the movement of water is slow and oil production has increased.

4.6 Summary

This chapter focused on evaluating the EOR process for the Kashkari oil field using the LSWF method. The advanced features of the CMG-GEM utilized to formulate a simulation model replicating the conditions of the oil field study.

Initially, the process of oil recovery was explored through a simulation model designed to imitate laboratory core flooding experiments. Developing this model allowed us to first investigate the feasibility of introducing the LSWF method in a controlled environment before forecasting its implications and success in the actual oil field.

Following the laboratory test simulation, another model (based on a sector of the field) was designed specifically to simulate the conditions of the Kashkari oil field. This model allowed us to apply and analyze the effects of the LSWF method within a representative environment of the oil field.

To evaluate the overall impact of LSWF injection on oil recovery, three simulation models: the base model, the FW injection model, and the LSW injection model were created and studied. The findings showed differing levels of oil recovery for these models, being 1.3%, 4.5%, and 6.4% respectively.

The results showed that implementing LSWF (with a salinity of 0.1%) had a significant impact on oil recovery in the model. Compared to the base model, the LSW injection resulted in a 5.1% increase in oil recovery, and a 1.9% increase compared to the model using FW injection. These findings suggest that utilizing LSWF (salinity 0.1%) could be an effective method for maximizing oil recovery in the Kashkari oil field.

Chapter Five

5 Sensitive Analysis of LSWF on Kashkari Oil Field Simulation Model

The factors that may impact the recovery development of the Kashkari oil field may include the following three factors: salinity concentration in water injection, flowing BHP, and salinity water injection rate. The following uses the single variable method to study the influence of various factors in the oil increase in the well group. The parameter and default values of each factor are shown in Table 5.1.

Table 5.1: Overall injection parameter adjustment of Kashkari oil field.

Influencing factors	Parameter value	Defaults
Salinity concentration (%)	0.1 0.5 1.0 2.0 3.0	0.1
Flowing bottom hole pressure (kPa)	15,000 20,000 25,000 30,000	25,000
Injection rate (m^3/d)	30 50 100 150 200	-
Timing of water injection (year)	0 10 20 30	0

5.1 Influence of Salinity Concentration

Given the influence of salinity concentration, five levels: 0.1%, 0.5%, 1%, 2%, and 3%, are designed. Corresponding to the production characteristic curves of each oil production well shown in Figures 5.1 and 5.2, the percentage of salinity is designed based on the formation of water salinity explained in table 5.2. Form the salinity sensitive analysis result it observed that the oil production increases with the decrease of salinity. A low concentration of salinity water injection such as 0.1 wt% is beneficial for increasing oil. The increased volume of the oil calculation process for a single well and well group is shown in Table 5.3.

Table 5.2: FW ion contents.

Ion Contents (PPM)	Cl^-	SO_4^{2-}	HCO^{3-}	Ca^{2+}	Mg^{2+}	Na^+	Total
FW (3%)	12488	4172	2091	402	75	10278	29506
SW(2%)	8324	2780	1394	268	50	6852	19668
SW (1%)	4162	1390	697	134	25	3426	9834
LSW (0.5%)	2081	695	348	67	12	1713	4916
LSW (0.1%)	416	139	69	13	2	343	982

Table 5.3: Oil increase of each well in a well group with different concentrations.

Salinity concentration (%)	Increased oil volume (m^3)					
	Kash-1	Kash-3	Kash-4	Kash-9	Kash-10	Well group
3	147,460	352,833	41,917	405,874	218,029	1,166,113
2	183,597	379,703	56,323	456,519	256,516	1,332,658
1	224,739	406,678	77,350	505,033	301,191	1,514,991
0.5	243,373	426,491	86,742	536,672	322,388	1,615,666
0.1	253,517	431,640	92,581	547,185	332,265	1,657,188

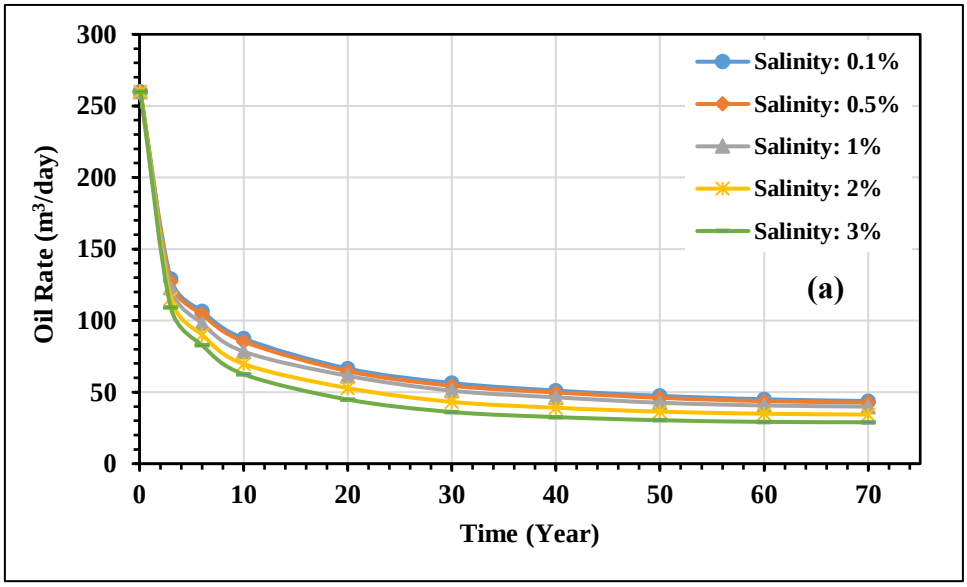

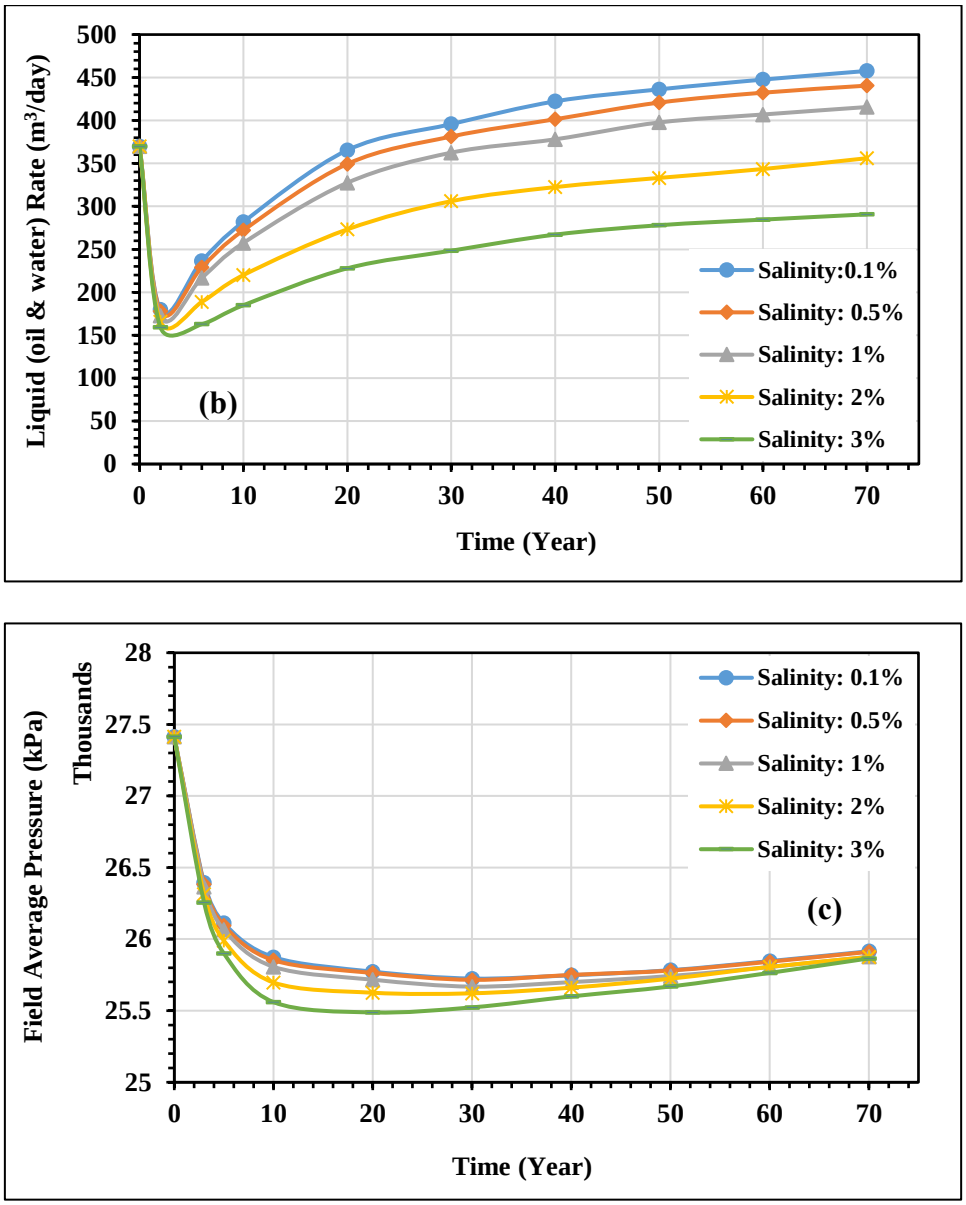

Figure 5.1: The influence of salinity concentration on the (a) daily oil production curve, (b) daily liquid production curve, and (c) pressure average of the oilfield.

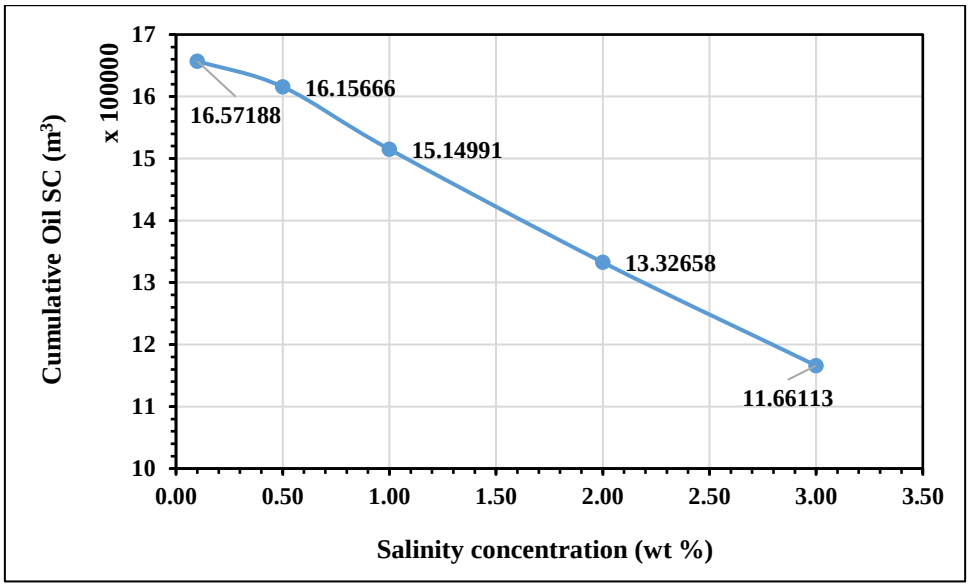

Figure 5.2: The influence of salinity concentration on the oil increase of the oilfield.

5.2 Influence of Flowing Bottom Hole Pressure

Given the influence of the flowing BHP, four levels: 15000, 20000, 25000, and 30000 kPa are designed, and the production characteristic curves corresponding to each oil production well in Figures 5.3 and 5.4. It seems from these figures that the oil increases with the increase in the flowing BHP. The increased volume of the oil calculation process for a single well and well group affected by flowing BHP optimization is shown in Table 5.4

Table 5.4: Oil increase of each well in a well group with different pressure rates.

Flowing bottom hole pressure (kPa)	Increased oil volume (m³)					
	Kash-1	Kash-3	Kash-4	Kash-9	Kash-10	Well group
15000	45,993	87,167	67,470	72804.51	71,065	344,499
20000	63,982	201,550	63,819	191814.6	167,407	688,573
25000	253,517	431,641	92,582	547185.6	332,266	1,657,191
30000	360,670	593,068	115,280	820389.3	410,144	2,299,552

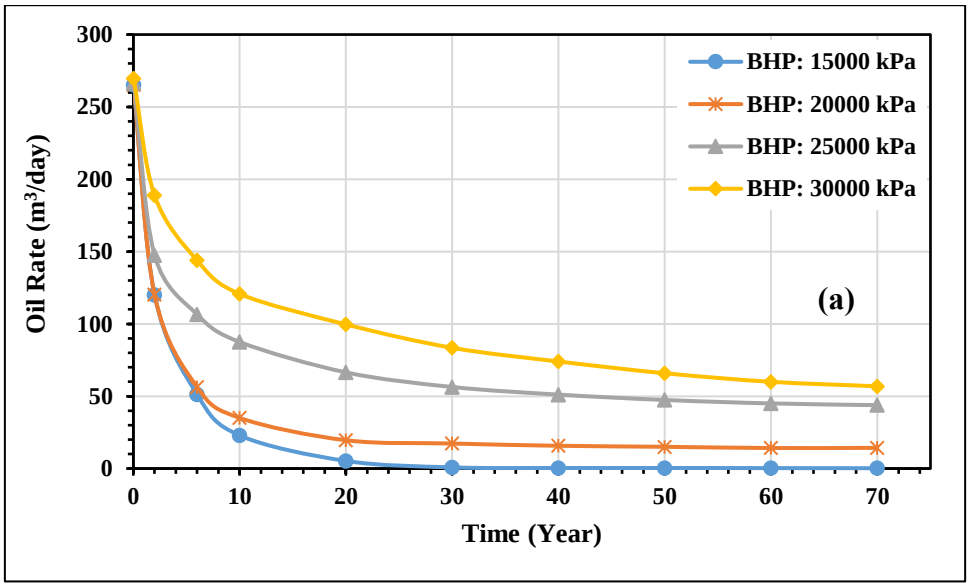
Oil Rate (m³/day)
300
250
200
150
100
50
0
0
10
20
30
40
50
60
70
Time (Year)
BHP: 15000 kPa
BHP: 20000 kPa
BHP: 25000 kPa
BHP: 30000 kPa
(a)

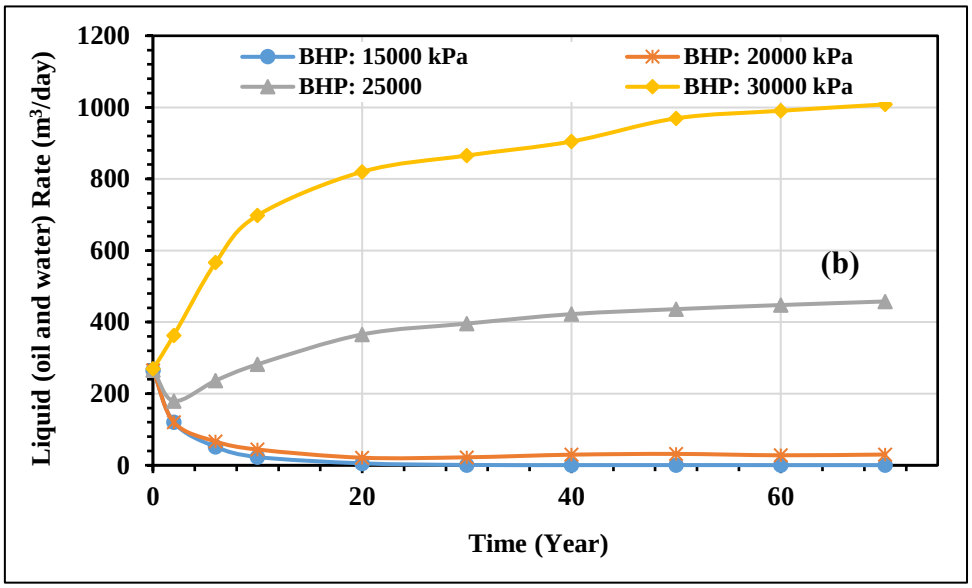
Liquid (oil and water) Rate (m³/day)
1200
1000
800
600
400
200
0
0
20
40
60
Time (Year)
BHP: 15000 kPa
BHP: 20000 kPa
BHP: 25000
BHP: 30000 kPa
(b)

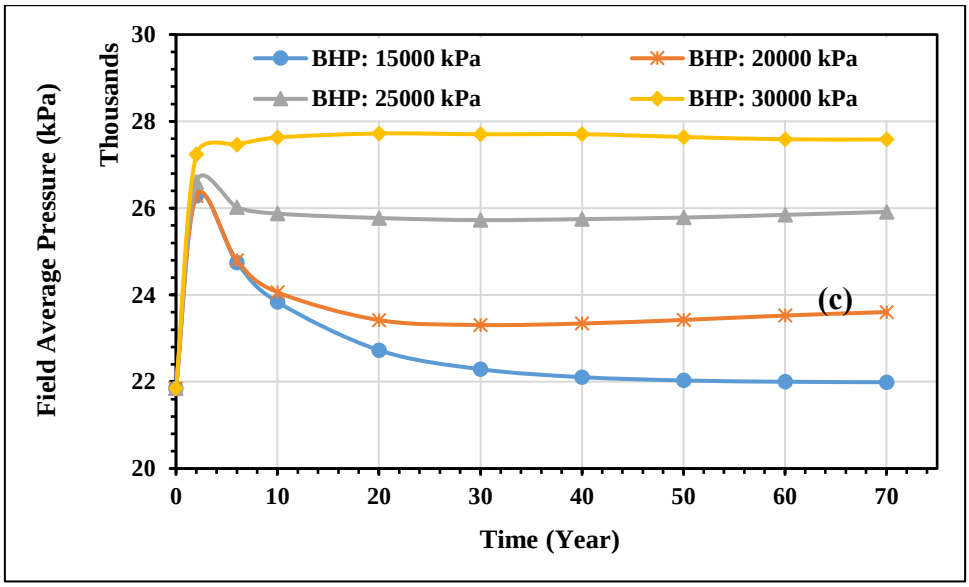

Figure 5.3: The influence of pressure rate on the (a) daily oil production curve, (b) daily liquid production curve, and (c) pressure average of the oilfield.

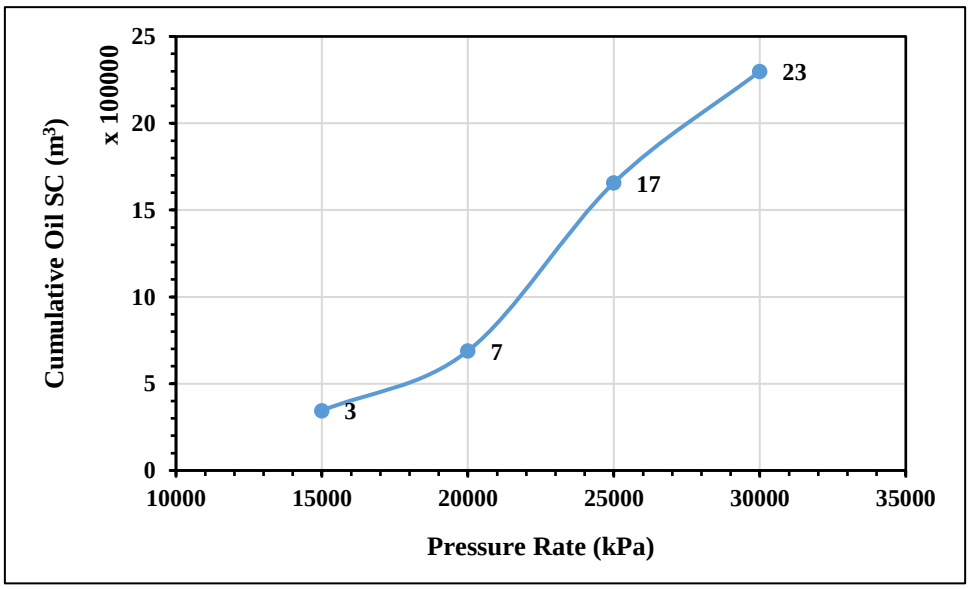

Figure 5.4: The influence of pressure rate on the oil increase of the oilfield.

5.3 Influence of Water Injection Rate

Given the influence of salinity water injection rate, five levels of 30 m³/day, 50 m³/day, 100 m³/day, 150 m³/day, and 200 m³/day are designed, and the corresponding production characteristic curves of oil production wells are shown in Figures 5.5 and 5.6. The more the water injection rate, the best effect of increasing oil in the well group; when the water injection rate is 200 m³/day, the oil production rate is at the highest

level, so the recommended water injection rate can be 200 m³/day. The increased volume of the oil calculation process for a single well and well group affected by the salinity water injection rate is shown in Table 5.5.

Table 5.5: Oil increase of each well in a well group with different water injection rates.

Injection rate (m³/day)	Increased oil volume (m³)					
	Kash-1	Kash-3	Kash-4	Kash-9	Kash-10	Well group
30	55,051	176,080	82,846	156,831	110,065	580,873
50	92,251	219,350	91,659	226,164	186,485	815,909
100	195,461	303,200	106,120	383,933	256,970	1,245,684
150	274,137	365,905	120,325	486,645	288,639	1,535,651
200	278,151	396,142	114,715	520,802	308,499	1,618,309

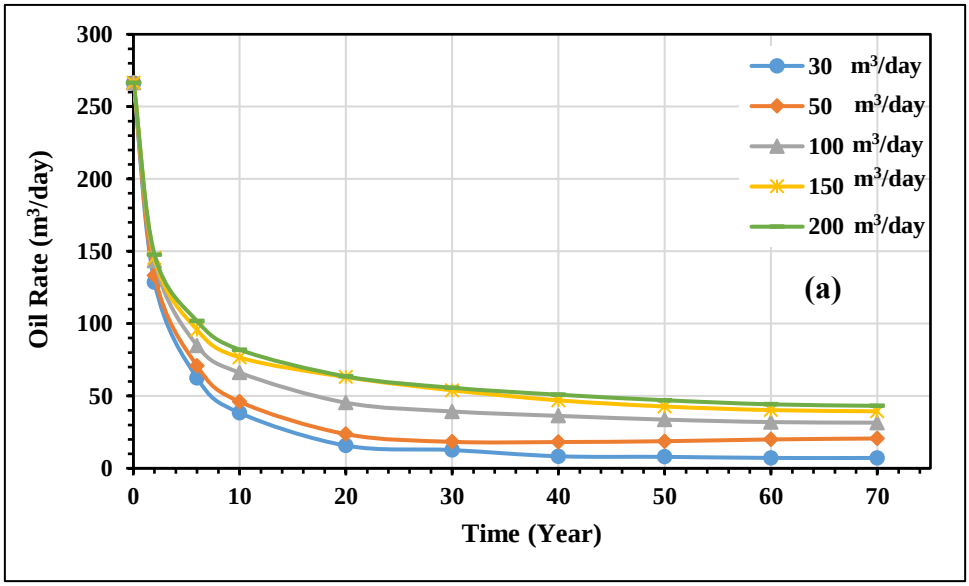

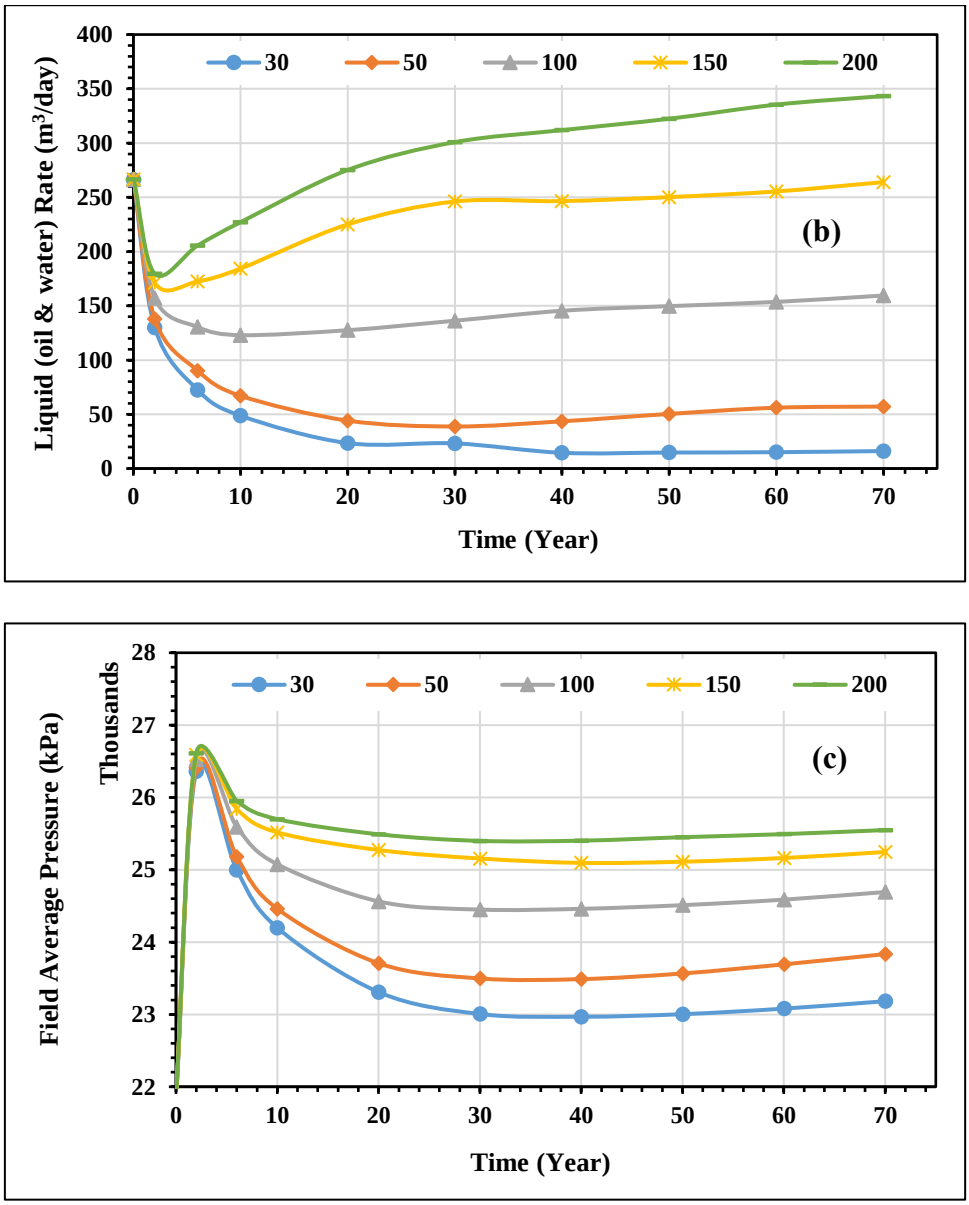

Figure 5.5: The influence of injection rate on the (a) daily oil production curve, (b) daily liquid production curve, and (c) pressure average of the oilfield.

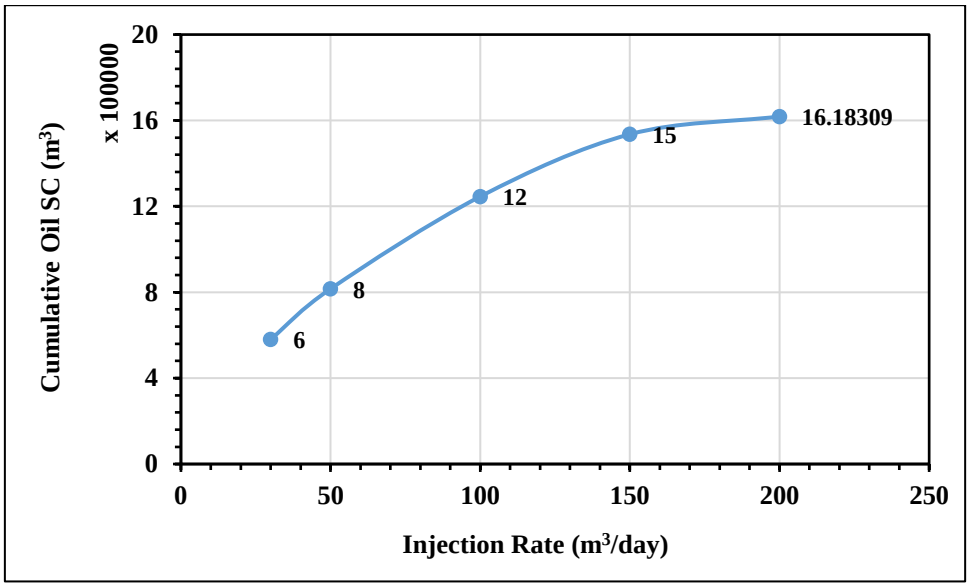

Figure 5.6: The influence of injection rate on the oil increase of the oilfield.

5.4 Timing of Salinity Water Injection

According to the timing of salinity water injection, as shown in Table 5.6, a total of four levels of 0 years which is the start of the simulation, after 10, 20, and 30 years are considered. The corresponding production characteristic curves of oil wells are shown in Figures 5.7 and 5.8. It seems from the results that as early as the salinity water injection is started the oil recovery gets higher. The increased volume of the oil calculation process for a single well and well group affected by different salinity injection timing is shown in Table 5.6.

Table 5.6: Oil increase of each well in a well group with salinity water injection timing.

Injection timing (year)	Increased oil volume (m³)					
	Kash-1	Kash-3	Kash-4	Kash-9	Kash-10	Well group
0	253,517	431,640	92,581	547,185	332,265	1,657,191
10	234,935	354,448	106,934	470,767	281,776	1,448,862
20	200,679	271,037	102,526	392,558	240,224	1,207,026
30	165,144	208,783	96,221	318,436	205,802	994,387

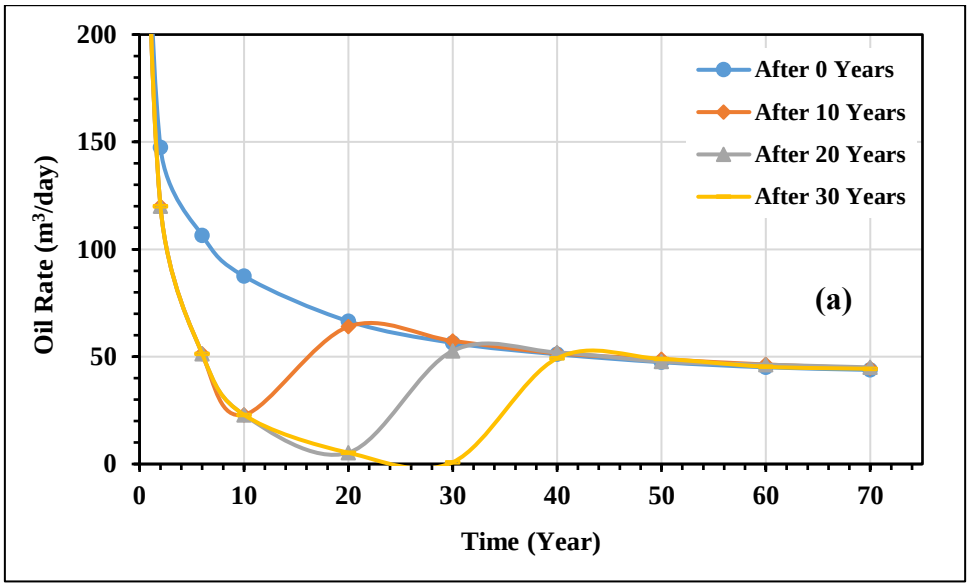
Oil Rate (m3/day)
Time (Year)
After 0 Years
After 10 Years
After 20 Years
After 30 Years
(a)

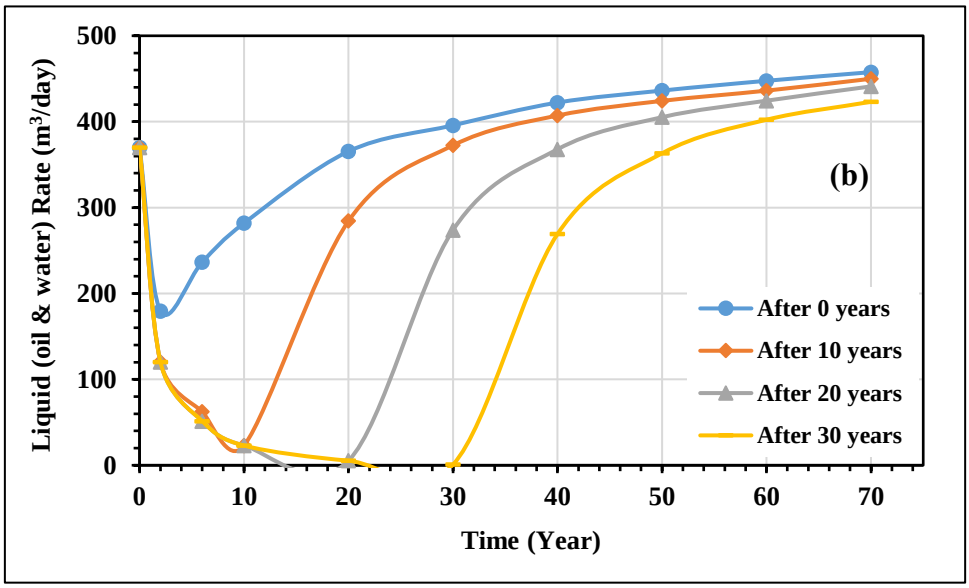
Liquid (oil & water) Rate (m3/day)
Time (Year)
After 0 years
After 10 years
After 20 years
After 30 years
(b)

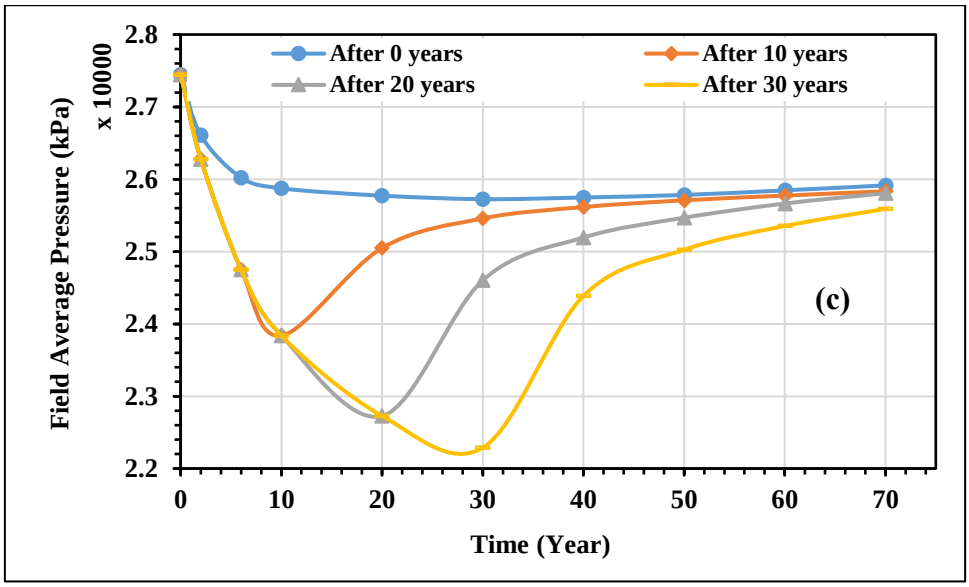

Figure 5.7: The influence of salinity injection timing on the (a) daily oil production curve, (b) daily liquid production curve, and (c) pressure average of the oilfield.

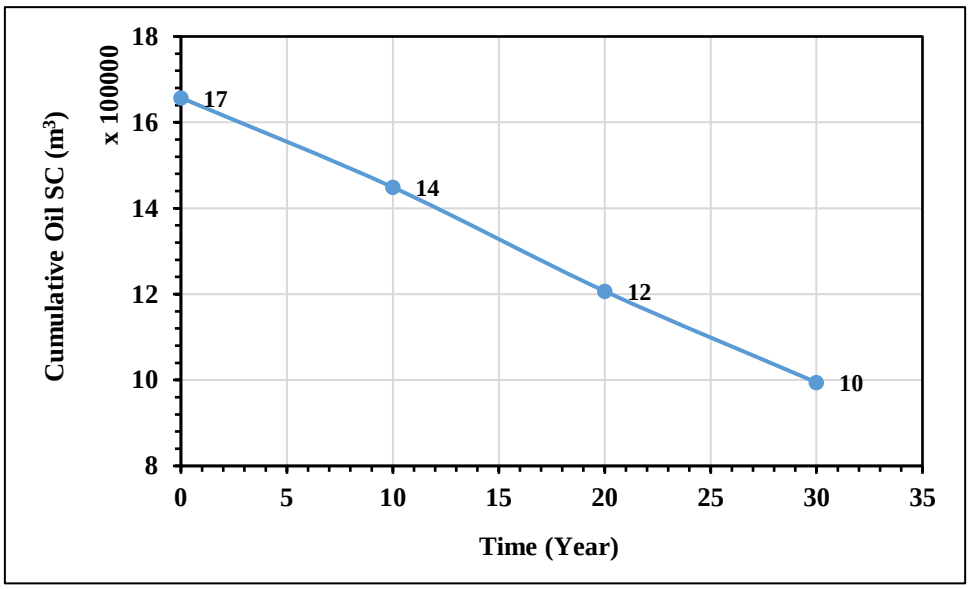

Figure 5.8: The influence of salinity water injection timing of the oil increase of the oilfield.

5.5 Summary

In this chapter, a comprehensive sensitivity analysis pertaining to the LSWF method in the well grouping of the Kashkari oil field was undertaken. The results indicate that the understanding of four key factors crucially impacts the outcomes. These entail the concentration of low salinity, different flowing bottom hole pressures (BHP), variances in the salinity water injection rate, and the timing of salinity water injection.

The findings suggest that using a low concentration of salinity water, such as 0.1 weight percent (wt%), significantly contributes to enhanced oil extraction. As the flowing BHP increases, a corresponding uptick in oil concentration was observed. Furthermore, we found that a high rate of water injection, scaling up to 200 m^3/day, results in an optimal increase in oil concentration. This leads us to recommend an injection rate of 200 m^3/day for ideal outcomes.

The analysis of timing for initiating the salinity water injection process revealed that an early start to the process leads to higher oil recovery factor. Therefore, it is recommended to launch the water injection process as soon as feasibly possible.

Upon analyzing the sensitivity of these specific parameters, we have been able to define both the lower and upper bounds of the relevant factors. These findings will work as a range of guidelines for future oil extraction processes in the Kashkari oil field, ultimately leading to optimize oil recovery strategies and increasing the overall efficiency of operations.

Chapter Six

6 Conclusion

Afghanistan, though tectonically complex due to historical plate collisions, houses potential petroleum reserves within its North Afghanistan's sedimentary Amu Darya basin. Specifically, this basin's geology, spanning Jurassic to Eocene epochs, features source rocks and reserves largely within Jurassic-Cretaceous rocks. Notably, clay shale of Lower to Middle Jurassic and marine shale of Upper Jurassic form the key source rocks, while Hauterivian Shatlyk Bed sandstone and Upper Jurassic carbonates are the primary reservoir rocks. The region's hydrocarbon traps are largely structural, created by broader anticlines during Neogene compression events. Lastly, the Kashkari to Tithonian Gaurdak Formation, comprising salt, anhydrite, and carbonate layers, seals these layers.

The Kashkari oil field, located in the Amu Darya basin of northern Afghanistan, has been a site of oil extraction since the first well was drilled in 1976. To date, a total of ten wells have been drilled in this field. However, as the global population continues to grow, so does the demand for oil, putting pressure on rapidly depleting conventional oil reserves. It's also known that around 80% of oil remains unrecovered after primary production. To address this, EOR techniques are being implemented to further extract oil and meet rising demands.

This study highlights the effectiveness of LSWF in boosting oil recovery, as demonstrated through laboratory core flooding tests. Significant increases in oil recovery were observed when applying LSWF at specific salinity levels of 1%, 0.5%, and 0.1%, with the maximum increase reaching 7% after the initial FW injection. The tests were conducted in steps, each with differing salinity levels, all contributing to the overall increase in oil recovery. Notably, a 4% increase in oil recovery was recorded at the 1% salinity level during the LSWF injection phase. The findings validate LSWF as an efficient EOR method, especially in reservoirs like the Kashkari oil field that has high clay content. The varying results at different salinity levels underscore the importance of selecting optimal salinity levels for practical LSWF application EOR strategies.

Through the application of a CMG-GEM simulation model, LSWF evaluated the EOR of the Kashkari oil field. To evaluate the effectiveness of the LSWF method, a

laboratory core flooding experiment was first simulated. Then, to determine whether the technology might be used in the actual oil field, the lab test simulation model was validated with the test result. The Kashkari oil field simulation model was created and the LSWF method was used to it. Three models (base, FW injection, and LSW injection) were considered in the Kashkari oil field simulation model to assess the impact of the LSWF injection of oil recovery. The oil recovery of these three models is 1.3%, 4.5%, and 6.4% respectively.

It may be inferred from this study that it is possible to simulate intra-phase interactions, ion exchange, and the dissolution or precipitation of minerals in CMG-GEM reservoir simulation software. It is also possible to observe the behavior of ionic liquids.

According to research on the sensitivity analysis of LSWF in the Kashkari oilfield's well group, four factors were recognized for this analysis: salinity concentration, different flowing BHP, injection rate, and timing of the injection. From the results, it is speculated that, a low concentration of salinity water injection such as 0.1 wt% is beneficial for increasing oil. The oil concentration increases with the increase in flowing BHP and similarly with the high-water injection rate, oil concentration increases, and it is recorded highest at 200 m^3/day, so it is a recommended water injection rate. From the simulation study of salinity water injection timings, it is evaluated that as early as the salinity water injection is started the oil recovery gets higher.

From the series of analysis conducted during this research, it is concluded that the LSWF technique is a suitable technique for EOR for the Kashkari oil field. The results of laboratory core flooding test, simulation model and the sensitivity analysis of low salinity suggested the efficiency of this technique and it is in the favor of EOR.

Abbreviation and Parameters	Definition
EoR	Enhanced Oil Recovery
CNPCI	China National Petroleum Corporation International
WOGL	Oil and Gas Group, Ltd
CMG	Computer Modeling Group
LSW	Low salinity water
LSWF	Low-salinity water flooding
PVI	Pore Volume Injection
PV	Pore Volume
OFT	Oil Finding Technology
STARS™	Thermal & Advanced Processes Simulator, software
GEM™	Compositional & Unconventional Simulator, software
SGS	SGS Afghanistan Ltd. Oil and Gas Testing Laboratory in Hairatan
SKUA-GOCAD™	Geomodelling software
EMERSON™	American multinational corporation
GEOLOG™	Geomodelling software
R_w	Water resistivity
S_{wi}	Irreducible water saturation
S_{orw}	Residual oil saturation
$k_{ro\ max}$, $k_{rw\ max}$, $k_{rg\ max}$	Maximum relative permeability
P_c	Capillary pressure
PARADIGM™	Reservoir model development software
Cf	Formation rock compressibility
San Saba	Core sample from San Saba, Texas
SRP-350	Apparatus used for core flooding test
n_h	Aqueous phase hydrocarbon components
n_a	Aqueous phase components
n_m	Aqueous mineral components
FW	Formation water
mol/kg	Moles per kilogram
A_γ, B_γ and $\dot{B}$	Are temperature-dependent coefficients
$\dot{a}_i$	The ion size parameter
z_i	Valence number of species i
m_i	Molality
r_β	The reaction rate
$\hat{A}_\beta$	The reactive surface area for mineral β
k_β, $K_{eq,\beta}$ and Q_β	The rate constant

$E_{a\beta}$ and $k_{o\beta}$	The activation energy for reaction β (J/mol)
R	The universal gas constant (8.314J/mol-K)
E_a	The activation energy
$\hat{A}_\beta^0$ and N_β^0	The reactive surface area
$\emptyset$	The new porosity
$\emptyset^*$	The reference porosity with no mineral dissolution/precipitation
$\widehat{\emptyset}^*$	The porosity with dissolution/precipitation
ρ_β	The mineral's molar density
$c_\emptyset$	The rock compressibility
p and p^*	Current and reference pressures
$\emptyset^0$	The initial porosity
k°	Initial permeability
CEC	Cation Exchanger Capacity
BHP	Bottom Hole Pressure
FDP	Field Development Plan
PHREEQC	Mathematical software
MMbbl	One million barrels
MIE	Multiple-component Ion Exchange
COBR	Crude Oil/Brine/Rock
RS	Reactivity Series
TPS	Total Petroleum System

Annex

Application of Buckley-Leverett Theory to the Kashkari Oil Field in the Northern Afghanistan

Hydrocarbon resources are important for the rehabilitation and sustainable development of Afghanistan's infrastructure. In this annex, the Buckley-Leverett's (BL) frontal displacement theory was used to examine the enhancement of oil production from the petroleum reservoirs located in the Kashkari oil field in the northern Afghanistan. The theory is investigated in a laboratory experiment, and a graphical method to a horizontal plane model is used to calculate the fluid flow properties through porous media. The experimental results are compared with the graphical calculations, and then the theory is applied to the oil field plane. The relative permeability of oil and water was obtained from the laboratory experiment published by author. Based on the water-oil displacement, residual oil saturation, the advance of the saturation front, and F_{BL} are determined. According to this investigation, a considerable amount of oil was estimated to be produced from the Kashkari oil field.

1. Introduction

In Afghanistan, decades of war have caused energy shortages, hindering the improvement of living standards. Food, clothing, shelter, heat, sanitation, and industry depend on the availability of energy. It has long been known that Afghanistan has petroleum resources, but the exploitation of these resources has been limited. To improve living standards and economic conditions in Afghanistan, the availability of energy must be increased, particularly by exploiting the country's petroleum resources. In this research, we proposed increasing oil production from one of the Afghanistan's oil reservoirs based on the BL theory. We investigate the displacement of oil by injecting water into the underlying petroleum reservoir, which is known as the waterflooding technique and it is applied to the Kashkari oil field in the northern Afghanistan. The Kashkari oil field was being under exploration and exploitation by the China National Petroleum Corporation (CNPC) and Watan Oil and Gas Group Ltd. (WOGL) from 2012 to 2016 [96, 97].

Oil companies maximize the value of a reservoir by extracting as much oil as possible. However, it is difficult to exploit all hydrocarbons from an oil field; only a certain amount of oil from a petroleum reservoir may be recovered. More oil is left behind in an oil field than can be recovered by the end of the field life. There is a big difference in the percentage of oil in place and recoverable oil. Many factors influence recovery from an oil field, such as geological complexity, fluid physics, and economics. Generally, the recovery factor of oil from petroleum reservoirs is 30–35% [98]. Oil recovery can be increased by changing the physical and chemical nature of the fluid formation, and many ways to increase the oil recovery from petroleum fields are being developed. Oil displacement by water is one of the oil recovery methods. A virgin reservoir may have sufficient pressure to push hydrocarbons to the surface. However, as the oil is exploited, the pressure decreases, and production efficiency drops. The effective pressure in the reservoir must be maintained for hydrocarbon withdrawal. In the waterflooding technique, to maintain the pressure artificially, water is injected into the reservoir during oil production, and it affords high oil production rates and high petroleum recovery when oil production rates begin to drop [99]. Water injection results in a recovery factor of 30–35%, increasing the recoverable reserves [100].

Injecting water into a reservoir displaces oil toward the production wells in an immiscible two-phase flow, known as the immiscible displacement of fluid flow in porous media. The mechanism of the immiscible displacement two-phase fluid flow has been studied extensively in investigations of fluid flow through porous media, and BL published an inventive, simple approach to this problem in 1942 [101]. The BL frontal displacement theory describes a method for calculating saturation profiles based on relative permeability, assuming that the effect of capillary pressure between the two fluids and the gravitational effects are neglected. The advance of a saturation front by the displacing fluid is mainly affected by the permeability of oil and water relative to the reservoir rock and the viscosity ratio between the two fluids [101].

In this chapter, the recovery of oil by the waterflooding technique in a horizontal displacement method was evaluated by a laboratory experiment and by graphical calculations based on BL's frontal displacement theory. The objective of this study is to increase the recoverable oil reserves in the Kashkari oil field through the implementation of BL techniques as an affordable and straightforward method. Based on this research, an oil production of 68.79 MMbbl from the under-study oil field was predicted.

2. Buckley-Leverett Theory

Buckley-Leverett theory is a simple, widely used method of investigating the advance of a fluid displacement front in an immiscible displacement process [99, 102]. The theory models the rate at which an injected water tank moves through a porous medium by using fractional flow theory. It assumes that the flow is linear and horizontal, water is injected into a petroleum reservoir, oil and water are incompressible and immiscible, and the effect of gravity and capillary pressure is negligible [102]. The theory of displacement is based on the concept of relative permeability [101]. Buckley-Leverett's advanced theory is an application of the law of mass conservation [102].

The one-dimensional flow rate of oil and water considering oil displacement by water in a completely saturated porous medium can be described by Darcy's law as:

$$q_w = -\frac{k_x k_{rw} A}{\mu_w} \frac{\partial p_w}{\partial x} \tag{A.1}$$

$$q_o = -\frac{k_x k_{ro} A}{\mu_o} \frac{\partial p_o}{\partial x} \tag{A.2}$$

Where k_x is the intrinsic permeability of the porous medium, A is the cross-sectional area, μ_o and μ_w are the dynamic viscosity of oil and water, p_o and p_w are the pore pressure of oil and water, and k_{ro} and k_{rw} are the relative permeability of oil and water, respectively. The relative permeability of oil and water (k_{ro} and k_{rw}) are given as a function of water saturation S_w, where S_{wi} and S_{or} are the irreducible water saturation and the residual oil saturation in the reservoir. The pressure difference at the contact surface between oil and water (i.e., capillary pressure) is denoted by $p_{o/w}$ and p_w in Eq. A.1. If the water pressure is replaced by capillary pressure water and oil, Eq. A.1 is rewritten as:

$$q_w = -\frac{k_x k_{rw} A}{\mu_w} \frac{\partial (p_o - p_{o/w})}{\partial x} \tag{A.3}$$

Subtracting Eq. A.1 from Eq. A.3, gives:

$$-\frac{1}{k_x A}\left(q_w \frac{\mu_w}{k_{rw}} - q_o \frac{\mu_o}{k_{ro}}\right) = -\frac{\partial p_{o/w}}{\partial x} \tag{A.4}$$

Eq. A.4 gives:

$$q_T = q_w(1+\frac{k_{ro}}{k_{rw}}\frac{\mu_w}{\mu_o})-\frac{k_x k_{ro} A}{\mu_o}\frac{\partial p_{o/w}}{\partial x} \tag{A.5}$$

Then, the fraction of pore water flow (i.e., fractional flow rate), f_w, is expressed as:

$$f_w=\frac{q_w}{q_T}=\frac{1+\frac{k_x k_{ro} A}{q_T \mu_o}\frac{\partial p_{o/w}}{\partial x}}{1+\frac{k_{ro}}{k_{rw}}\frac{\mu_w}{\mu_o}} \tag{A.6}$$

Capillary pressure $p_{o/w}$ is small compared with the oil/water pressure when water displaces oil in the reservoir. If the effect of capillary pressure is neglected, for the horizontal flow, the fractional flow equation is expressed simply as:

$$f_w=\frac{1}{1+\frac{k_{ro}}{k_{rw}}\frac{\mu_w}{\mu_o}} \tag{A.7}$$

The continuity equation may be introduced to consider the conservation of fluid mass [103], and this is expressed as:

$$-\frac{\partial q_w}{\partial x}=A\phi\frac{\partial S_w}{\partial t} \tag{A.8}$$

Where φ is the porosity of the reservoir rock. Using the relations $q_w = f_w q_T$ and f_w (S_w), Eq. A.8 is rewritten as:

$$\frac{\partial S_w}{\partial t}=-\frac{q_T}{A\phi}(\frac{df_w}{dS_w}\frac{\partial S_w}{\partial x}) \tag{A.9}$$

Because $S_w(x, t)$, we can express the saturation change as:

$$dS_w=\frac{\partial S_w}{\partial x}dx+\frac{\partial S_w}{\partial t}dt \tag{A.10}$$

In Eq. A.10, if the fluid is at constant saturation during the displacement process, we can rewrite it as:

$$0 = \frac{\partial S_w}{\partial x} dx + \frac{\partial S_w}{\partial t} dt \tag{A.11}$$

Then, it follows that:

$$\frac{\partial S_w}{\partial t} = -\frac{\partial S_w}{\partial x} \frac{dx}{dt} \tag{A.12}$$

Substituting Eq. A.12 into Eq. A.9, the following equation will be obtained:

$$\frac{\partial x}{\partial t} = \frac{q_T}{A\phi} \left(\frac{df_w}{dS_w}\right) \tag{A.13}$$

Eq. A.13 is the BL equation, which implies that the rate of advance of a plane of fixed saturation S_w is proportional to the rate of change of the stream composition with saturation. Because f_w is not an explicit function of t, Eq. A.13 can be integrated to give the position of a particular saturation value as a function of time.

$$x_{S_w} = \frac{q_T t}{A\phi} \left(\frac{df_w}{dS_w}\right) + x_0 \tag{A.14}$$

Here, x_0 is the position of the water saturation at time $t = 0$.

According to Eq. A.14, saturation advances into the system at a rate directly proportional to $f_w' = d f_w / dS_w$. The shape of the saturation profile calculated by Eq. A.14 is expressed by curve *abcd* in Figure A.1, but it does not display a sharp leading edge for the saturation front.

Morel-Seytoux [104] applied the conservation of mass over the front position so that $A = B$, and explained that the saturation established in the flowing system immediately behind the front S_{BL} can be evaluated from tangent point c on the fractional flow curve in Figure A.1. The abrupt front in the saturation profile is given by line *cf*.

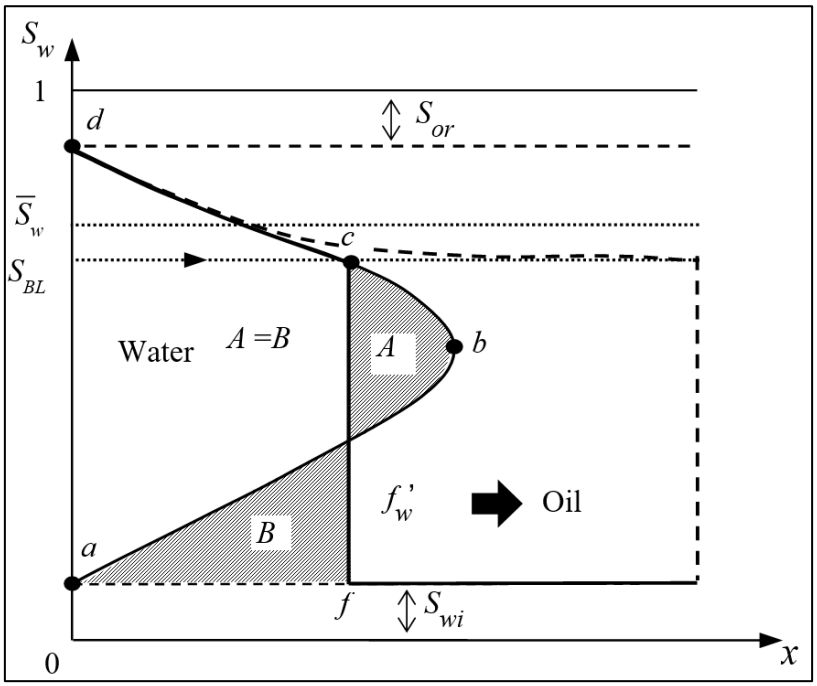

Figure A.1: Tentative saturation profile.

3. Relative Permeability of Oil and Water Used for BL Method

Relative permeability is an important parameter that controls the immiscible displacement of two-phase fluid flows in porous media. Many factors affect the relative permeability such as fluid saturation, the magnitude of the initial-phase saturation (S_{wi}), wettability, the effect of rock pore structure, and temperature. The relative permeability value is measured through laboratory tests by steady-state methods and unsteady-state methods [100]. The wetting fluid saturation curves are usually water (S_w) extending from the irreducible wetting-phase saturation to the residual oil saturation. As the relative permeability curves of water increase, the relative permeability of oil, k_{ro}, decreases with the desaturation of oil, and the relative permeability of water gradually increases and reaches its maximum value k_{rws} (endpoint water permeability) at which time k_{ro} is 0 because water is the only phase that is mobile and at its maximum saturation [105].

Figure A.2 shows the relative permeability curves of oil and water measured experimentally by the steady state-method. We have previously published the laboratory method for measuring oil and water [105]. As the relative permeability curve of water, k_{rw}, increases, the relative permeability curve of oil, k_{ro}, gradually decreases.

The irreducible water saturation (S_{wr} = 0.12) is visible at the left-hand side of the graph and the residual oil saturation (S_{or} = 0.27) is visible at the right-hand side.

Relative permeability curves with different residual oil and water saturations are used for designing the waterflooding technique to evaluate the amount of oil recovered by artificially injecting water into the reservoir. The rate of advance of the waterfront can be calculated based on the BL frontal displacement theory using fractional flow curves that are evaluated from the relative permeability curves [106].

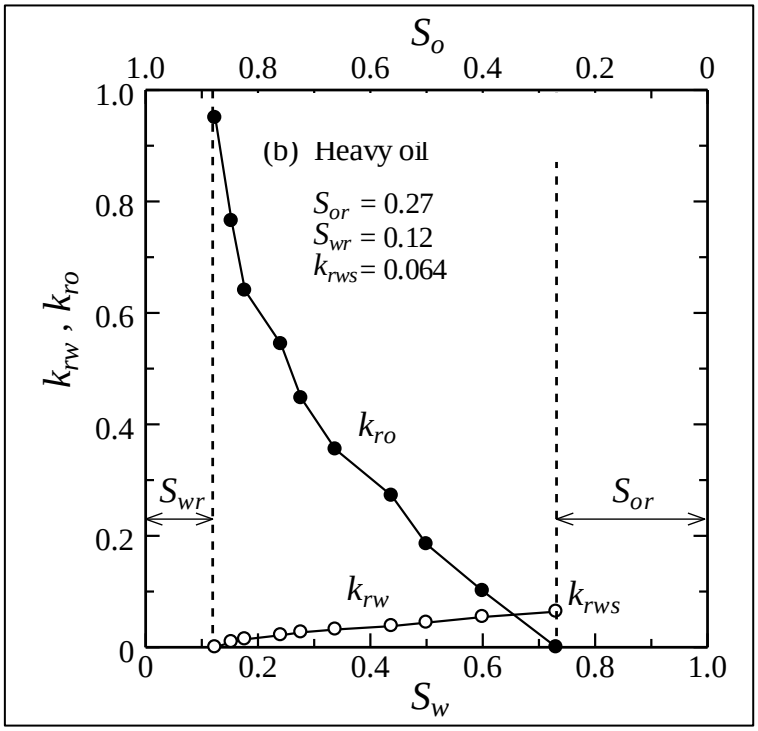

Figure A.2: Relative permeability curves for oil displacement by water [107]

4. Experimental Investigation of Buckley-Leverett Theory

The apparatus shown in Figure A.3 was used to investigate oil displacement by water. Toyoura sand (particle diameter D = 0.105–0.425 mm) was packed with a uniform density of ρ_s = 2.65 g/cm³ in a horizontal square plane model 60 cm long with a cross-sectional area of 120 cm². The sand was saturated with oil for oil displacement by water. On both sides of the model, the piezometer pressure was kept constant. There was a water supply tank on the left side of the model. The model was designed so that the fluid flow characteristics through porous media could be observed. The model was

made from glass and had nine observation wells, with upstream and downstream levels that were set to evaluate the hydraulic head from the fluid flow pressure. We evaluated the horizontal immiscible displacement of the fluid flow through porous media. During the experiment, the water displaced the oil from the left to the right side of the plane, toward the outlet. The displaced fractional fluid discharge was collected at the right edge of the model.

Figure A.4 shows the fractional flow discharge of oil and water through the horizontal square plane model. Oil was displaced by water ($q_o = q_T$, where q_T is the total input rate). When the soil pores in the horizontal square plane were saturated with oil, the fractional discharge at the outlet, f_{od}, was 1 up to some pore volume, and thereafter some amount of water was discharged. Therefore, only oil was discharged during the first 120 min. After 120 min, the oil fractional discharge decreased, and the water discharge increased. After 180 min, only water was discharged ($f_{wd} = 1$) and the fluid flow reached a steady state. There was still residual oil in the plane, referred to as the residual oil saturation ($S_{or} = 0.27$). The total amount of oil displaced by water up to 120 min was 1073 cm³ ($Q_o = 0.39$ PV) calculated from the total pore volume ($PV = V \times n = 2767$ cm³). After the full 180 min, the total discharge of fluids was $Q_T = 1610$ cm³.

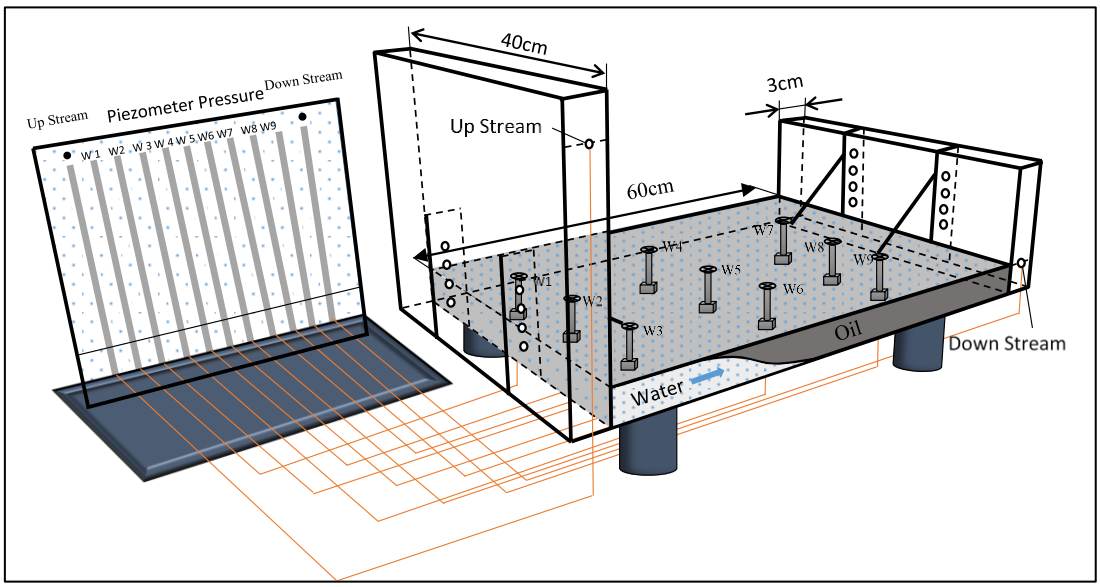

Figure A.3: Schematic diagram of the experimental apparatus.

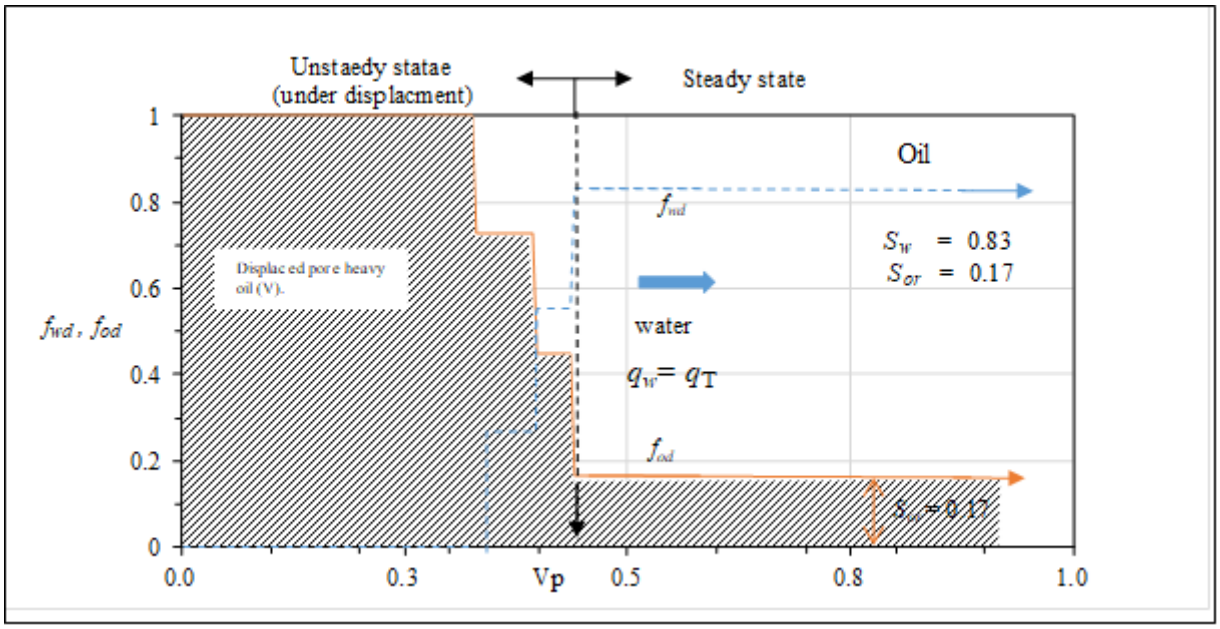

Figure A.4: Experimental fractional discharge of pore oil and water.

5. Application of Buckley-Leverett Theory to the Experimental Model

The relative permeability of oil and water is shown in Figure A.2 were used. Figure A1.5 shows the relative permeability of water and oil curves that were expressed as the following cubic functions concerning effective water saturation for convenience [108].

$$k_{rw} = k_{rws} S_e^{\,3} \tag{A.15}$$

$$k_{ro} = (1 - S_e)^3 \tag{A.16}$$

Here, S_e is the effective (normalized) saturation given by:

$$S_e = \frac{S_w - S_{wi}}{1 - S_{wi} - S_{or}} \tag{A.17}$$

The fractional flow of water and oil can be calculated by Eq. A.7. As a quantitative demonstration of the BL analysis, an artificial petroleum reservoir with a cross-sectional area of A = 120 cm², length of x = 60 cm, and porosity of φ = 0.44 is considered (Figure A.3). The viscosities of water and oil are assumed to be identical for simplicity. The total amount of water injected is $q_T = q_W$ = 9 cm³/min, and a graphical method shows that the water saturation at the front is S_{BL} = 0.51, and the average saturation behind the front is S_W = 0.56. Figure A.4 shows that the water flow fraction is an S shape, and the S_{BL} and f_{BL} are calculated by using the intersection between the tangent line and f_W = 1.

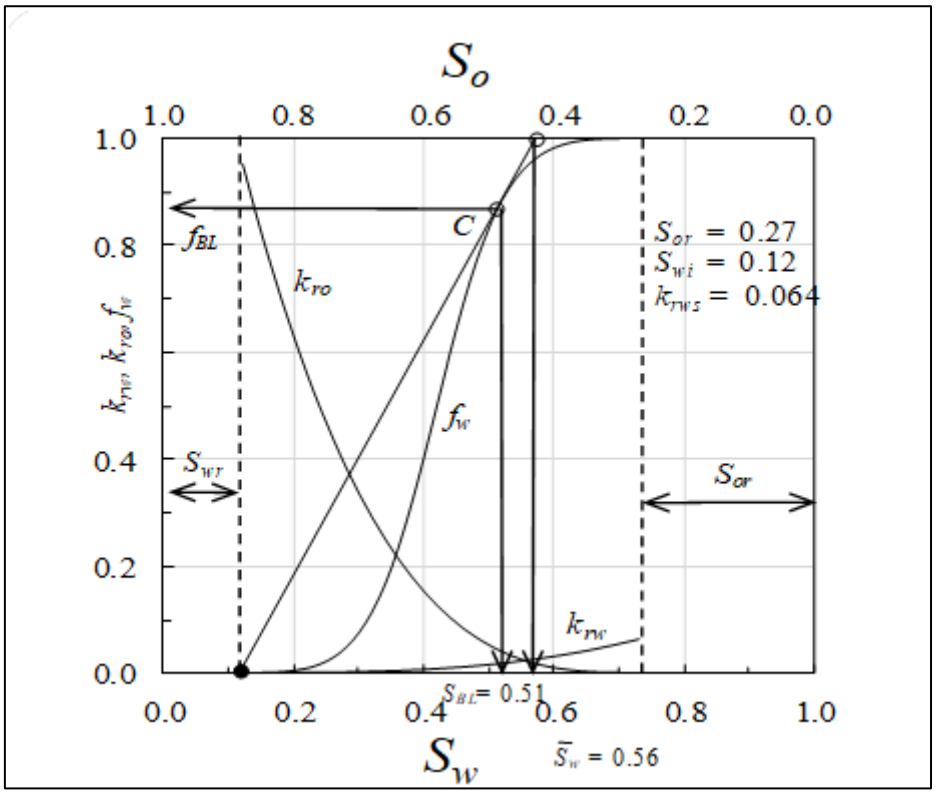

Figure A.5: Relative permeability for oil and water and fractional flow curves.

Figure A.6 shows the analysis of oil displacement by water based on the BL frontal displacement theory. The saturation front progresses toward the outlet at a constant speed, and breakthrough occurs at t = 147 min when the front reaches the edge of the plane. However, there is still some residual oil in the plane model, which may be discharged with the water.

The amount of oil produced may be calculated for a reservoir of area A and distance B by writing Eq. A.13 as:

$$dx/B = f_w' q_T dt/A\phi B = f_w' q_T dt/V_p = f_w' dv_p \qquad \text{(A.18)}$$

Where $V_p = A\varphi B$ is the pore volume of the reservoir and dv_p is the pore volume of water injected. Because the saturation is steady, the equation can be integrated to obtain the front swept by water.

$$x = B f_w' v_p \qquad \text{(A.19)}$$

Where v_p is the pore volume of water injected. When x reaches B, the water saturation at the front is S_{BL}, which makes it possible to evaluate f_w' and calculate v_p,

the total amount of oil displaced by water in units of pore volume [100]. The oil recovery factor of this condition can be calculated by:

$$RF = \frac{\bar{S}_w - S_{or}}{1 - S_{or}} \tag{A.20}$$

$$RFD = \frac{\bar{S}_w - S_{wi}}{1 - S_{wi} - S_{or}} \tag{A.21}$$

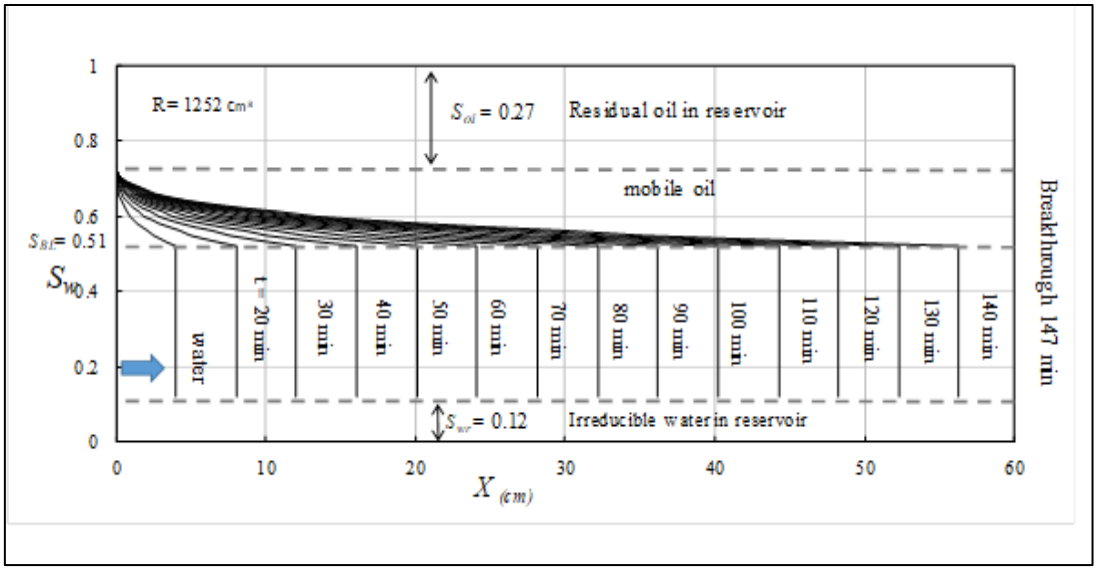

Figure A.6: Saturation profile calculated by BL analysis for oil displacement.

The oil recovery factor calculated from Eq. A.20 is RF = 0.40, from which the amount of water produced up to break through is A φ B × RF = 1252 cm³ (0.45 PV) from the total pore volume (PV = 2746 cm³) for the experimental plane model.

6. Application of Buckley-Leverett Theory to the Kashkari Oil Field

The relative permeability of oil and water shown in Figure A.5 was used to calculate oil displacement by water through BL frontal displacement theory in the Kashkari oil field. The fractional flow of water and oil was calculated with Eq. A.7. The asymmetric anticline Kashkari reservoirs were approximated as a cubic reservoir under the active water drive with a cross-sectional area of: 1. For the Albian reservoir group XIa, the area A = 3428 m², distance x = 3500 m, and the porosity n = 0.18; for the Aptian reservoir group XIIa, the area A = 10,440 m², distance x = 3750 m, and the porosity n = 0.2 (Figure

A.7 (a)); and for the Albian reservoir group XIIb, the area A = 4790 m², distance x = 3500 m, and the porosity n = 0.17; and for the Hauterivian reservoir group XIV, the area A = 15,504 m², distance x = 4750 m, and the porosity n = 0.2 (Figure A.7 (b)) were considered. The water injection wells near the oil-water contact in the western part of the reservoir were considered. The flow was approximated as a horizontal linear flow. The water injection rate in the effective underlying reservoir (q_T = 1000 m³/day) was considered.

For water pumped at a rate of q_T = 1000 m³/day through the reservoir, the water saturation at the front was calculated by a graphical method as S_{BL} = 0.51and the average saturation behind the front was S_W = 0.56. Figure A.8 illustrated the cross-sectional map of the Kashkari oil reservoirs.

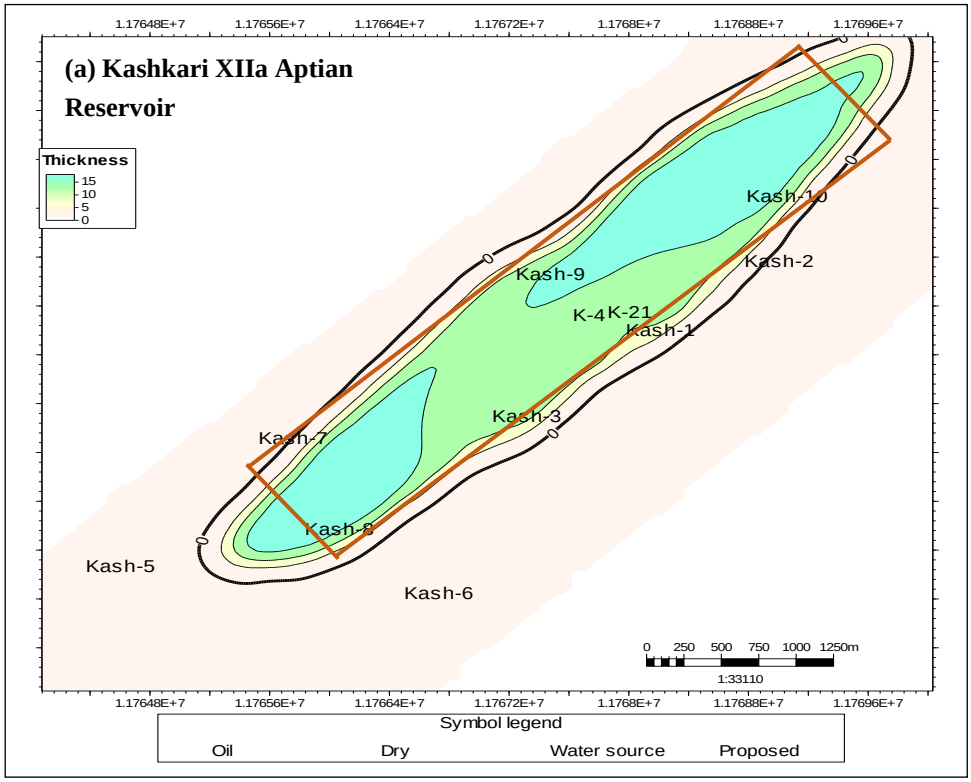

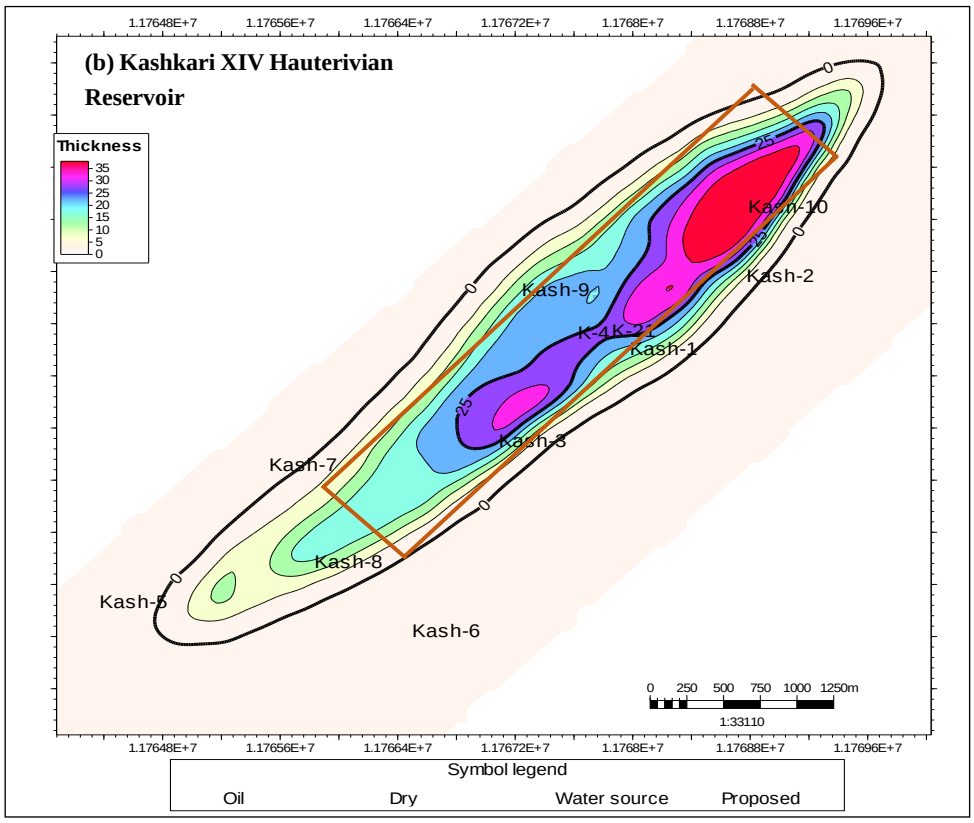

Figure A.7: Isopach maps of the petroleum reservoir in the Kashkari oil field (a) Aptian reservoir group XIIa, and (b) Hauterivian reservoir group XIV.

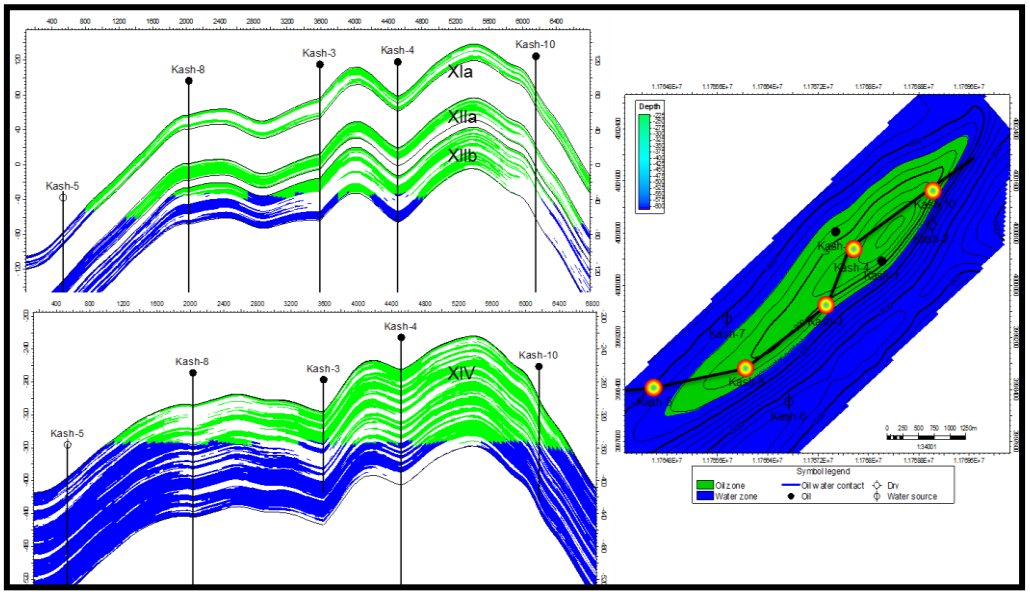

Figure A.8: Cross-sectional map of the Kashkari oil field from different wells shows the four reservoir groups XIa, XIIa, XIIb, and XIV.

Figure A.9 shows the oil displacement by water calculated by BL frontal displacement theory. The saturation front progresses with a constant speed toward the production wells, and breakthrough occurs at different times for different reservoirs. Figure A.9 (a) shows the oil displacement by water in the Albian group XIa reservoir, toward the production wells, and the breakthrough occurred at t = 900 days. The oil recovery factor in this reservoir was also calculated as RF = 0.40 from Eq. A.20, from which the amount of oil produced up to break through was $A\,\varphi\,B \times RF$ = 5.39 MMbbl. The OOIP is estimated by CNPC to be 9.10 MMbbl.

Based on the BL frontal displacement calculation shown in Figure A.9 (b) the oil displaced by water in the Aptian group XIIa reservoir moved toward the outlet and the breakthrough occurred at t = 3200 days. The oil produced up to the breakthrough was 19.5 MMbbl. In this reservoir, the OOIP was estimated by CNPC to be 42.6 MMbbl. The breakthrough for the Aptian XIIb occurred at t = 1200 days and total oil production was calculated to be 7.1 MMbbl. The OOIP for this reservoir was estimated by CNPC to be 12.2 MMbbl. The Hauterivian group XIV is the biggest reservoir in the Kashkari oil field. Figure A.9 (d) shows the frontal saturation profile calculated from the BL theory. Based on graphical calculation breakthrough occurred at t = 6200 days. The total oil produced from the Hauterivian reservoir was calculated to be Q_T = 36.8 MMbbl. The OOIP estimated at 2013 by CNPC was 70.28 MMbbl. There would still be residual oil in the reservoirs that could be discharged with the water.

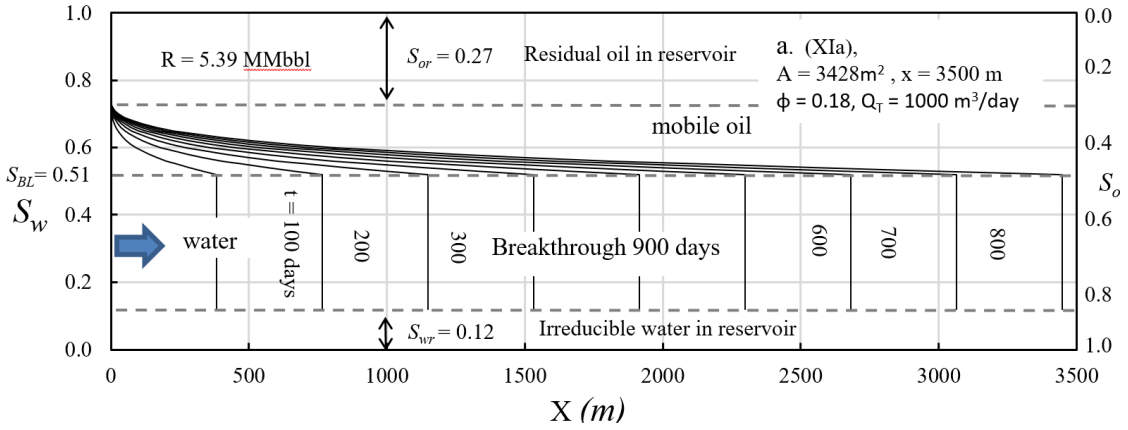

(a) XIa

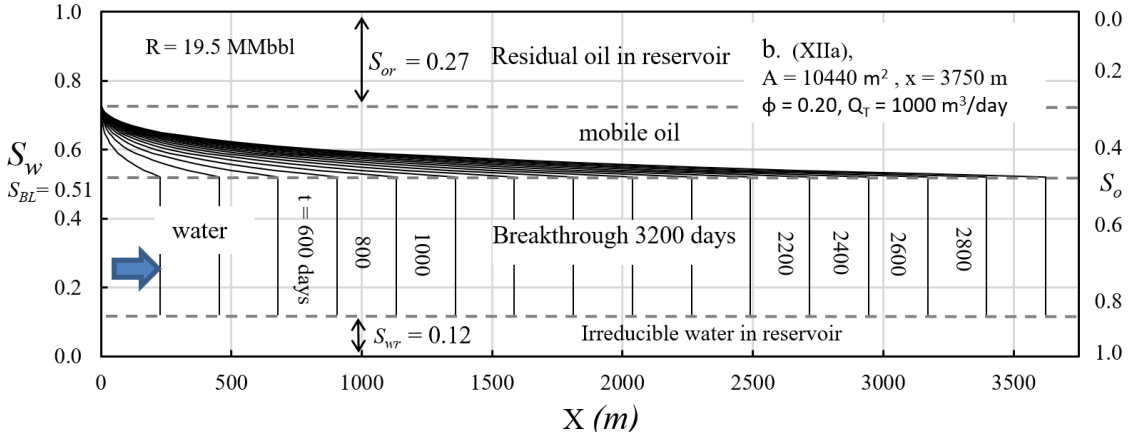

(b) XIIa

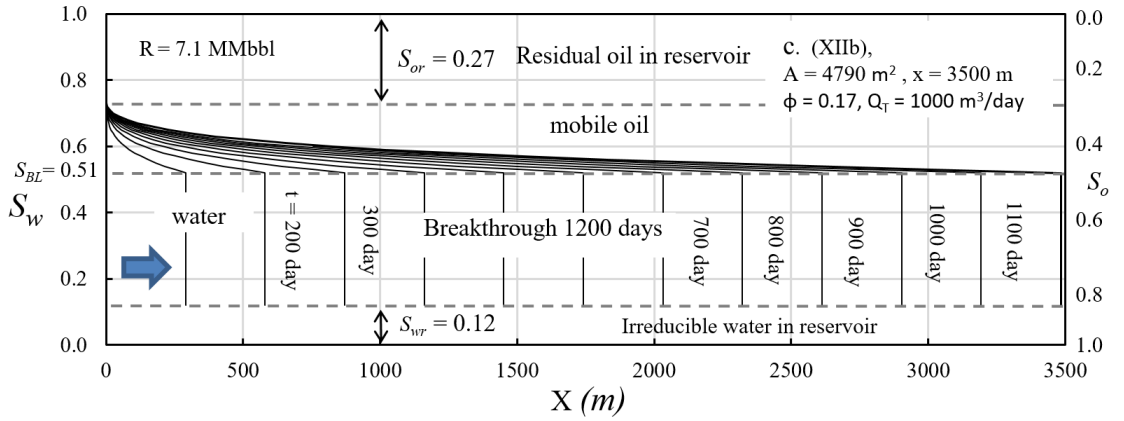

(c) XIIb

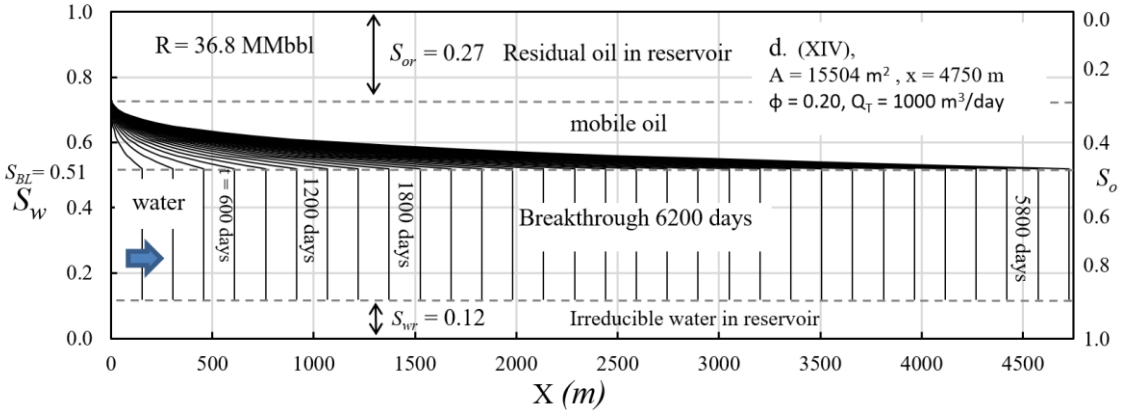

(d) XIV

Figure A.9: Saturation profile calculated by BL analysis of the Kashkari oil field (a) the Albian reservoir group XIa, (b) the Aptian reservoir group XIIa, (c) the Albian reservoir group XIIb, and (d) the Hauterivian reservoir group XIV.

CNPC estimated the geological reserves of the Kashkari oil field in 2013 to be 133.99 MMbbl. Table A.1 shows the calculation results of the oil reserves for each zone.

Table A.1: Calculation of Kashkari oil field reserves by CNPC [109].

Zone	Oil-bearing area (km^2)	h (m)	Por (f)	S_o (f)	ρo (g/cm^3)	B_{oi}	OOIP (MMbbl)
Xia	8.57	2.14	0.183	0.478	0.851	1.05	9.10
XIIa	5.28	11.6	0.203	0.586	0.852	1.02	42.60
XIIb	2.41	9.58	0.174	0.542	0.86	1.09	12.02
XIV	5.17	19.38	0.206	0.568	0.89	1.04	70.28
Total	8.57	42.7					133.99

From 1978 to 2012, seven organizations evaluated the reserves in the Kashkari field, and the estimates have been revised from 99.48 to 137.40 MMbbl (Table A.2). For the reserve calculations by the Research Institute of the former Soviet Union, Academy of Sciences of the Ministry of Geology of the former Soviet Union, and Sofregaz, more data was available and there are only small differences among these calculation results.

Table A.2: Comparison of estimated reserves [110].

Parties	Categories of Reserves (MMbbl)	
	OOIP	Recoverable
Gustavson	99.48	26.12
Russian Reserves Estimates		41.86
Soviet Union (1978)	122.99	47.60
Research Institute of Soviet Union (1980)	137.40	44.67
Geological Institute of Soviet (1987)	137.40	44.67
Sofregaz (2004)	137.31	44.57
CNPC (2013/01)	133.99	43.58
Buckley-Leverett Theory (This study)		68.79

7. Summary

The experiment was conducted by building an acrylic model of having nine observation wells. We evaluated the horizontal linear immiscible displacement of the fluid flow through porous media. In this test, the total amount of oil displaced by water up to 120 min was 1073 cm^3 (Q_o = 0.39 PV) calculated from the total pore volume ($PV = V \times n = 2767$ cm^3).

Then the BL graphical calculation was compared with the test result. The saturation front progresses toward the outlet at a constant speed, and breakthrough occurs at t = 147 min. The amount of water produced up to break through is = 1252 cm^3 (0.45 PV) from the same amount of pore volume for the experimental plane model.

In light of the negligible temporal disparities between the test results and the BL graphical calculations, the volumes of oil produced were insignificantly varied, thus, illustrating the potential applicability of the graphical calculation method within future case studies.

Then, the theory was applied to the Kashkari oil field. The asymmetric anticline Kashkari reservoirs were approximated as a cubic reservoir under the active water drive with a specific cross-sectional area.

According to the BL graphical calculations, the oil produced from the various geological groupings, namely Albian group XIa, Aptian group XIIa, Aptian group XIIb, and Hauterivian group XIV, amounted to 5.39, 19.5, 7.1, and 36.8 MMbbls respectively, yielding a sum total of 68.7 MMbbl. Furthermore, CNPC had previously estimated the geological reserves of the Kashkari oil field in 2013 to be 133.99 MMbbl, with recoverable reserves approximated at 43.58 MMbbl.

Consequently, amidst the economically challenging climate of the country, we advocate for the use of our proposed cost-effective, simplistic yet adaptable approach in the management of the Kashkari oil field. This method offers Afghanistan's authorities an affordable and comprehensive solution, enabling a clear image of recoverable oil estimation.

Reference

1. Fink, J., *Petroleum engineer's guide to oil field chemicals and fluids*. 2021: Gulf Professional Publishing.

2. Bello, A., J. Ozoani, and D. Kuriashov, *Proppant transport in hydraulic fractures by creating a capillary suspension.* Journal of Petroleum Science and Engineering, 2022. **208**: p. 109508.

3. Lake, L.W., *Enhanced oil recovery.* 1989.

4. Eftekhari, A.A., R. Krastev, and R. Farajzadeh, *Foam stabilized by fly ash nanoparticles for enhancing oil recovery.* Industrial & engineering chemistry research, 2015. **54**(50): p. 12482-12491.

5. Osei-Bonsu, K., N. Shokri, and P. Grassia, *Foam stability in the presence and absence of hydrocarbons: From bubble-to bulk-scale.* Colloids and Surfaces A: Physicochemical and Engineering Aspects, 2015. **481**: p. 514-526.

6. Alharthy, N., et al., *Enhanced oil recovery in liquid–rich shale reservoirs: laboratory to field.* SPE Reservoir Evaluation & Engineering, 2018. **21**(01): p. 137-159.

7. Arshad, A., et al. *Carbon dioxide (CO2) miscible flooding in tight oil reservoirs: A case study*. in *Kuwait International Petroleum Conference and Exhibition*. 2009. OnePetro.

8. Shojaei, M.J., et al., *Foam flow investigation in 3D-printed porous media: fingering and gravitational effects.* Industrial & Engineering Chemistry Research, 2018. **57**(21): p. 7275-7281.

9. Dang, C., et al. *Modeling low salinity waterflooding: ion exchange, geochemistry and wettability alteration*. in *SPE Annual Technical Conference and Exhibition*. 2013. OnePetro.

10. Zeinijahromi, A., et al., *Case study of low salinity water injection in Zichebashskoe field.* Journal of Petroleum Science Research, 2015. **4**(1): p. 16-31.

11. Reiter, P.K., *A water-sensitive sandstone flood using low salinity water*. 1961, University of Oklahoma.

12. Bernard, G.G. *Effect of floodwater salinity on recovery of oil from cores containing clays*. in *SPE California Regional Meeting*. 1967. OnePetro.

13. Tang, G. and N.R. Morrow, *Salinity, temperature, oil composition, and oil recovery by waterflooding.* SPE Reservoir Engineering, 1997. **12**(04): p. 269-276.

14. Purswani, P., M.S. Tawfik, and Z.T. Karpyn, *Factors and mechanisms governing wettability alteration by chemically tuned waterflooding: a review*. Energy & Fuels, 2017. **31**(8): p. 7734-7745.

15. Jadhunandan, P. and N.R. Morrow, *Effect of wettability on waterflood recovery for crude-oil/brine/rock systems.* SPE reservoir engineering, 1995. **10**(01): p. 40-46.

16. Yildiz, H.O. and N.R. Morrow, *Effect of brine composition on recovery of Moutray crude oil by waterflooding.* Journal of Petroleum science and Engineering, 1996. **14**(3-4): p. 159-168.

17. Austad, T., et al., *Seawater in chalk: An EOR and compaction fluid.* SPE Reservoir Evaluation & Engineering, 2008. **11**(04): p. 648-654.

18. Austad, T., et al., *Conditions for a low-salinity enhanced oil recovery (EOR) effect in carbonate oil reservoirs.* Energy & fuels, 2012. **26**(1): p. 569-575.

19. Fathi, S.J., T. Austad, and S. Strand, *"Smart water" as a wettability modifier in chalk: the effect of salinity and ionic composition.* Energy & fuels, 2010. **24**(4): p. 2514-2519.

20. Zhang, P., M.T. Tweheyo, and T. Austad, *Wettability alteration and improved oil recovery in chalk: The effect of calcium in the presence of sulfate.* Energy & fuels, 2006. **20**(5): p. 2056-2062.

21. Qiao, C., et al., *A mechanistic model for wettability alteration by chemically tuned waterflooding in carbonate reservoirs.* SPE Journal, 2015. **20**(04): p. 767-783.

22. Qiao, C., R. Johns, and L. Li, *Modeling low-salinity waterflooding in chalk and limestone reservoirs.* Energy & Fuels, 2016. **30**(2): p. 884-895.

23. Bader, M., *Seawater versus produced water in oil-fields water injection operations.* Desalination, 2007. **208**(1-3): p. 159-168.

24. Puntervold, T., S. Strand, and T. Austad, *New method to prepare outcrop chalk cores for wettability and oil recovery studies at low initial water saturation.* Energy & Fuels, 2007. **21**(6): p. 3425-3430.

25. Shariatpanahi, S.F., S. Strand, and T. Austad, *Evaluation of water-based enhanced oil recovery (EOR) by wettability alteration in a low-permeable fractured limestone oil reservoir.* Energy & Fuels, 2010. **24**(11): p. 5997-6008.

26. Strand, S., et al., *"Smart water" for oil recovery from fractured limestone: a preliminary study.* Energy & fuels, 2008. **22**(5): p. 3126-3133.

27. Zhang, Y., X. Xie, and N.R. Morrow. *Waterflood performance by injection of brine with different salinity for reservoir cores*. in *SPE annual technical conference and exhibition*. 2007. OnePetro.

28. Tang, G.-Q. and N.R. Morrow, *Influence of brine composition and fines migration on crude oil/brine/rock interactions and oil recovery.* Journal of petroleum science and engineering, 1999. **24**(2-4): p. 99-111.

29. Jerauld, G.R., et al., *Modeling low-salinity waterflooding.* SPE Reservoir Evaluation & Engineering, 2008. **11**(06): p. 1000-1012.

30. Zhang, P., M.T. Tweheyo, and T. Austad, *Wettability alteration and improved oil recovery by spontaneous imbibition of seawater into chalk: Impact of the potential determining ions Ca2+, Mg2+, and SO42−.* Colloids and Surfaces A: Physicochemical and Engineering Aspects, 2007. **301**(1-3): p. 199-208.

31. Webb, K., C. Black, and I. Edmonds. *Low salinity oil recovery–The role of reservoir condition corefloods*. in *IOR 2005-13th European Symposium on Improved Oil Recovery*. 2005. European Association of Geoscientists & Engineers.

32. Morrow, N.R., et al., *Prospects of improved oil recovery related to wettability and brine composition.* Journal of Petroleum science and Engineering, 1998. **20**(3-4): p. 267-276.

33. Berg, S., et al., *Direct experimental evidence of wettability modification by low salinity.* Petrophysics-The SPWLA Journal of Formation Evaluation and Reservoir Description, 2010. **51**(05).

34. Mahani, H., et al. *Analysis of field responses to low-salinity waterflooding in secondary and tertiary mode in Syria*. in *SPE Europec/EAGE Annual Conference and Exhibition*. 2011. OnePetro.

35. Mohamed, I., J. He, and H.A. Nasr-El-Din, *Effect of Brine Composition on CO_2/Limestone Rock Interactions during CO_2 Sequestration.* Journal of Petroleum Science Research, 2013. **2**(1): p. 14-26.

36. Takahashi, S. and A.R. Kovscek, *Wettability estimation of low-permeability, siliceous shale using surface forces.* Journal of Petroleum Science and Engineering, 2010. **75**(1-2): p. 33-43.

37. Webb, K., A. Lager, and C. Black. *Comparison of high/low salinity water/oil relative permeability*. in *International symposium of the society of core analysts, Abu Dhabi, UAE*. 2008.

38. Zhang, Y. and N.R. Morrow. *Comparison of secondary and tertiary recovery with change in injection brine composition for crude-oil/sandstone combinations*. in *SPE/DOE symposium on improved oil recovery*. 2006. OnePetro.

39. Webb, K., C.a. Black, and H. Al-Ajeel. *Low salinity oil recovery-log-inject-log*. in *SPE/DOE Symposium on Improved Oil Recovery*. 2004. OnePetro.

40. McGuire, P., et al. *Low salinity oil recovery: An exciting new EOR opportunity for Alaska's North Slope*. in *SPE western regional meeting*. 2005. OnePetro.

41. Lager, A., et al. *LoSal enhanced oil recovery: Evidence of enhanced oil recovery at the reservoir scale*. in *SPE symposium on improved oil recovery*. 2008. OnePetro.

42. Skrettingland, K., et al., *Snorre low-salinity-water injection—coreflooding experiments and single-well field pilot.* SPE Reservoir Evaluation & Engineering, 2011. **14**(02): p. 182-192.

43. Austad, T., et al. *Seawater as IOR fluid in fractured chalk*. in *SPE international symposium on oilfield chemistry*. 2005. OnePetro.

44. Hognesen, E.J., S. Strand, and T. Austad. *Waterflooding of preferential oil-wet carbonates: Oil recovery related to reservoir temperature and brine composition*. in *SPE Europec/EAGE annual conference*. 2005. OnePetro.

45. Morrow, N. and J. Buckley, *Improved oil recovery by low-salinity waterflooding.* Journal of petroleum Technology, 2011. **63**(05): p. 106-112.

46. Dang, C., et al., *Mechanistic modeling of low salinity water flooding.* Journal of Petroleum Science and Engineering, 2016. **146**: p. 191-209.

47. Mehrad, A.T., et al. *Assessment of oil and gas resources of northern Afghanistan and their impact on energy security in the country*. in *IOP Conference Series: Materials Science and Engineering*. 2020. IOP Publishing.

48. *Formation Evaluation & Geomodeling Study, KASHKARI FIELD, AFGHANISTAN*, in *PARADIGM GEOPHYSICAL*. 2017, Watan Oil and Gas Group: UAE, Dubai. p. 91.

49. *Kashkari oilfield development plan (1st phase)*. 2013: Kabul. p. 140.

50. Sabawon, A., et al., *Estimation of petroleum source rocks based on the crude oil geochemistr y in*

Amu Dar ya Basin, northern Afghanistan. Journal of the Japanese Association for Petroleum Technology, 2016. **81**(3): p. 230-242.

51. Gas, W.G.O., *Kashkari Field, Afghanistan 2017 Field Development Plan*, S.W. Steve Major, Editor. 2017, Sarotaga Technology. p. 183.

52. GEOPHYSICAL, P., *Formation Evaluation & Geomodeling Study, KASHKARI FIELD, AFGHANISTAN*, C.B. Brijesh Singh, Stuart Walley, Ramiro Losada, Steve Major, Editor. 2017, EMERSON, PARADIGM GEOPHYSICAL: UAE, Dubai. p. 91.

53. *Promotion of Oil and Gas Producing Areas to the Private Sector, Executive Summery*. 2005, Gustavson Associates. p. 221.

54. *Kashkari Oilfield, Well No.: Kash-1, Geological Design for Workover*. 2012, CNPCI Watan Oil and Gas Afghanistan Ltd. p. 29.

55. *Kashkari Oilfield, Well No.: Kash-3, Geological Design for Workover*. 2012, CNPCI WATAN Oil and Gas Afghanistan Ltd. p. 30.

56. *Kashkari Oilfield, Well No.: Kash-4, Geological Design for Workover*. 2012, CNPCI WATAN Oil and Gas Afghanistan Ltd. p. 31.

57. *Kashkari Oilfield, Well No.: Kash-9, Geological Design for Workover*. 2012, CNPCI WATAN Oil and Gas Afghanistan Ltd. p. 29.

58. *Kashkari Oilfield, Well No.: Kash-10, Geological Design for Workover*. 2012, CNPCI WATAN Oil and Gas Afghanistan Ltd. p. 28.

59. *Kashkari Oilfield, Well No.: Kash-21, Geological Design for Workover*. 2012, CNPCI WATAN Oil and Gas Afghanistan Ltd. p. 7.

60. KANSUN, G. and A.O. AFZALI, *Geology, Petrographic Characteristics and Tectonic Structure of Paleoproterozoic basement of Kabul Block (North Eastern Afghanistan), Initial Findings.* International Journal of Multidisciplinary Studies and Innovative Technologies, 2022. **6**(1): p. 117-133.

61. Steinmüller, K., et al., *The metalliferous mineral potential of Afghanistan. Synthesis of geology and metallogeny with suggestions for mineral resource development.* Islamic Republic of Afghanistan, Ministry of Mines, 2010.

62. Kingston, J., *The undiscovered oil and gas of Afghanistan*. 1990: Department of the Interior, US Geological Survey.

63. Ulmishek, G.F., *Petroleum geology and resources of the Amu-Darya basin, Turkmenistan, Uzbekistan, Afghanistan, and Iran*. Vol. 2201. 2004: US Department of the Interior, US Geological Survey Iran.

64. Klett, T., et al., *Assessment of undiscovered technically recoverable conventional petroleum resources of northern Afghanistan.* US Geological Survey open-file report, 2006. **2006**: p. 1253.

65. Petroconsultants, *Petroleum Exploration and Production* 1996.

66. Sokolova, I.M., Abryutina, N.I., Makarov, V.V., Kuldzhaev, and R. B.A., G.V., and Petrov, Al.A.,, *Biomarkers*

in gas condensates of eastern Turkmenistan. Geokhimiya,

no. 1, p. 123–130, 1993.

67. Melikhov, V.N., Sibirev, V.S., Ashirmamedov, M.A., Ataev, and P. A.A., O.N., and Rozhkov, E.L.,, *Geologic basis and ways of realization of petroleum potential of the Bakhardok slope and Kopet-Dag foredeep, Information Review, Series Petroleum Geology and Geophysics* 1987.

68. Ibragimov, A.G., and Ivanov, E.V.,, *Genesis of abnormally high formation pressure in Upper Jurassic carbonate rocks of the northern Amu-Darya basin.* : Geologiya Nefti i Gaza, no. 1, p. 15–19, 1984.

69. Tashliev, M.S., Yuferov, R.F., Tovbina, S.Z., Davydov, A.N., and D.E. Kosoy, and Kuryleva, A.M.,, *Lithostratigraphy of hydrocarbon-productive rocks of Turkmenistan [Litostratigrafiya neftegazonosnykh otlozheniy Turkmenistana]:* . Ashkhabad, Turkmenistan, Ylym, 230 p, 1985.

70. Yixin, Y., et al., *Division and resources evaluation of hydrocarbon plays in the Amu Darya basin, central Asia.* Petroleum Exploration and Development, 2015. **42**(6): p. 819-826.

71. Gustavson, *Promotion of Oil and Gas Production Areas to the Private Sector Grant Agreement, No. H007-AF, Gustavson Associates report, Jul-2005.* 2005.

72. Mahdi, Z., et al. *Waterflooding Technique to the Kashkari Oilfield in the North Part of Afghanistan*. in *5th International Conference on Chemical Investigation and Utilization of Natural Resource (ICCIUNR-2021)*. 2021. Atlantis Press.

73. Mahdi, Z., et al., *Increasing Recoverable Oil in Northern Afghanistan Kashkari Oil Field by Low-Salinity Water Flooding.* Energies, 2023. **16**(1): p. 534.

74. CNPCI, W.O.a.G., Afghanistan, *KASHKARI OILFIELD DEVELOPMENT PLAN (1st PHASE)* 2013, CNPCI Watan Oil and Gas Afghanista: Afghanistan.

75. Ghulami, M.R., et al. *Numerical Simulation Study on Gas Miscibility of an Oil Field Located in Afghanistan*. in *SPWLA Formation Evaluation Symposium of Japan*. 2015. SPWLA.

76. Katende, A. and F. Sagala, *A critical review of low salinity water flooding: Mechanism, laboratory and field application.* Journal of Molecular Liquids, 2019. **278**: p. 627-649.

77. Dang, C., et al. *State-of-the art low salinity waterflooding for enhanced oil recovery*. in *SPE Asia Pacific Oil and Gas Conference and Exhibition*. 2013. OnePetro.

78. *Russian Production Report*, T.P.R.o.K.F. Afghanistan, Editor. 1980, State Institute on Design and Research in Oil Industry: USSR Ministry of Oil Industry.

79. Derkani, M.H., et al., *Low salinity waterflooding in carbonate reservoirs: Review of interfacial mechanisms.* Colloids and Interfaces, 2018. **2**(2): p. 20.

80. Al-Shalabi, E.W., K. Sepehrnoori, and M. Delshad. *Does the double layer expansion mechanism contribute to the LSWI effect on hydrocarbon recovery from carbonate rocks?* in *SPE Reservoir characterization and simulation conference and exhibition*. 2013. OnePetro.

81. Dang, C., et al. *Modeling and optimization of low salinity waterflood*. in *SPE Reservoir Simulation Symposium*. 2015. OnePetro.

82. Awolayo, A.N., H.K. Sarma, and L.X. Nghiem. *A comprehensive geochemical-based approach at modeling and interpreting brine dilution in carbonate reservoirs*. in *SPE reservoir simulation conference*. 2017. OnePetro.

83. Tunnish, A., E. Shirif, and A. Henni, *History matching of experimental and CMG-STARS results.* Journal of Petroleum Exploration and Production Technology, 2019. **9**(1): p. 341-351.

84. *CMG-GEM Technical Manual*, C.M.G. Ltd, Editor. 2021.

85. Adegbite, J.O., E.W. Al-Shalabi, and B. Ghosh, *Geochemical modeling of engineered water injection effect on oil recovery from carbonate cores.* Journal of Petroleum Science and Engineering, 2018. **170**: p. 696-711.

86. Ghahfarokhi, A.J. and O. Torsaeter. *Numerical Simulation Of Low Salinity Water Flooding: Wettability Alteration Considerations*. in *ECMOR XVI-16th European Conference on the Mathematics of Oil Recovery*. 2018. European Association of Geoscientists & Engineers.

87. Ghahfarokhi, A.J. and O. Torsaeter. *Modeling wettability alteration in low salinity water flooding*. in *81st EAGE Conference and Exhibition 2019*. 2019. European Association of Geoscientists & Engineers.

88. Bethke, C., *Geochemical reaction modeling: Concepts and applications.* 1996.

89. Delany, J. and S. Lundeen, *The LLNL thermodynamic database.* Lawrence Livermore National Laboratory Report UCRL-21658. Lawrence Livermore National Laboratory, Livermore, California, USA, 1990.

90. Kharaka, Y.K., *SOLMINEQ. 88, a computer program for geochemical modeling of water-rock interactions*. Vol. 88. 1988: Department of the Interior, US Geological Survey.

91. Nghiem, L., et al. *Modeling CO2 storage in aquifers with a fully-coupled geochemical EOS compositional simulator*. in *SPE/DOE symposium on improved oil recovery*. 2004. OnePetro.

92. RezaeiDoust, A., et al., *Smart water as wettability modifier in carbonate and sandstone: A discussion of similarities/differences in the chemical mechanisms.* Energy & fuels, 2009. **23**(9): p. 4479-4485.

93. Appelo, C. and D. Postma, *Geochemistry.* Groundwater and pollution, 2005. **536**.

94. *KASHKARI OILFIELD*

DEVELOPMENT PLAN (1st PHASE). 2013, CNPCI Watan Oil and Gas Afghanistan Ltd. p. 140.

95. Gas, W.G.O., *Kashkari Field, Afghanistan 2017 Field Development Plan; Sarotaga Technology: 2017; p. 183.* 2017.

96. Petzet, A., *CNPC gets three Afghanistan Amu Darya blocks.* Oil Gas J. http://www. ogj. com/articles/2012/01/cnpc-gets-three-afghanistan-amu-darya-blocks. html, 2016.

97. Dullien, F.A., *Porous media: fluid transport and pore structure*. 2012: Academic press.

98. Shepherd, M., *Factors influencing recovery from oil and gas fields.* 2009.

99. Ezekwe, N., *Petroleum reservoir engineering practice*. 2010: Pearson Education.

100. Dandekar, A.Y., *Petroleum reservoir rock and fluid properties*. 2006: CRC press.

101. Buckley, S. and M. Leverett. *Mechanism of Fluid Displacement in Sands, Transact*. 1942. AIME.

102. Fanchi, J.R., *Principles of applied reservoir simulation*. 2005: Elsevier.

103. Bear, J., *Dynamics of fluids in porous media*. 1988: Courier Corporation.

104. Wooding, R.A. and H.J. Morel-Seytoux, *Multiphase fluid flow through porous media.* Annual review of fluid mechanics, 1976. **8**(1): p. 233-274.

105. Seddiqi, K.N., Z. Mahdi, and S. Honma, *Laboratory measurement of relative permeabilities of oil and water in sand.* Proc. School of Eng. of Tokai University, 2016. **41**: p. 47-51.

106. Nazari, J., et al., *Influence of relative permeability and viscosity ratio on oil displacement by water in petroleum reservoir.* Proceedings of School of Engineering of Tokai University, 2015. **40**: p. 15-20.

107. Seddiqi, K.N., Mahdi, Z., & Honma, S., *Laboratory measurement of relative permeabilities of oil and water in sand.* Proc. School of Eng. of Tokai University, 41, 47-51., 2016.

108. Arabzai, A. and S. Honma, *numerical simulation of the Buckley-Leverett problem.* Proceedings of School of Engineering of Tokai University, 2013. **38**: p. 9-14.

109. Arshad, A.A.-M., A.A.; Menouar, H.; Muhammadain, A.M.; Mtawaa, B. , *Carbon dioxide (CO2) miscible flooding in tight oil reservoirs: A case study.* In Proceedings of the Kuwait International Petroleum Conference and Exhibition, 2009., 2019.

110. Kabul, *Kashkari oilfield development plan (1st phase).* 2013.